PART I. CHEMICAL REACTIONS DURING FLOW IN ROCKET NOZZLES

PART II. GAS DISCHARGE RATES THROUGH DE LAVAL NOZZLES AND THE EXPERIMENTAL DETERMINATION OF DESORPTION RATES

Thesis by

John William Porter, Jr.

In Partial Fulfillment of the Requirements

For the Degree of

Doctor of Philosophy

California Institute of Technology

Pasadena, California

1963

ACKNOWLEDGEMENTS

The author is indebted to Dr. S. S. Penner for his guidance throughout the course of this research.

Financial support for this research has been provided by the Daniel and Florence Guggenheim Foundation in the form of a Guggenheim Jet Propulsion Fellowship to the author for the academic year 1961-62, by the California Institute of Technology through tuition scholarships for the years 1960-63, and by the Office of Ordnance Research, United States Army, under Contract No. DA 04-495-ORD-1634 and Grant No. DA-ARO(D)-31-124-G289. This support is gratefully acknowledged.

The author is also grateful to Mrs. Madeline Fagergren and Mrs. Barbara Mullican for their assistance in preparing this manuscript.

ABSTRACT

In Part I, some of the important physical ideas that have been used in an analysis of chemical changes in rocket nozzles are reviewed with particular reference to the three-body recombination reaction. Modified forms of the simple near-equilibrium flow criterion developed about 15 years ago are shown to lead to results that are substantially equivalent to estimates derived from a criterion of Bray. The influence of surface-catalyzed processes on atomic recombination rates in rocket nozzles is considered and found likely to be important in present solid-propellant rocket engines.

In Part II, studies of the effective desorption rates of gases (Ar, He, and CO_2) from sand and from silica gel are described. These rates have been determined experimentally by measuring, as a function of time, the pressure drop in a vessel containing the solids when the gases are allowed to discharge through a small de Laval nozzle. The dependence of the desorption rate on temperature has been investigated. A theoretical expression for the rate of desorption from porous solids has been developed assuming that the overall process is diffusion controlled. The experimentally determined desorption rates of Ar, He, and CO_2 from silica gel have been compared with this theoretical expression.

TABLE OF CONTENTS

PART II. GAS DISCHARGE RATES THROUGH DE LAVAL NOZZLES AND THE EXPERIMENTAL DETERMINATION OF DESORPTION RATES

PART I. CHEMICAL REACTIONS DURING FLOW IN ROCKET NOZZLES

I. APPROXIMATIONS USED IN THE THREE-BODY RECOMBINATION REACTION IN ROCKET NOZZLES

A. Lighthill's Approximation

In the literature we find frequent reference to Lighthill's "ideal diatomic gas".[1] This "ideal diatomic gas" refers to the classical harmonic oscillator-rigid rotator approximation[2] for diatomic molecules and includes only consideration of the electronic ground state for the atom A and the molecule A_2 which participate in the homogeneous recombination reaction

$$A_2 + X \underset{k_R}{\overset{k_D}{\rightleftharpoons}} 2A + X \qquad (1)$$

where k_D and k_R represent, respectively, specific reaction rate constants for dissociation and recombination and X denotes either A or A_2.

The equilibrium constant based on ratios of partial pressures (K_p) is then related to the equilibrium constant based on ratios of mass fractions (K_Y) through the expression [cf. ref. 2, Eq. (36) on p. 123]:

$$K_p = \frac{p_A^2}{p_{A_2}} = K_Y (RT\rho)\, W_A^{-2}\, W_{A_2} = \frac{(Y_A)^2}{1-Y_A}\, \rho RT\, \frac{2}{W_A}$$

or

$$\frac{(Y_A)^2}{1-Y_A} = \frac{W_A}{2}\, \frac{1}{\rho RT}\, K_p \equiv \frac{m}{2}\, \frac{1}{\rho kT}\, K_p . \qquad (2)$$

Here p_A and p_{A_2} denote the partial pressures of species A and A_2, respectively; Y_A and Y_{A_2} are the corresponding mass fractions; R is the molar gas constant; T represents the absolute temperature; ρ is the density of the gas mixture; W_A and W_{A_2} are the molecular weights of species A and A_2, respectively; $m = W_A/N$ (where N = Avogadro's number) is the mass per atom of species A; $k = R/N$ is the Boltzmann constant.

For an ideal gas it follows from statistical mechanics that [cf. ref. 2, Eqs. (29) and (30) on p. 193]

$$K_p = \exp(-\Delta F^\circ/RT)$$

where

$$\Delta F^\circ = 2F_A{}^\circ - F_{A_2}{}^\circ$$

is the standard Gibbs free energy difference (i.e., the free energy difference at unit pressure) for the chemical process described in Eq. 1. But [cf. ref. 2, Eq. (29) on p. 193]

$$F_A{}^\circ = RT\ln\left[\frac{h^3}{(2\pi m)^{3/2}}\ \frac{1}{(kT)^{5/2}}\ \frac{1}{Q'_{\text{int, A}}}\right] + \varepsilon_A N$$

and

$$F_{A_2}{}^\circ = RT\ln\left[\frac{h^3}{2^{3/2}(2\pi m)^{3/2}}\ \frac{1}{(kT)^{5/2}}\ \frac{1}{Q'_{\text{int, A}_2}}\right] + \varepsilon_{A_2} N$$

where (cf. ref. 2, p. 194)

$$Q'_{\text{int, A}} \simeq g_A{}^\circ$$

and [cf. ref. 2, Eqs. (46), (53), (54) and (40) on pp. 200-202]

$$Q'_{int, A_2} = g_{A_2}{}^{o}\left[1-\exp(-h\nu/kT)\right]^{-1}(kT/shcB).$$

Here $Q'_{int, A}$ is the internal partition function for species A when the energy levels of A are referred to the ground level of species A, $g_A{}^{o}$ is the statistical weight of the ground state of species A, and it has been assumed that the temperature is sufficiently low to justify neglect of all electronic energy levels above the ground level. The quantity Q'_{int, A_2} represents the internal partition function of molecule A_2 in the ground electronic state with statistical weight $g_{A_2}{}^{o}$ when A_2 is treated as a combination of (a) a rigid rotator with rotational constant B where

$$hcB = h^2/8\pi^2 I$$

(h = Planck's constant, c = velocity of light, I = moment of inertia of A_2) and (b) a harmonic oscillator of frequency ν ; all energy levels in the expression for Q'_{int, A_2} are measured with respect to the ground state of A_2. The quantity s is the symmetry number of the diatomic molecule and equals unity for heteropolar molecules and two for homopolar molecules. The energies $\mathcal{E}_A$ and $\mathcal{E}_{A_2}$ represent, respectively, the zero point energies of the atom A and of the molecule A_2. Combination of the preceding expressions shows that

$$K_p = \left[\frac{(km)^{3/2}\, s(g_A{}^{o})^2}{8\pi^{1/2}\, h\, I\, g_{A_2}{}^{o}}\right] T^{3/2}\left[1-\exp(-h\nu/kT)\right]\exp(-2d_A/kT) \qquad (3)$$

where $2\mathcal{E}_A - \mathcal{E}_{A_2} \equiv 2d_A$ is the dissociation energy for one molecule of A_2. Combining Eqs. 2 and 3, we now obtain the expression

$$\frac{Y_A^2}{1-Y_A} = \frac{\rho_d}{\rho} \exp(-2d_A/kT) \tag{4}$$

where

$$\rho_d = \frac{m^{5/2} \epsilon \nu^{1/2}}{16\pi^{1/2} h^{1/2} I} \frac{(g_A^{\,o})^2}{g_{A_2}^{\,o}} \frac{1-\exp(-h\nu/kT)}{(h\nu/kT)^{1/2}} \tag{5}$$

is a characteristic density. Lighthill noted that $\left[1-\exp(-x)\right] x^{-1/2}$ is a slowly varying function of x and proposed to replace it by an effective mean value. This "Lighthill approximation" is well justified for the range of values of x actually encountered in conventional rocket nozzles. A plot of $(kT/h\nu)^{1/2}\left[1-\exp(-h\nu/kT)\right]$ as a function of $h\nu/kT$ is shown in Fig. 1. Reference to Fig. 1 shows that $(kT/h\nu)^{1/2}\left[1-\exp(-h\nu/kT)\right]$ varies very slowly with temperature near $kT/h\nu \simeq 1$; it approaches zero as the temperature approaches infinity. Values of $kT/h\nu \simeq 1$ are of interest in connection with conventional nozzle flow calculations.

We may easily show that the statement

$$1-\exp(-h\nu/kT) \propto \left(\frac{h\nu}{kT}\right)^{1/2} \tag{6}$$

corresponds to the assumption that the vibrational energy of the molecule is half excited. Thus the specific vibrational energy of A_2 is given by the expression

$$u_{A_2,\,vib} = \frac{k}{2m} T^2 \frac{d \ln Q_{vib}}{dT}$$

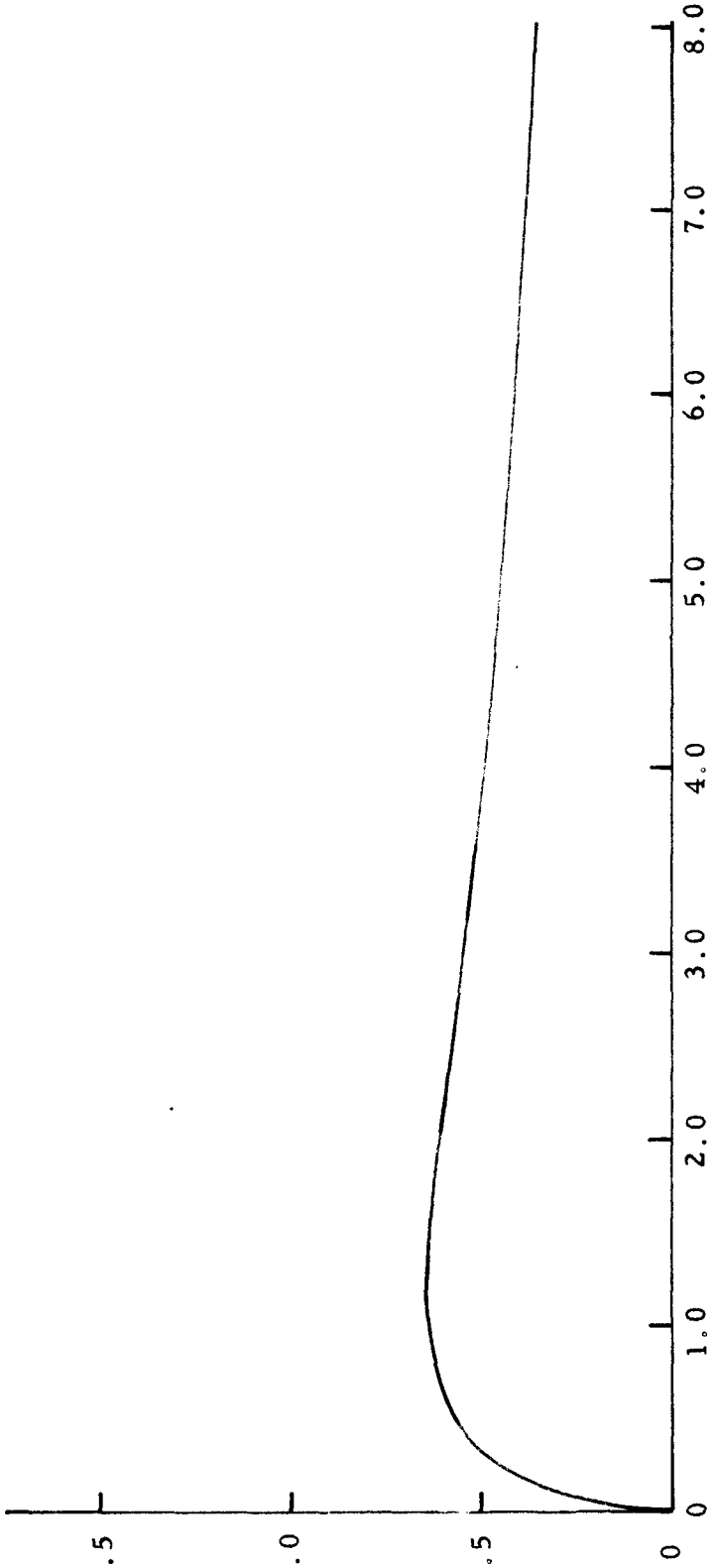

Fig. 1. The quantity $x^{-1/2}[1-\exp(-x)]$ as a function of x.

where

$$Q_{vib} = \frac{\exp(-\frac{1}{2} h\nu/kT)}{1-\exp(-h\nu/kT)} ;$$

hence

$$u_{A_2, vib} = \frac{1}{2m}(\tfrac{1}{2} h\nu) - \frac{kT^2}{2m} \frac{d \ln\left[1-\exp(-h\nu/kT)\right]}{dT} . \qquad (7)$$

Here the quantity $(\frac{1}{2} h\nu)/2m$ represents the specific vibrational energy associated with the zero-point energy. For unexcited molecules, $h\nu/kT \gg 1$ and the second term in Eq. 7 becomes negligibly small compared to the zero-point energy. For fully excited molecules, $h\nu/kT \ll 1$ and

$$-\frac{kT^2}{2m} \frac{d}{dT} \ln\left[1-\exp(-h\nu/kT)\right] \simeq -\frac{kT^2}{2m} \frac{d}{dT} \ln\left(\frac{h\nu}{kT}\right) = \frac{kT}{2m} .$$

On the other hand, if we use Eq. 6, then

$$-\frac{kT^2}{2m} \frac{d}{dT} \ln\left[1-\exp(-h\nu/kT)\right] \simeq -\frac{kT^2}{2m} \frac{d}{dT} \ln\left(\frac{h\nu}{kT}\right)^{1/2} = \frac{1}{2} \frac{kT}{2m} .$$

Thus it follows that Eq. 6 corresponds to the approximation that the vibrational degrees of freedom are half excited and that

$$2mu_{A_2, vib} = (\tfrac{1}{2} h\nu) + \tfrac{1}{2} kT. \qquad (8)$$

The internal energy of unit mass of fluid mixture, when the ground vibrational state of the molecule is chosen as energy zero, becomes

$$u = \frac{Y_A}{m}\left(\frac{3}{2} kT + d_A\right) + \frac{1-Y_A}{2m}\left[\frac{3}{2} kT + 2mu_{A_2, rot} + \left(2mu_{A_2, vib} - \frac{1}{2} h\nu\right)\right] ,$$

where

$$2mu_{A_2,\,rot} = kT;$$

hence,

$$u = \frac{Y_A d_A}{m} + \frac{3}{2m} kT . \tag{9}$$

The enthalpy per unit mass of mixture is

$$h = u + \frac{p}{\rho} \qquad (\rho = \text{density of the fluid mixture})$$

where $p = p_A + p_{A_2}$, $p_A = Y_A \rho (kT/m)$, $p_{A_2} = (1-Y_A)\rho (kT/2m)$,

$$p = \frac{1+Y_A}{2m} \rho\, kT$$

and

$$h = (4 + Y_A) \frac{kT}{2m} + \frac{Y_A d_A}{m} . \tag{10}$$

The approximations involved in (a) neglecting the influence of excited electronic states, (b) assuming that the vibrational degrees of freedom are only half excited, (c) neglecting anharmonicity terms in the vibrational partition function, and (d) neglecting vibration-rotation interactions in the partition function for A_2 are all ultimately justified because of the low accuracy inherent in nozzle-flow calculations because chemical reaction rates are usually not known to better than an order of magnitude.

B. The Reaction Rate

For the chemical process described by Eq. 1, the rate of reaction may be written in the form (cf. ref. 1, Chapter XVII)

$$\frac{dY_A}{dt} = \frac{W_A}{\rho}\,\frac{d(A)}{dt} = \frac{2}{\overline{W}}\left[k_D\,\frac{\rho\,(1-Y_A)}{2} - k_R\,\frac{\rho^2\,Y_A^2}{W_A}\right] \qquad (11)$$

where $\overline{W}$ is the average molecular weight of the mixture $= 2W_A/(1+Y_A)$ and the other symbols have their usual meaning. But detailed balancing leads to the requirement [cf. ref. 2, Chapter XVII and Eq. (36) on p. 123]

$$\frac{k_D}{k_R} = K_c = \frac{K_p}{NkT} = \frac{2\rho\,Y_A^2}{W_A(1-Y_A)} \quad .$$

Combining this last relation with Eq. 4 we now find that

$$\frac{k_D}{k_R} = \frac{2}{W_A}\,\rho_d \exp(-2d_A/kT) \quad . \qquad (12)$$

For the specific reaction rate constant for dissociation we use the conventional approximation

$$k_D = CT^{-s'} \exp(-2d_A/kT) \qquad (13)$$

where C is a constant. Using Eqs. 12 and 13, we find from Eq. 11 the result

$$\frac{dY_A}{dt} = \left(\frac{1+Y_A}{2W_A}\right)(CT^{-s'})\left[\rho\,(1-Y_A)\exp(-2d_A/kT) - \frac{\rho^2}{\rho_d}\,Y_A^2\right] . \qquad (14)$$

Equation 14 differs from the expression given by Freeman[3] and used by Bray[4] and others through the occurrence of the factor $(1+Y_A)$ in place of unity. It is easily shown that $(1+Y_A)$ should be replaced by unity when the process described in Eq. 1 occurs as a minor reaction

in a gas mixture. In any case, the relation given in Eq. 14 involves implicitly the erroneous assumption that atoms and molecules are equally effective as third bodies in the recombination of atoms.

II. BRAY'S APPROXIMATE CRITERION FOR FREEZING AND PENNER'S CRITERION FOR NEAR-EQUILIBRIUM FLOW

A. Introduction

Among the first studies of chemical reactions during flow through rocket nozzles are approximate numerical calculations by Penner and Altman,[5] the development of approximate procedures for defining "near-equilibrium" flow and "near-frozen" flow by Penner[6] in which earlier work of Schäfer[7] was used, and presumably exact* numerical solutions of flow with recombination of hydrogen atoms by Krieger.[8] In assessing the early ideas relating to rocket applications, it is important to remember the context in which this work was done: the knowledge of chemical reaction rates was still sparser than it is today, machine computations of composition changes during equilibrium flow were unknown, and the objectives of the early work were simply to define the problem within rational limits. After some 15 years of work in this field, the essential physical arguments have not changed, as is evident from the following quotation:

---

* Actually Krieger made a slight error in his work since he treated the flow problem as isentropic.[8] Revised calculations have been published recently.[9]

> "This study of the equilibrium involving nitric oxide, nitrogen, and oxygen suggests the occurrence of practically frozen flow below a certain temperature." (Penner, 1950).

The near-equilibrium and near-frozen flow criteria [cf. ref. 2, Chapter XXIII] had as objective the determination of the point in a nozzle where effective freezing of chemical equilibria would occur. A serious difficulty arose in the practical application of these criteria in 1949 and 1950 because there existed at the time essentially no precise data which could be used not for conservative but rather for practical applications of the criteria. Owing to the concentration of effort in this field in recent years,[4, 10-13] we are now in a position to refine the method of application of the criteria. That this is indeed useful has been pointed out recently by Barrère[14] who showed that the near-equilibrium criterion could be made to yield substantially equivalent results to those of Bray[4, 10] for Wegener's experimental studies on the system $N_2 + 2NO_2 \rightleftharpoons N_2 + N_2O_2$.[15] Since both procedures define the initial location in a nozzle where significant departures from near-equilibrium flow occur, Barrère's conclusion might well have been anticipated. We shall verify Barrère's observation by an analytical comparison between the methods of Bray and Penner for the reaction

$$B + 2A \rightleftharpoons B + A_2 \qquad (15)$$

where B represents an inert carrier that is present in vast excess.

B. Refinement of Bray's Approximate Procedure

Retaining the physical ideas of Bray, a modified derivation is presented.

For the chemical reaction described by Eq. 15, it is readily shown that

$$-\frac{d\alpha}{dt} = 2k_R \rho^2 \alpha^2 \frac{Y_B (Y_A)_o}{W_B W_A} \left(1 - \frac{K}{K_e}\right) \equiv R \left(1 - \frac{K}{K_e}\right) , \tag{16}$$

where

$$\alpha = \frac{Y_A}{Y_A + Y_{A_2}} = \frac{Y_A}{(Y_A)_o} , \tag{17}$$

$$R = 2k_R \rho^2 \alpha^2 \frac{Y_B (Y_A)_o}{W_B W_A} , \tag{18}$$

and

$$K = Y_{A_2} / Y_A^2 , \qquad K_e = (Y_{A_2} / Y_A^2)_e , \tag{19}$$

with the subscript e identifying local equilibrium conditions and the subscript o denoting initial (or nozzle entrance) conditions. It has also been assumed that $(Y_{A_2})_o = 0$ so that $Y_A + Y_{A_2} = (Y_A)_o$.*

The deviations from local equilibrium are conveniently described through the parameter

$$r = \frac{Y_A}{(Y_A)_e} = \frac{Y_A / (Y_A)_o}{(Y_A)_e / (Y_A)_o} = \frac{\alpha}{\alpha_e} \geq 1 . \tag{20}$$

---

* The analysis is now specifically applicable to the system $A = NO_2$.[15]

In terms of r, Eq. 19 becomes

$$\frac{K}{K_e} = \frac{1}{r^2} \frac{(Y_A)_o - Y_A}{(Y_A)_o - (Y_A)_e} = \frac{1}{r^2} \frac{(1 - r\alpha_e)}{(1 - \alpha_e)}$$

and Eq. 16 may be written in the form

$$-\frac{d\alpha}{dt} = R\left[1 - \frac{1}{r^2} \frac{(1-r\alpha_e)}{(1-\alpha_e)}\right] \equiv R - D \tag{21}$$

where R is the recombination rate and D represents the dissociation rate. For static equilibrium, Eq. 21 yields

$$\frac{d\alpha}{dt} = 0 ;$$

however, in order to have equilibrium flow in a nozzle, R must be infinite, in which case Eq. 21 becomes indeterminate and should be replaced by the law of mass action.

If R is sufficiently large, near-equilibrium flow obtains,

$$1 - \frac{1}{r^2} \frac{(1-r\alpha_e)}{(1-\alpha_e)} \ll 1$$

and, therefore,

$$-\frac{d\alpha}{dt} \ll R \frac{1}{r^2} \frac{(1-r\alpha_e)}{(1-\alpha_e)} \tag{22}$$

for near-equilibrium flow. On the other hand, when large deviations from equilibrium flow occur, $r = Y_A/(Y_A)_e$ becomes much larger than unity,

$$\frac{1}{r^2} \frac{(1-r\alpha_e)}{(1-\alpha_e)} \ll 1$$

and, therefore,

$$-\frac{d\alpha}{dt} \gg R\,\frac{1}{r^2}\,\frac{(1-r\alpha_e)}{(1-\alpha_e)} \tag{23}$$

for large deviations from equilibrium flow. Comparison of Eqs. 22 and 23 shows that

$$-\frac{d\alpha}{dt} = R\,\frac{1}{r^2}\,\frac{(1-r\alpha_e)}{(1-\alpha_e)} = D \tag{24}$$

between near-equilibrium flow and large deviations from near-equilibrium flow. The spatial location where Eq. 24 is satisfied is identified by the coordinate $x=x_o$.

If it is indeed true that a well-defined, narrow, spatial region exists in the nozzle where an abrupt transition occurs from near-equilibrium flow to near-frozen flow, then Eqs. 22 to 24 must all be satisfied in a small spatial region near x_o.

Bray now assumes that $r \simeq r_e = 1$, $\alpha \simeq \alpha_e$ and $-d\alpha/dt \simeq -d\alpha_e/dt$ up to the location x_o, in which case Eq. 24 reduces to the expression

$$-\frac{d\alpha_e}{dt} \simeq R_e \simeq D_e. \tag{25a}$$

Bray has also replaced the preceding expression by the empirical equation

$$-\frac{d\alpha_e}{dt} = K\,D_e \qquad \text{(Bray's criterion)} \tag{25b}$$

and states that K is a constant expected to be of order unity.

It appears more logical to use Eqs. 21 and 24 first to define conditions at x_o. Thus

$$(R - D)_{x_o} = (D)_{x_o}$$

or

$$\left(\frac{D}{R}\right)_{x_o} = \left[\frac{1}{r^2}\,\frac{(1-r\alpha_e)}{1-\alpha_e}\right]_{x_o} = \frac{1}{2} \quad . \tag{26}$$

Hence Eq. 24, which defines x_o, may be rewritten as

$$-\left(\frac{d\alpha}{dt}\right)_{x_o} = (D)_{x_o} = \left(\frac{R}{2}\right)_{x_o} . \tag{27}$$

Hence, again assuming that near equilibrium flow is maintained to $x = x_o$, with sudden freezing at x_o, we find

$$-\left(\frac{d\alpha_e}{dt}\right)_{x_o} \simeq \left(\frac{R_e}{2}\right)_{x_o} . \tag{28}$$

Equation 28 is a modified version of Bray's criterion.

Equation 26 may be used to obtain the value of r at x_o, viz.,

$$(r)_{x_o} = \left(\frac{\alpha_e}{1-\alpha_e}\right)\left[\left(1 + \frac{2(1-\alpha_e)}{\alpha_e^2}\right)^{1/2} - 1\right] \quad . \tag{29}$$

Reference to Eq. 29 leads to the conclusion that r at $x = x_o$ is not equal to unity but actually depends on the value of α_e at x_o. The assumption of equilibrium flow up to x_o, sudden freezing at x_o, and frozen flow downstream of x_o necessarily implies a jump in r at x_o. Indeed, the definition of x_o at the position where

$$-\frac{d\alpha}{dt} = D = \frac{R}{2}$$

obviously precludes the possibility that D = R up to x_o except in the case where D is not a continuous function of x.

It is clear that what is required here is an honest perturbation calculation that is substantially equivalent to the precise solution of the problem.

The important quantities appearing in the complete expression for $-d\alpha/dt$ given in Eq. 21 are plotted in the schematic diagram shown in Fig. 2. In an actual experiment, r does not remain equal to unity to $x = x_o$ and, therefore, the curve for R_e may lie anywhere between R and D. From the definitions of R and r given in Eqs. 18 and 20 and from the value of $(D/R)_{x_o}$ given in Eq. 26, it follows that

$$\left(\frac{R-R_e}{R-D}\right)_{x_o} = \left(\frac{1-R_e/R}{1-D/R}\right)_{x_o} = 2\left[1 - \frac{1}{(r^2)_{x_o}}\right] \tag{30}$$

from which it can be seen that the position of R_e, with respect to R and D, at $x = x_o$ depends on the value of $(\alpha_e)_{x_o}$ through the dependence of $(r)_{x_o}$ on $(\alpha_e)_{x_o}$ given in Eq. 29. We may estimate the value of $(\alpha_e)_{x_o}$ required to locate R_e midway between $(D)_{x_o}$ and $(R)_{x_o}$. Thus we use the relation

$$\left(\frac{R-R_e}{R-D}\right)_{x_o} = \frac{1}{2}$$

as well as Eq. 29 to find the results

$$\frac{1}{(r^2)_{x_o}} = \left(\frac{R_e}{R}\right)_{x_o} = \frac{3}{4}$$

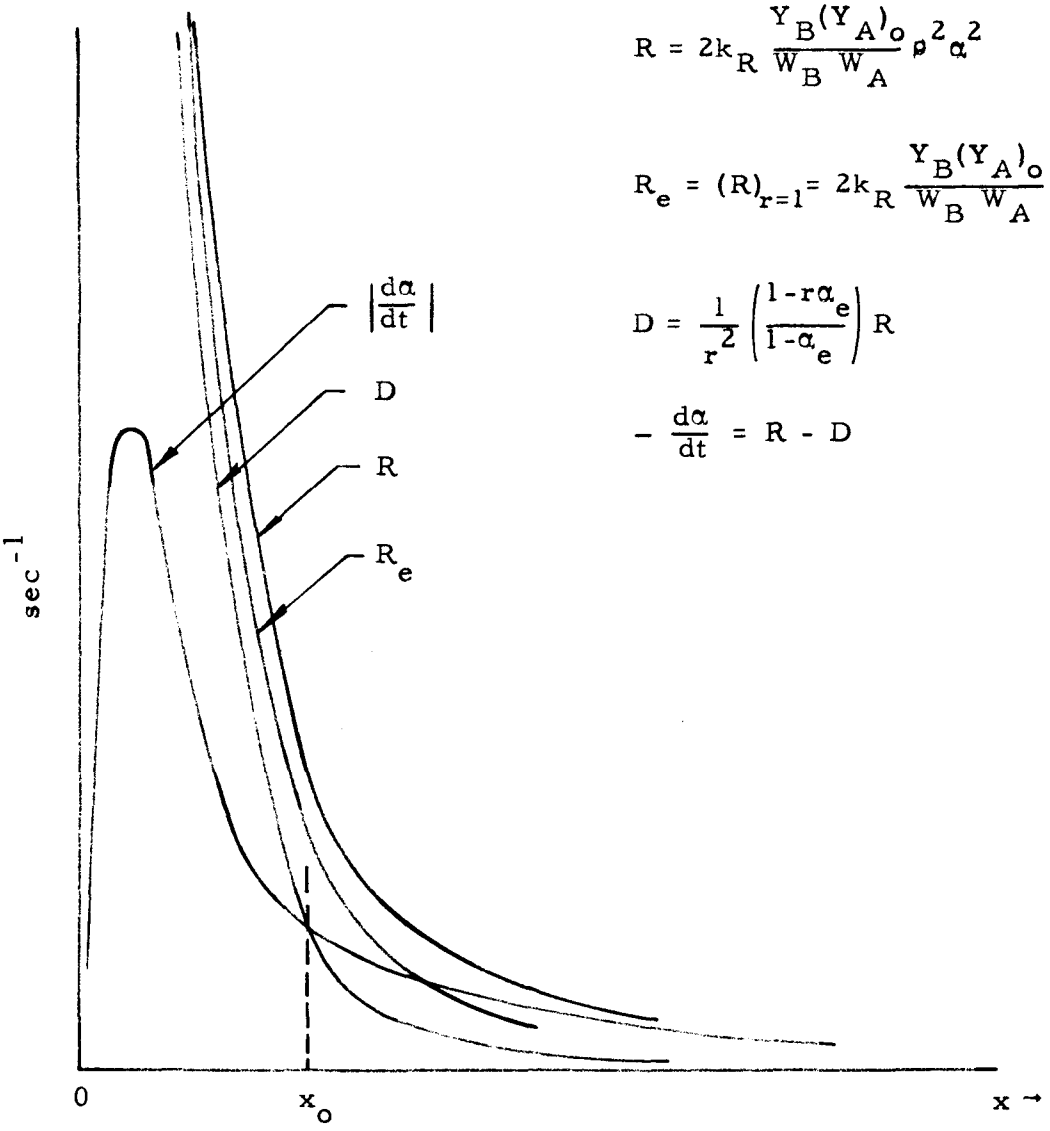

Fig. 2. Schematic diagram showing the rate terms in equation $- \frac{d\alpha}{dt} = R - D$ as a function of distance measured along nozzle centerline.

and

$$(a_e)_{x_o} = 0.68.$$

The preceding results may be summarized by the statement that for $(a_e)_{x_o} = 0.68$, $(r^2)_{x_o} = 4/3$ and R_e lies halfway between R and D at x_o. From Eqs. 29 and 30 it may now be seen that, for $(a_e)_{x_o} > 0.68$, $(R_e)_{x_o}$ lies relatively closer to $(R)_{x_o}$ whereas, for $(a_e)_{x_o} < 0.68$, $(R_e)_{x_o}$ lies relatively closer to $(D)_{x_o}$.

C. Comparison Between Bray's Modified Criterion and Penner's Near-Equilibrium Criterion

Since

$$-\left(\frac{da_e}{dt}\right) = -\left(\frac{\partial \ln a_e}{\partial \ln T}\right)_S a_e \left(\frac{d\ln T}{dt}\right)$$

it follows that the modified criterion of Bray given in Eq. (25b) may be written in the form

$$K = \left[\frac{a_e}{R_e}\left(\frac{d\ln T}{dt}\right)\left(-\frac{\partial \ln a_e}{\partial \ln T}\right)_S\right]_{x_o} \tag{31}$$

where the subscript S identifies isentropic flow. Barrère has noted that the right-hand side of Eq. 31 is essentially Damköhler's first similarity group D_I (cf. ref. 2, Chapter XXV) and that we may regard it as the ratio of a chemical time

$$(\tau_{ch})_B = \frac{a_e}{R_e}\left(-\frac{\partial \ln a_e}{\partial \ln T}\right)_S$$

to a convection time

$$(\tau_{mech}) = \frac{dt}{d\ell nT} \quad .$$

This observation is of considerable value since we expect, on the basis of very general principles for reacting flow systems, that large deviations from equilibrium flow will occur for a specified value of this important similarity group.

Penner's approximate criterion for near-equilibrium flow is [cf. ref. 2, Eq. (9) on p. 299]

$$\frac{T'-T}{T} \simeq -z\left(\frac{d\ell nT}{dt}\right) \tag{32}$$

where [cf. ref. 2, Eq. (7) on p. 299]

$$\frac{T'-T}{T} = \frac{K-K_e}{K_e}\left(\frac{\partial \ell nT}{\partial \ell nK_e}\right)_S \tag{33}$$

and K and K_e have been defined in Eq. 19. The quantity z is a reaction time which becomes, for the chemical process described in Eq. 15 [cf. ref. 2, Eq. (10) on p. 300],

$$z = \left(\frac{1}{k_R(B)(A)^2\left[(A_2)^{-1} + 4(A)^{-1}\right]}\right)_e$$

where molar concentrations (B), (A), and (A_2) are used. In terms of the quantities α and R defined in Eqs. 17 and 18, respectively,

$$z = \left[\frac{1}{R\left(\frac{1}{1-\alpha} + \frac{2}{\alpha}\right)}\right]_e . \tag{34}$$

It is apparent that $(T'-T)/T$ again represents a form of Damköhler's first similarity group.

When the near-equilibrium criterion was first developed in 1947, there were no experimental data available that could be used to ascertain the magnitude of the term $(T'-T)/T$ required for significant deviations from near-equilibrium flow. Today this identification can be performed in a meaningful manner by utilizing Wegener's results.[15] The utility of this approach has already been demonstrated (Wegener 1960, Barrère 1961). The only quantity that must be changed is the absolute value of $(T'-T)/T$, which was originally chosen for very conservative estimates to assure near-equilibrium flow. Thus we may assume that T' has the magnitude corresponding to a mass fraction Y_A which has deviated from the local equilibrium mass function $(Y_A)_e$ such that

$$r = \frac{Y_A}{(Y_A)_e}$$

at the point in the flow where effective freezing occurs. If we now define $(T'-T)/T$ at the point x_o where Eq. 26 applies, then Bray's modified criterion and Penner's near equilibrium criterion should yield identical results. Substituting

$$\left(\frac{K-K_e}{K_e}\right) = -\frac{1}{2}$$

into Eq. 33 for $(T'-T)/T$ yields

$$\frac{T'-T}{T} = -\frac{1}{2}\left(\frac{\partial \ell n T}{\partial \ell n K_e}\right)_S \qquad (35)$$

at the point where significant departure from near-equilibrium flow occurs. But

$$\ell n K_e = \ell n K_p - \Delta n \, \ell n p + \Delta n \, \ell n \bar{W} - \sum_{j=1}^{n} (\nu_j' - \nu_j'') \, \ell n \, W_j$$

for the chemical process

$$\sum_{j=1}^{n} \nu_j' \, M_j \rightleftharpoons \sum_{j=1}^{n} \nu_j'' \, M_j$$

if

$$\Delta n = \sum_{j=1}^{n} (\nu_j'' - \nu_j') \, ;$$

also

$$\ell n \, K_p = - \frac{\Delta H^\circ}{RT} + \frac{\Delta S^\circ}{R} \quad .$$

Here K_p is the equilibrium constant expressed in terms of pressure ratios, ΔH° is the standard molar heat of reaction, ΔS° is the standard molar entropy change, $\bar{W}$ represents the average molecular weight of the gas mixture, and W_j is the molecular weight of species j. For Hugoniot experiments, $\Delta n = -1$ and $\bar{W}$ is effectively constant. Hence it follows that

$$\left(\frac{\partial \ell n K_e}{\partial \ell n T}\right)_S \simeq \left(\frac{\partial \ell n K_p}{\partial \ell n T}\right)_S + \left(\frac{\partial \ell n p}{\partial \ell n T}\right)_S \simeq \frac{-1}{T}\left[\frac{\partial \ell n K_p}{\partial (1/T)}\right]_S + \frac{\bar{\gamma}}{\bar{\gamma} - 1} \simeq \frac{\Delta H^\circ}{RT} + \frac{\bar{\gamma}}{\bar{\gamma} - 1}$$

where $\bar{\gamma}$ is an effective value of γ. Thus Eq. 35 becomes

$$\left(T'-T\right) \simeq \frac{-T/2}{(\Delta H^{o}/RT) + \bar{\gamma}/(\bar{\gamma}-1)} \quad .$$

For Wegener's experiments,[15] $\Delta H^{o} \simeq -13,000$ cal/mole, $\bar{\gamma} \simeq 1.3$, and $T \simeq 300^{o}K$ whence it follows that $T'-T \simeq 9^{o}K$. This value is in good accord with the observed experimental results (cf. Wegener, ref. 15, Fig. 5).

III. INFLUENCE OF SURFACE-CATALYZED PROCESSES ON ATOMIC RECOMBINATION RATES IN ROCKET NOZZLES[16]

A. Introduction

In two-phase nozzle flow processes, it is of interest to consider the relative importance of a three-body gas-phase recombination reaction and a succession of heterogeneous two-body reactions.

We consider a uniform mixture of gaseous hydrogen and small liquid or solid particles. We will show that, for the particle concentrations actually encountered in some rocket nozzles, the rate of heterogeneous two-body reactions may be equal to or larger than the rate of the three-body gas-phase recombination reaction. It is therefore clearly important to consider such heterogeneous two-body recombination reactions in quantitative rocket performance evaluation.

The following considerations are also of interest in connection with the development of experimental procedures for improving the performance of nuclear rockets using hydrogen as driving fluid. Finally, they may be modified to infer conditions under which the flow processes in hypersonic, air-breathing engines can be influenced by

induced, heterogeneous chemical reactions.

B. Outline of Theoretical Considerations

The two assumed reaction paths for the recombination of hydrogen atoms are:

$$2H + X \xrightarrow{k_3} H_2 + X \tag{36}$$

and

$$H + Y \xrightarrow{k_{2a}} H\text{---}Y , \tag{37a}$$

$$H + H\text{---}Y \xrightarrow{k_{2b}} H_2 + Y . \tag{37b}$$

The quantities k_3, k_{2a}, k_{2b} denote appropriate specific reaction rate coefficients, X represents either H or H_2, Y is a small solid or liquid particle, and H---Y denotes a hydrogen atom adsorbed on the surface of Y.

According to Eqs. 36, 37a and 37b, the rate of disappearance of hydrogen atoms by three body processes is

$$-\left[\frac{d(H)}{dt}\right]_3 = 2k_3(H)^2(X)$$

or

$$-\left[\frac{dn_H}{dt}\right]_3 = \frac{2k_3}{N^2} n_H^2 n_X \tag{38}$$

where n_X denotes the number of particles of species X per unit volume; the rate of disappearance of hydrogen atoms by two-body processes is

$$-\left[\frac{d(H)}{dt}\right]_2 = k_{2a}(H)(Y) + k_{2b}(H)(H\text{---}Y)$$

or

$$-\left[\frac{dn_H}{dt}\right]_2 = \frac{1}{N}\left(k_{2a} n_H n_Y + k_{2b} n_H n_{H---Y}\right). \tag{39}$$

Hence the ratio

$$R \equiv \frac{-(dn_H/dt)_2}{-(dn_H/dt)_3} = \frac{N(k_{2a} n_H n_Y + k_{2b} n_H n_{H---Y})}{2k_3 n_H^2 n_X} \tag{40}$$

is a measure of the relative importance of heterogeneous two-body to three-body processes in the removal of hydrogen atoms.

We shall now estimate this ratio in terms of $(n_Y + n_{H---Y})/n_H$. Observations by various investigators have shown conclusively that the three-body recombination process occurs without appreciable activation energy.[17] We denote by α the fractional number of collisions that lead to adsorption in reaction 37a and by β the fractional number of collisions leading to H_2 formation in reaction 37b.

For a mixture of gases containing rigid, elastic-sphere molecules of different sizes and concentrations, the total number of collisions of molecules of type 1 with molecules of type 2 in unit volume in unit time is[18]

$$Z_{1,2} = 2n_1 n_2 \sigma_{1,2}^2 \sqrt{2\pi kT\left(\frac{1}{m_1} + \frac{1}{m_2}\right)} \tag{41}$$

if $\sigma_{12} = \frac{1}{2}(\sigma_1 + \sigma_2)$ represents the collision diameter, and σ_1 and σ_2 are the diameters of the separate species. Hence

$$-\left[\frac{dn_H}{dt}\right]_2 = \alpha Z_{H,Y} + \beta Z_{H,H---Y} \tag{42}$$

and

$$-\left[\frac{dn_H}{dt}\right]_2 = 2\alpha n_H n_Y \sigma^2_{H,Y}\sqrt{2\pi kT\left(\frac{1}{m_H}+\frac{1}{m_Y}\right)} + 2\beta n_H n_{H---Y}\sigma^2_{H,H---Y}\sqrt{2\pi kT\left(\frac{1}{m_H}+\frac{1}{m_{H---Y}}\right)}. \quad (43)$$

For the case where $m_Y \gg m_H$, $m_{H---Y} \gg m_H$, and $\sigma_Y \simeq \sigma_{H---Y} \gg \sigma_H$, we obtain

$$-\left[\frac{dn_H}{dt}\right]_2 \simeq \sqrt{\frac{2\pi kT}{m_H}}\ \frac{n_H}{2}\ \sigma_Y^2(\alpha n_Y + \beta n_{H---Y}). \quad (44)$$

If the concentrations (H), (Y), and (H---Y) are small compared with (H_2), then $n_X \simeq n_{H_2}$ and we obtain for R from Eqs. 38, 40 and 44 the result

$$R = \sqrt{\frac{2\pi kT}{m_H}}\ \frac{N^2\sigma_Y^2}{4k_3 n_{H_2}}\left(\frac{\alpha n_Y + \beta n_{H---Y}}{n_H}\right). \quad (45)$$

C. Numerical Estimates and Conclusions

The ratio R has been calculated from Eq. 45 for the following numerical values: $T = 1365^\circ K$, pressure = 5 atmos, $\sigma_Y = 3 \times 10^{-6}$ cm, $\sigma_H = 3 \times 10^{-8}$ cm, and[19] $k_3 = 3 \times 10^{15}$ mole^{-2}-(cm^3)^2-sec^{-1}. We find that

$$R \simeq (5 \times 10^6)\left(\frac{\alpha n_Y + \beta n_{H---Y}}{n_H}\right).$$

Therefore, the heterogeneous two-body processes will become of comparable importance with the three-body gas-phase collisions if

$$\frac{\alpha n_Y + \beta n_{H---Y}}{n_H} \gtrsim 2 \times 10^{-7}$$

or

$$\frac{n_Y + n_{H---Y}}{n_H} \gtrsim 2 \times 10^{-6}$$

for $\alpha \sim \beta \sim \frac{1}{10}$. But, for a representative propellant system in two-phase nozzle flow, $(n_{H_2}) \simeq 10^{20}$ cm^{-3}, $(n_H) \simeq 10^{18}$ cm^{-3}, and $\left[(n_Y) + (n_{H---Y})\right] \simeq 10^{12}$ to 10^{15} cm^{-3}. Hence $(n_Y + n_{H---Y})/n_H \simeq 10^{-6}$ to 10^{-3}, i. e., the heterogeneous recombination processes may actually become dominant.

The product $\alpha\beta$ appears to be of the order of 10^{-2} for the conditions existing in representative rocket nozzles.[20, 21]

REFERENCES FOR PART I

1. M. J. Lighthill, J. Fluid Mech. 2, 1 (1957).

2. S. S. Penner, Chemistry Problems in Jet Propulsion, Pergamon Press, Ltd., London 1957.

3. N. C. Freeman, J. Fluid Mech. 4, 407 (1958).

4. K. N. C. Bray, Aeronautical Research Council, London, Report 19, 983, March 1958.

5. S. S. Penner and D. Altman, J. Franklin Inst. 245, 421 (1948); D. Altman and S. S. Penner, J. Chem. Phys. 17, 56 (1949).

6. S. S. Penner, J. Am. Chem. Soc. 71, 788 (1949); J. Franklin Inst. 249, 441 (1950); J. Chem. Phys. 19, 877 (1951); 20, 341 (1952).

7. K. Schäfer, "On the Thermodynamics of Rocket Propulsion, I", Wright-Patterson Air Force Base, Dayton, Ohio, February 1947.

8. F. J. Krieger, J. Amer. Rocket Soc. 21, 179 (1952).

9. R. Reichenbach and S. S. Penner, Eighth International Combustion Symposium, pp. 359-366, Williams and Wilkins Co., Baltimore 1962.

10. K. N. C. Bray, J. Fluid Mech. 6, 1 (1959); Fourth AGARD Combustion and Propulsion Colloquium, pp. 279-285, Pergamon Press, Ltd., London 1961.

11. M. Rudin, Phys. Fluids 1, 384 (1958).

12. J. C. Hall and A. L. Russo, Cornell Aeronautical Lab., Inc., AFOSR TN-59-1090, Buffalo, New York, November 1959.

13. A. G. Eschenroeder, D. W. Boyer and J. C. Hall, "Exact Solutions for Nonequilibrium Expansions of Air with Coupled Chemical Reactions", Report No. AF-1413-A-1, Contract No. AF 49(638)-792, Cornell Aeronautical Laboratory, Inc., Buffalo 21, New York, May 1961.

14. M. Barrère, Fourth AGARD Combustion and Propulsion Colloquium, pp. 261-277, Pergamon Press, Ltd., London 1961.

15. P. P. Wegener, Phys. of Fluids 2, 264 (1959); ARS Journal 30, 322 (1960); Fourth AGARD Combustion and Propulsion Colloquium, pp. 261-277, Pergamon Press, Ltd., London 1961.

16. S. S. Penner and J. W. Porter, Astronautica Acta 8, 240 (1962).

17. W. Steiner, Trans. Faraday Soc. 31, 623 (1935); I Amdur and A. L. Robinson, J. Am. Chem. Soc. 55, 1395 (1933).

18. J. Jeans, Kinetic Theory of Gases, p. 137, Cambridge University Press, London 1940.

19. W. C. Gardiner, Jr., and G. B. Kistiakowsky, J. Chem. Phys. 35, 1765 (1961).

20. D. S. Hacker, S. A. Marshall and M. Steinberg, J. Chem. Phys. 35, 1788 (1961).

21. E. J. Wood and H. Wise, Rarefied Gas Dynamics, pp. 51-59, edited by L. Talbot, Academic Press, Inc., New York 1961.

PART II. GAS DISCHARGE RATES THROUGH DE LAVAL NOZZLES AND THE EXPERIMENTAL DETERMINATION OF DESORPTION RATES

I. INTRODUCTION

Successful measurements of chemical reaction rates during nozzle flow have been performed[1] for the mixture $2NO_2 \rightleftharpoons N_2O_4$ by using a large-scale apparatus. Cruder data have been obtained, by a number of investigators, on rocket engines of various sizes. In order to utilize the full potential of this technique for studying the interplay between chemical reaction rates and subsonic or supersonic flow, it is clearly desirable to develop a small-scale laboratory apparatus which can be constructed at low cost. Unfortunately, the use of a small, closed vessel as gas source reduces the (pseudo-) steady flow conditions to very short periods of time, thereby leading to the requirement that kinetic studies be performed with very high time resolution. As a first step for increasing the testing time, we have studied experimentally the discharge rates of He, Ar, and CO_2 through a de Laval nozzle from a small, closed reaction vessel containing sand or silica gel beads. The results and an approximate interpretation for the measurements are described in the following sections.

The experimental technique developed by us appears to be useful for the empirical determination of desorption rates from porous solid particles under isothermal conditions (see Appendix A for justification of the assumed isothermal conditions) during the initial stages of desorption. The dependence on temperature of the rates of desorption

of Ar, He, and CO_2 from silica gel has been investigated. A theoretical expression has been developed for the rate of desorption of gas from a porous solid under our experimental conditions (see Appendix B). Study of the data derived from the decay of chamber pressure with time indicates that the assumed model for desorption from porous spheres yields reasonable results for the heats of desorption of He, Ar, and CO_2 from silica gel.

II. OUTLINE OF THEORETICAL CONSIDERATIONS

A. Derivation of Equations for the Chamber Pressure as a Function of Time for Systems Without Mass Addition

Consider adiabatic expansion of a perfect gas, characterized by a constant value of γ, from a closed container through a de Laval nozzle. The equation for conservation of mass in the container is

$$-\frac{d(\rho V)}{dt} = \rho_t v_t A_t \qquad (1)$$

where V denotes the constant chamber volume, $\rho_t = p_t/R_g T_t$ is the gas density at the nozzle throat if R_g denotes the gas constant per unit mass, $T_t = \left[2/(\gamma+1)\right] T$ represents the temperature at the nozzle throat when the chamber temperature is T, $p_t = \left[2/(\gamma+1)\right]^{\gamma/(\gamma-1)} p$ represents the pressure at the nozzle throat when the chamber pressure is p, and $v_t = \sqrt{\gamma R_g T_t}$. Hence Eq. 1 may be written in the form

$$-\frac{d}{dt}\left[\left(\frac{p}{p_o}\right)\left(\frac{T_o}{T}\right)\right] = \frac{p}{p_o}\sqrt{\frac{T_o}{T}}\,\frac{A_t\sqrt{\gamma R_g T_o}}{V}\left(\frac{2}{\gamma+1}\right)^{(\gamma+1)/2(\gamma-1)} \qquad (2)$$

where the subscript o identifies initial conditions in the chamber.

1. Isothermal Expansion in Chamber

For isothermal gases in a closed chamber, the integral of Eq. 2 becomes

$$\frac{p}{p_o} = \exp\left(-\frac{t}{t^*}\right) \qquad \text{for } T = T_o, \tag{3}$$

where

$$t^* = \left(V/A_t\sqrt{\gamma R_g T_o}\right)(1/\Gamma) = m_o/\dot{m}_o \tag{4}$$

and

$$\Gamma = \left(\frac{2}{\gamma+1}\right)^{(\gamma+1)/2(\gamma-1)} \simeq \frac{0.1047}{\gamma} + 0.5048. \tag{5}$$

Here t^* represents a characteristic time involving chamber and nozzle parameters, $m_o = \rho_o V$ is the initial mass of gas in the chamber, and $\dot{m}_o = \rho_o A_t \sqrt{\gamma R_g T_o}\,\Gamma$ represents the initial mass flow rate of gas through the nozzle.

2. Adiabatic Equations with Modified Values of γ

For adiabatic expansion in the chamber,

$$\frac{T}{T_o} = \left(\frac{p}{p_o}\right)^{(\gamma_c-1)/\gamma_c}$$

where we use the symbol γ_c to denote an effective constant value of the specific heat ratio in the chamber. The differential equation becomes now

$$-\frac{d}{dt}\left[\left(\frac{p}{p_o}\right)^{1/\gamma_c}\right] = \left(\frac{p}{p_o}\right)^{(\gamma_c+1)/2\gamma_c}\frac{1}{t^*}$$

and we obtain, after integration between the limits $p/p_o = 1$ at $t = 0$ and p/p_o at t, the result

$$\left(\frac{p}{p_o}\right)^{(1-\gamma_c)/2\gamma_c} = 1 + \left(\frac{\gamma_c - 1}{2}\right)\frac{t}{t^*} \quad . \tag{6}$$

In the limit, as the gas-bead system in the chamber assumes an infinite specific heat, γ_c approaches unity and, therefore,

$$\lim_{\gamma_c \to 1}\left[\frac{\left(\frac{p}{p_o}\right)^{(1-\gamma_c)/2\gamma_c} - 1}{(\gamma_c - 1)/2}\right] = -\ln\frac{p}{p_o} \quad .$$

Thus, Eq. 6 reduces now to the isothermal case described by Eq. 3.

In comparing the theoretical formulas with experimental data, it is reasonable to treat γ_c as a variable parameter that is adjusted in order to fit the experimental data. In this manner, we may use the proximity of γ_c to unity as an indication of the efficiency with which heat is transferred from the beads to the gases.

It should be noted that the statements $T = T_o$ and $(p/p_o) = (T/T_o)^{\gamma_c/(\gamma_c-1)}$ constitute effectively two different energy conservation assumptions, both of which correspond to unobservable limiting cases. The isothermal limit ($T=T_o$) will constitute a fair approximation if the heat transfer rates from the solids to the gases are very high. The

adiabatic limit for unmodified γ, on the other hand, represents a reasonable approximation if the discharge rates are fast compared with the heat transfer rates.

B. Derivation of Chamber Pressure as a Function of Time for Limiting Cases Involving Heat and Mass Transfer From the Beads to the Gas

For strongly adsorbed gases, mass addition by desorption (rather than heat transfer) will dominate the observed pressure-time behavior. This limiting condition should obtain when the rate of decay of chamber pressure with time for chambers filled with beads is appreciably slower than the rate of decay for the case of discharge of gases from an isothermal chamber.

1. Mass Addition Under Isothermal Conditions in the Chamber

As a first step in interpreting the experimental results, we assume that the desorption rates are constant and independent of the instantaneous value of the chamber pressure. We may obtain some insight into the physical conditions under which this assumed desorption model applies by noting that desorption rates from highly porous materials (e.g., silica gel beads) should be controlled by diffusion processes.[2, 3]

If the average pore radius is small compared to the mean free path of the gas molecules but large compared to the dimensions of a molecule, the flow of gas in the pores will occur by Knudsen diffusion.

The average pore radius for silica gel satisfies this condition (see Appendix B for details). A concentration gradient in the gas phase within the pores produces a concentration gradient in the adsorbed phase on the pore walls, i. e., the flow of gas in a porous solid such as silica gel occurs by diffusion in the gas phase and by surface diffusion in the adsorbed phase. Of course, only molecules possessing sufficient energy to separate from the local adsorption sites will be able to migrate over the surface. The activation energy required for surface diffusion is equal to or smaller than the heat of adsorption (for details, see, for example, ref. 4, Fig. 12 on p. 54).

The solution of the diffusion problem involves the external density, $\rho(t)$, as a boundary condition. We have used for this density the expression for an isothermal system with a constant rate of mass addition. The density boundary condition has then been justified by showing that results derived from it are, approximately, consistent with the assumption of a constant rate of mass addition under isothermal conditions.

For a constant rate of mass addition, $\dot{m}_d$, Eq. 1 becomes

$$-\frac{d}{dt}(\rho V) = \rho_t v_t A_t - \dot{m}_d$$

or

$$-\frac{d}{dt}\left[\left(\frac{p}{p_o}\right)\left(\frac{T_o}{T}\right)\right] = \frac{p}{p_o}\left(\frac{T_o}{T}\right)^{1/2}\frac{1}{t^*} - \nu_o \qquad (7)$$

where $\nu_o = \dot{m}_d / m_o$ is a characteristic desorption frequency and V = free volume = (chamber volume - total apparent volume of beads). For

isothermal gases, Eq. 7 may be integrated directly with the result

$$\frac{\rho}{\rho_o} = \frac{p}{p_o} = \exp\left(-\frac{t}{t^*}\right) + b_o\left[1-\exp\left(-\frac{t}{t^*}\right)\right] \qquad \text{for } T = T_o \tag{8}$$

where $b_o = \nu_o t^*$ is a constant.

Using Eq. 8 as the boundary condition, the diffusion equation may be solved (see Appendix B for details) for the total rate of mass addition $\dot{m}_d$. The resulting expression for $\dot{m}_d$ is

$$\dot{m}_d = \frac{m_o}{t^*}\left[6\epsilon\left(\frac{1-f}{f}\right)\right](1-b_o)(1+A)\left(\frac{t^*}{t_d}\right)\sum_{n=1}^{\infty}\left\{\frac{\exp\left(-\frac{t}{t^*}\right) - \exp\left[-n^2\pi^2\left(\frac{t^*}{t_d}\right)\left(\frac{t}{t^*}\right)\right]}{\left(n^2\pi^2\frac{t^*}{t_d} - 1\right)}\right\} \tag{9}$$

where $(1-f)/f$ is equal to $\rho_o m_b / \rho_b m_o$ if f is the fractional void in the bed, ρ_o is the initial density of gases in the chamber, ρ_b is the apparent density of the porous spheres = mass of beads/apparent volume of beads, m_b is the total mass of the beads, $m_o = \rho_o V$ is the initial mass of free gas in the chamber, ϵ is the porosity of the bead which is defined as the pore volume divided by the total volume of the bead, $t_d = a^2/D$ is a characteristic diffusion time, a is the radius of a single spherical bead, $D = (D_g + AD_a)/(1+A)$ is an effective diffusion coefficient, D_g and D_a are, respectively, the Knudsen diffusion coefficient and the apparent surface diffusion coefficient, and A is a function of the temperature. Since Eq. 8 fits the experimental results rather well (see Figs. 6 to 54), Eq. 9 should constitute an acceptable expression for $\dot{m}_d$ subject to the assumption of diffusion-controlled

desorption. It is apparent that Eq. 9 is consistent with the statements $\dot{m}_d = 0$ at $t = 0$ and the limit of $\dot{m}_d = 0$ as $t \to \infty$.

A graph of Eq. 9 is shown in Fig. 1 for representative values of the parameters. Reference to Fig. 1 indicates that, to a first approximation, $\dot{m}_d$ may indeed be treated as a constant for t greater than about $t^*/4$.

A second approximation to the pressure in the chamber is obtained by deleting the assumption that $\nu = \dot{m}_d / m_o$ is constant in Eq. 7 and by using instead the relation for $\dot{m}_d$ given by Eq. 9. In this case, Eq. 8 should be replaced by the expression

$$\frac{\rho}{\rho_o} = \frac{p}{p_o} =$$

$$\left[1 - 6\varepsilon \left(\frac{1-f}{f} \right) (1-b_o)(1+A) \left(\frac{t^*}{t_d} \right) \sum_{n=1}^{\infty} \left\{ \frac{1 - (n^2\pi^2 \frac{t^*}{t_d} - 1)\frac{t}{t^*} - \exp\left(-n^2\pi^2 \frac{t^*}{t_d} + 1 \right) \frac{t}{t^*}}{\left(n^2\pi^2 \frac{t^*}{t_d} - 1 \right)^2} \right\} \right]$$

$$\times \left[\exp\left(-\frac{t}{t^*} \right) \right]. \qquad (10)$$

Equation 10 is the first step in obtaining an improved solution to the problem. In the next laborious, though straightforward iteration, Eq. 10 serves as boundary condition in the derivation of an improved expression for $\dot{m}_d$ according to the procedure described in Appendix B.

2. Adiabatic Conditions and a Constant Rate of Mass Addition in the Chamber

For the case of adiabatic expansion in the chamber, Eq. 8 should be replaced by the expression

$$\int_1^{p/p_o} \frac{dx}{x^{(\gamma_c-1)/\gamma_c}\left[1-(1/\nu_o t^*)x^{(\gamma_c+1)/2\gamma_c}\right]} = \gamma_c \nu_o t \ .$$

The preceding relation may be integrated for $\gamma_c = 5/3$ with the result

$$\gamma_c \nu_o t = \left(\frac{5}{2}b^{3/4}\right) \times \left\{\frac{1}{2} \ln \left|\frac{1+x^{1/5}b_o^{-1/4}}{1-x^{1/5}b_o^{-1/4}}\right| \left|\frac{1-b_o^{-1/4}}{1+b_o^{-1/4}}\right| - \left[\tan^{-1}(x^{1/5}b_o^{-1/4})\right] + \left[\tan^{-1}(b_o^{-1/4})\right]\right\}$$

where $x=p/p_o$ and b_o is again equal to $\nu_o t^*$. There is no obvious experimental procedure for realizing near-adiabatic conditions with mass addition.

C. A More Complete Analysis of Gas Discharge Through a Nozzle From a Two-Phase System

Thus far we have derived applicable relations without proper consideration of the actual form of the energy equation in the two-phase system under discussion. For a more complete analysis, we must use all of the conservation equations and obtain a solution after imposition of suitable boundary conditions.

The equation for conservation of mass, using the ideal gas equation of state, has been given in Eq. 7 and may be rewritten in the form

$$\frac{d}{dt}\left(\frac{p}{p_o}\right) + \frac{p}{p_o}\frac{d}{dt}\ln\left(\frac{T_o}{T}\right) = \nu\left(\frac{T}{T_o}\right) - \frac{1}{t^*}\frac{p}{p_o}\sqrt{\frac{T}{T_o}} \qquad (11)$$

where ν is a function of pressure and temperature. An approximate expression for conservation of energy is (see Appendix C for details)

$$\frac{d}{dt}(mc_vT) = \dot{Q} + \dot{m}_d c_p T_d - \dot{m}_e c_p T \qquad (12)$$

where m represents the total mass of free gas in the chamber, c_v and c_p denote, respectively, the specific heats of the gas at constant volume and at constant pressure, $\dot{Q}$ is the total rate of energy addition to the gas by heat conduction and radiation, $\dot{m}_d$ is the rate of mass addition of free gas by desorption from the beads at the temperature T_d (we assume that the specific heat of the added gas is the same as that of the chamber gas), and $\dot{m}_e$ represents the mass discharge rate of gases through the nozzle.

Since

$$m = pV/R_gT ,$$

$$\dot{m}_e = \frac{m_o}{t^*}\frac{p}{p_o}\sqrt{\frac{T_o}{T}} ,$$

and

$$\dot{m}_d = \nu m_o ,$$

Eq. 12 may be rewritten as

$$\frac{d}{dt}\left(\frac{p}{p_o}\right) = \frac{\dot{Q}}{m_o c_v T_o} + \gamma_c \nu \frac{T_d}{T_o} - \frac{\gamma_c}{t^*}\frac{p}{p_o}\sqrt{\frac{T}{T_o}} . \qquad (13)$$

All of the results derived in the preceding sections may be obtained by starting from Eqs. 11 and 13.

For the isothermal case without mass addition ($T=T_o$, $\nu=0$), Eq. 11 yields

$$\frac{p}{p_o} = \exp\left(-\frac{t}{t^*}\right)$$

which was previously obtained in Eq. 3. In addition, Eq. 13 yields the rate at which heat must be added to the system to maintain T equal to T_o, viz.,

$$\frac{\dot{Q}}{m_o c_v T_o} = \frac{1}{t^*}\left(\gamma_c - 1\right) \exp\left(-\frac{t}{t^*}\right) . \tag{14}$$

For the case without heat or mass addition ($\dot{Q} = 0$, $\nu = 0$), Eqs. 11 and 13 give the following results:

$$\frac{T}{T_o} = \left[1 + \frac{\left(\gamma_c - 1\right)}{2} \frac{t}{t^*}\right]^{-2} \tag{15}$$

and

$$\frac{p}{p_o} = \left[1 + \frac{\left(\gamma_c - 1\right)}{2} \frac{t}{t^*}\right]^{2\gamma_c/(1-\gamma_c)} = \left(\frac{T}{T_o}\right)^{\gamma_c/(\gamma_c - 1)} . \tag{16}$$

The first equality in Eq. 16 was obtained previously in Eq. 6 for adiabatic expansion.

For the isothermal case with a constant rate of mass addition ($T = T_o$, $\nu = \nu_o$ = constant), Eq. 11 yields

$$\frac{p}{p_o} = \exp\left(-\frac{t}{t^*}\right) + \nu_o t^* \left[1 - \exp\left(-\frac{t}{t^*}\right)\right]$$

which was previously obtained in Eq. 8. Equation 13 may be used to obtain again the rate of heat addition necessary to maintain $T = T_d = T_o$. The result is

$$\frac{\dot{Q}}{m_o c_v T_o} = \frac{1}{t^*} (\gamma_c - 1)(1-b_o) \exp\left(-\frac{t}{t^*}\right) . \qquad (17)$$

In the general case where both heat and mass addition occur, it is necessary to specify both $\dot{Q}$ and $\dot{m}_d$ explicitly and then to solve the resulting coupled relations, viz., Eqs. 11 and 13. We shall not pursue this approach further since acceptable fits are obtained to the experimental data of pressure as a function of time on the assumption that isothermal conditions and a constant rate of mass addition prevail in the chamber.

III. EXPERIMENTAL PROCEDURE AND RESULTS

We shall now describe the experimental procedure for the determination of chamber pressure as a function of time, show how these measurements may be used to obtain desorption rates, and finally interpret the observed data in terms of the previously derived theoretical expressions.

A. Experimental Apparatus and Procedure

A schematic diagram of the apparatus is shown in Fig. 2. The apparatus consisted of a reaction vessel with a volume of 1110 cm^3 (1) which contained the gas and the solid particles, a de Laval nozzle (2) with a throat diameter of 4.4 mm, a rapidly-opening[5] valve (3), and a dump tank (4). The dump tank, the volume of which was ten times that of the reaction vessel, was evacuated to a pressure much lower

than the chamber pressure (the initial pressures in the dump tank and in the reaction vessel were about 0.5 mm of Hg and about 740 mm of Hg, respectively). The valve at the nozzle exit position opened in less than 10^{-3} sec, and pseudo-steady discharge of gas from the reaction vessel began in about one millisec. A Type 535 Tektronix oscilloscope (5), equipped with a Polaroid camera, was used to record the time dependence of the pressure as measured by a Consolidated Electrodynamic Corporation strain-gage pressure transducer (6) installed in the reaction vessel. The temperature of the contents of the reaction vessel was regulated by using either a heating mantle or an acetone-dry ice cooling bath (7). Five iron-constantan thermocouples were used to record the temperature of the gas in the reaction vessel. The top of the reaction vessel could be removed to allow introduction of solid particles. A 100-mesh screen (8) was located upstream of the de Laval nozzle to prevent solid particles from being blown into the nozzle. The reaction vessel was evacuated and filled with gas by means of a three-way stopcock (9). The gas was passed through a dry ice water-trap (10) before entering the reaction vessel.

For each gas (CO_2, Ar, and He), the chamber pressure was measured as a function of time for (a) initial temperatures ranging from -50°C to 120°C with the chamber filled with 6-16 mesh silica gel, (b) an initial temperature of about 22°C with the chamber filled with 12-mesh quartz sand, and (c) an initial temperature of about 22°C with the chamber empty. The same material, consisting of 696g of 6-16 mesh silica gel with an apparent density ρ_b=1.2 to 1.3 g/cm^3 and a

true density ρ = 2.2 g/cm^3 (Grade 42, the Davison Chemical Company) was used in all of the experiments performed under (a); in the experiments (b), the same sample of 1331g of 12-mesh quartz sand with a density of 2.6 g/cm^3 (Crystal Silica Company, Oceanside, California) was used.

The system containing silica gel was prepared for a series of experiments with each of the adsorbed gases by heating the reaction vessel and its contents to about 130°C, evacuating and flushing the system with the gas, and finally allowing the system to reach equilibrium at a pressure of about one atmosphere and at a temperature of about 120°C. The first measurement of pressure as a function of time was made at about 120°C, and succeeding measurements were made at successively reduced temperatures using intervals of 15°C to 20°C down to about -50°C.

The system with quartz sand was thoroughly evacuated and then flushed with each of the gases used before performing an experiment.

B. Experimental Determination of Desorption Rates

Since the calculations given in Appendix A, as well as the experimental measurements of chamber temperature, indicate that the free chamber gases are nearly isothermal for $t > 0$, Eq. 11 may be used with $T = T_o$ and $d(T/T_o)/dt = 0$ for the direct determination of $b = \dot{m}_d t^*/m_o = \nu t^*$. Thus b may be derived from the experimental data of pressure as a function of time by using the expression

$$b(\tau) = \frac{p}{p_o} + \frac{d}{d\tau}\left(\frac{p}{p_o}\right) \tag{18}$$

where $\tau = t/t^*$.

C. Experimental Results

The results of experimental measurements are plotted in Figs. 3 to 65. The data in Figs. 3, 4 and 5 refer to the pressure drop as a function of time during the discharge of CO_2, Ar, and He, respectively, from a vessel containing no solid adsorbent. The dashed curves were calculated from the theoretical equation for adiabatic expansion (Eq. 6) by using theoretical estimates for the applicable specific heat ratios. The values of γ_c were chosen to obtain the best fit of Eq. 6 to the experimental curves. The values of t^* were computed from Eq. 4 by using these values of γ_c. The values of γ_c and t^* are shown in the figures. Reference to Figs. 3, 4 and 5 shows that the theoretical estimates for γ_c apply very closely, at least during the initial phases of the experiments.

The results shown in Figs. 6 to 18 refer to the pressure drop during the discharge of CO_2 when the reaction vessel contained 6-16 mesh silica gel at various initial temperatures. Figures 19 to 44 and Figs. 45 to 54 contain similar data for Ar and for He, respectively. The results shown in Figs. 55 to 58 refer to the discharge of CO_2, Ar, and He, when the reaction vessel contained 12 mesh quartz sand at room temperature initially. The dashed curves in Figs. 6 to 57 represent computer-calculated, least-squares fits of Eq. 8 to the experimental curves; the values of b_o determined in this way are indicated in the figures. The dashed curve in Fig. 58 was calculated from the theoretical equation for an isothermal chamber without mass addition (Eq. 3). The values of t^* were computed according to Eq. 4

by using for γ the appropriate value for the gas as calculated at $T=T_o$. Tables I, II and III and Fig. 59 show b_o as a function of the initial temperature T_o for the CO_2-, Ar-, and He-silica gel systems. It is apparent that the empirically determined values of $b_o = \nu_o t^*$, together with the calculated values of t^*, provide an estimate for the characteristic desorption frequency ν_o. The value of the free chamber volume V used in Eq. 4 for the evaluation of t^* was determined by taking the difference between the volume of the reaction vessel and the volume of the beads. The volume of the beads includes the pore volume and corresponds to the ratio m_b/ρ_b where m_b is the total mass of the beads; the density ρ_b for silica gel was supplied by the manufacturer (i.e., the Davison Chemical Company), and ρ_b for the quartz sand was determined by the author experimentally using the water-displacement method.

Experimental curves of the dimensionless desorption rate $b=\dot{m}_d t^*/m_o$ as a function of the reduced time $\tau = t/t^*$ for the CO_2-, Ar-, and He-silica gel systems have been determined by using the procedure outlined in Section III-B, together with the experimental data shown in Figs. 6 to 54. The results may be represented by curves of b as a function τ for each gas for a given initial temperature. Representative experimental curves of the dimensionless desorption rates are shown in Fig. 60.

The theoretical equation (see Eq. 9) for $b(\tau)=\dot{m}_d t^*/m_o$ was fitted to each of the experimental curves of $b(\tau)$. The fit was accomplished by choosing suitable values of the parameter $a = t^*/t_d$

and of the factor $\left[6\epsilon\,(1-f)/f\right](1-b_o)(1+A)$. For Ar and He, the theoretical curves of $b(\tau)$ fit the experimental curves very closely for all τ, and both a and $\left[6\epsilon\,(1-f)/f\right](1-b_o)(1+A)$ were, therefore, determined as functions of the temperature. Figures 61 and 62 show theoretical curves of $b(\tau)$ fitted to representative experimental curves for Ar and He, respectively.

For CO_2, the experimental curves were best fitted by using the limiting form of Eq. 9 for small a (see Appendix B, Eq. B-21). However, the fits were not very good, particularly at the lower temperatures. Furthermore, only the product $\left[6\epsilon\,(1-f)/f\right](1-b_o)(1+A)\sqrt{a}$ could be determined. Figure 63 shows the theoretical curves of $b(\tau)$ fitted to representative experimental curves of $b(\tau)$ for CO_2.

The dependence of b_o on temperature for the He-, Ar-, and CO_2-silica gel systems is given in Tables I, II, and III, respectively, and in Fig. 59, and the factor $6\epsilon\,(1-f)/f$ is a known constant equal to 2.6 (calculated using apparent density $\rho_b = 1.25$ g/cm^3, true density $\rho = 2.2$ g/cm^3, total mass of the beads $m_b = 696$g, and chamber volume $V = 1110$ cm^3) which was the same for all of the experiments; hence, for He and Ar, it was possible to determine a and A as functions of temperature (see Tables I and II), but, for CO_2, only the product $\sqrt{a}(1+A)$ was determined as a function of temperature (see Table III).

D. Interpretation of Experimental Results in Terms of Theoretical Equations

The deviations of the experimentally determined curves of pressure as a function of time, for the discharge of Ar and He from a

vessel containing no solid adsorbent, from the theoretical equation for adiabatic expansion (see Figs. 4 and 5) are probably due to heat transfer from the walls of the vessel to the gas as the gas cooled. Initially, the expansion was very nearly adiabatic, but heat transfer began to affect the chamber pressure for τ greater than about 0.6. The corresponding experimental curve for CO_2 (see Fig. 3) suggests that the influence of heat transfer was offset by an increase in γ during the discharge (heat transfer tended to increase the pressure whereas cooling tended to increase γ). As the result of fortuitous compensation, a very close fit was obtained to the theoretical equation for adiabatic expansion.

The results shown in Fig. 58 refer to the discharge of CO_2, Ar, and He when the reaction vessel contained 12-mesh quartz sand. The broken curve represents the theoretical equation for an isothermal system without mass addition. The relatively small differences between the experimental curves for the different gases indicate that very little mass addition by desorption occurred during the experiments. Furthermore, the close agreement of the experimental curves with the theoretical curve for isothermal gases indicates that nearly isothermal conditions existed in the chamber during the discharge. The results for sand are thus seen to be very different from those obtained with silica gel where strong adsorption and mass addition during discharge dominated the observed pressure-time behavior (compare Figs. 10, 28 and 50).

Figure 60 shows representative experimental curves of the dimensionless desorption rate b as a function of the reduced time

$\tau = t/t^*$. As is to be expected, the reduced desorption rates increase rapidly as the temperatures are reduced because larger amounts of gas are initially adsorbed at lower temperatures.

The values of a and $\underline{A}$ obtained by fitting the theoretical equation for the dimensionless desorption rate $b(\tau)$ to the experimental curves of $b(\tau)$ for He are shown in Table I. Earlier experiments by other investigators indicate that He is not measurably adsorbed (i.e., $A \simeq 0$) except at very low temperatures.[6, 7] For $A = 0$, the quantity

$$a \equiv \frac{t^*(D_g + AD_a)}{a^2(1+A)} \tag{19}$$

becomes

$$a = \frac{t^* D_g}{a^2} \tag{20}$$

which is independent of the temperature since $t^* \propto 1/\sqrt{T}$ and $D_g \propto \sqrt{T}$. Our experimental values for a and $\underline{A}$ for He agree with these findings within the limits of experimental error. The percentage error in the quantity $(1+A)$ for He is estimated to be about $\pm$ 15%.

The experimental values of a and $(1+A)$ were used in Eq. 19 to obtain the quantity $(D_g + AD_a)$. Theoretical values of the Knudsen diffusion coefficient $(D_g)_{theor}$ (see Appendix B) were calculated for each experiment. Both $(D_g + AD_a)$ and $(D_g)_{theor}$ are presented in Table I. Within the limits of experimental error, we obtained the result

$$(D_g + AD_a) \simeq (D_g)_{theor} \quad .$$

The percentage error in the experimental value of $(D_g + AD_a)$ is at least as great as the ± 15% error in (1+A), and the percentage error in $(D_g)_{theor}$ is estimated to be about ± 25% (because of uncertainty in the value of the pore radius a_p).

The results for Ar listed in Table II indicate that both a and $\underline{A}$ are functions of the temperature. Assuming that $A \propto \exp(Q/RT)$, where Q is the molar heat of adsorption, a plot of $\ln A$ as a function of $1/T$ should yield a straight line with slope of Q/R, if Q is constant. The plot of $\ln A$ as a function of $1/T$ for Ar is shown in Fig. 64. The slope of the dashed line through these points yields $Q \simeq 4200$ cal/mole. In the literature, the value of the molar heat of adsorption for Ar on silica gel is stated to be about 3000 cal/mole.[8]

The quantity $(D_g + AD_a)$ for Ar was calculated by using Eq. 19 together with the experimental values of a and (1+A). In addition, theoretical values of the Knudsen diffusion coefficient $(D_g)_{theor}$ for Ar were calculated using for D_g the equation given in Appendix B. Both $(D_g + AD_a)$ and $(D_g)_{theor}$ are listed in Table II. The values of $(D_g + AD_a)$ begin to decrease rapidly, compared to $(D_g)_{theor}$, in the neighborhood of $T = 280^{\circ}K$. This change may possibly be explained by assuming that the porosity of the silica gel, $\mathcal{E}$, is effectively reduced because of the volume occupied by the adsorbed molecules. For example, the cross-sectional area of a pore with a radius of 20 Å is reduced by a factor of $(16/20)^2 = 0.64$ due to a single adsorbed layer of molecules with collision diameters approximately equal to 4 Å.

Since (1+A) is proportional to $1/\mathcal{E}$, $(D_g + AD_a)$ is also proportional to $1/\mathcal{E}$ (see Eq. 19). Therefore, a reduction in $\mathcal{E}$ as the temperature decreases (i. e., as the amount of adsorption increases) would result in larger values for $(D_g + AD_a)$ than those which were obtained in Table II by using a constant value of $\mathcal{E}$.

The percentage error in the quantity (1+A) for Ar is estimated to be about ± 5 to ± 10%. The percentage error in the experimental value of $(D_g + AD_a)$ is at least as great as the percentage error in the quantity (1+A), and again the uncertainty in $(D_g)_{theor}$ is estimated to be about ± 25%.

The results in Tables I and II indicate that as the temperatures are increased, the values of α and (1+A) for Ar approach the corresponding values of α and (1+A) for He. This is to be expected because (a) as the temperatures are increased, the amount of Ar initially adsorbed becomes very small (i. e., $A \to 0$), and (b) for $A \to 0$, α approaches the value $t^* D_g / a^2$ (see Eq. 20) which is independent of molecular weight and is, therefore, the same for gases with the same value of the ratio of specific heats γ (see Eq. 4 and the equation for D_g in Appendix B).

As was indicated in Section III-C, the product $\sqrt{\alpha}(1+A)$ was determined experimentally for CO_2. References 8 and 9 indicate that the value of $\underline{A}$ for CO_2 at 150°C is approximately the same as the value of $\underline{A}$ for Ar at -22°C; the experimental results for Ar in Table II show that $A \simeq 16$ at $T_o = -22°C$; hence, we may assume that $A \gg 1$ for CO_2 in the temperature range from -50°C to 120°C. Using Eq. 19, the

product $\sqrt{a}(1+A)$ may be written as

$$\sqrt{a}(1+A) = \left[\frac{t^*(1+A)(D_g + AD_a)}{a^2}\right]^{1/2}$$

or, for $A \gg 1$,

$$\sqrt{a}(1+A) \simeq \left[\frac{t^*A(D_g + AD_a)}{a^2}\right]^{1/2} . \tag{21}$$

Assuming that $D_g \ll AD_a$, Eq. 21 becomes

$$\sqrt{a}(1+A) \simeq A\left(\frac{t^*D_a}{a^2}\right)^{1/2} . \tag{22}$$

Substituting D_a = (constant) $\sqrt{T}\exp(-E/RT)$,[10] where E is the molar activation energy for surface diffusion, and A = (constant) $\exp(Q/RT)$ into Eq. 22 yields the following temperature dependence for $\sqrt{a}(1+A)$:

$$\sqrt{a}(1+A) \propto \exp\left[Q-(E/2)\right]/RT. \tag{23}$$

In this case, a graph of $ln\left[\sqrt{a}(1+A)\right]$ as a function of $1/T$ should yield a straight line with slope $\left[Q-(E/2)\right]/R$.

Assuming on the other hand, that $D_g \gg AD_a$, Eq. 21 reduces to

$$\sqrt{a}(1+A) \simeq \left(\frac{t^*AD_g}{a^2}\right)^{1/2} . \tag{24}$$

Again substituting A = (constant) $\exp(Q/RT)$ and using the proportionality $D_g \propto \sqrt{T}$ in Eq. 24, we find

$$\sqrt{a}(1+A) \propto \exp(Q/2RT). \tag{25}$$

In this case, a graph of $\ell n \left[\sqrt{a}\,(1+A)\right]$ as a function of 1/T should yield a straight line with slope Q/2R.

Figure 65 shows the experimental results for CO_2 plotted in the form of $\ell n \left[\sqrt{a}\,(1+A)\right]$ as a function of 1/T. A straight line with a slope of 1400°K may be drawn through the points for $T \gtrsim 300$°K. Hence Eq. (25) implies that

$$Q \simeq 5800 \text{ cal/mole} \qquad \text{for } D_g \gg AD_a \tag{26}$$

and, because E is necessarily smaller than Q, Eq. 23 implies that

$$Q \leq 5800 \text{ cal/mole} \qquad \text{for } D_g \ll AD_a. \tag{27}$$

The temperature dependence of the heat of adsorption of CO_2 on silica gel has been investigated by Kälberer and Schuster.[8] For pressures much smaller than one atmosphere, they obtained 7200 cal/mole at 0°C and 5370 cal/mole at 75°C -- a decrease of 1830 cal/mole for a temperature increase of 75°C. For pressures near 1/2 atmosphere, they obtained about 6300 cal/mole at 0°C and about 5600 cal/mole at 75°C -- a decrease of 700 cal/mole for a temperature increase of 75°C. In our experiments, the pressure varied from about 740 mm Hg to 100 mm Hg; hence, estimates for the heats of desorption based on literature data are about 6600 cal/mole for $T \simeq -40$°C and about 5100 cal/mole for $T \simeq 120$°C and are, therefore, in fair agreement with our experimentally determined results.

APPENDIX A

APPROXIMATE JUSTIFICATION OF THE ASSUMPTION THAT THE SILICA GEL-GAS SYSTEM REMAINS EFFECTIVELY ISOTHERMAL

Furnas[11] studied experimentally the heat transfer rates from a stream of heated gases to a bed of particles in a cylindrical pipe. The particles were initially at a uniform temperature T_o. The temperature of the gas at the pipe entrance was constant and equal to $T_1 > T_o$. The outside surface of the pipe was insulated; hence, as $t \to \infty$, the temperature of the entire bed approached T_1. The heat transfer coefficient determined under these conditions should approximate closely the heat transfer coefficient in our experiments. Furnas used experimental measurements of the temperature of the gas at the pipe exit, together with the theoretical results of Schumann,[12] to determine the dependence of the heat transfer coefficient per cm^3 of bed h (in $cal/cm^3\text{-}sec\text{-}^oC$) on velocity v (in cm/sec), temperature T (in ^oK), particle diameter d (in cm), and fractional void f of the bed. His expression for the heat transfer coefficient is

$$h = \frac{B(v/1000)^{0.7} T^{0.3} 10^{1.68f - 3.56f^2}}{d^{0.9}} \qquad (A\text{-}1)$$

where the velocity v refers to flow in the empty pipe and B is a constant which depends on the physical properties of the particles.

As a reasonable first approximation, we assume that the velocity v in our experiments varies linearly with the distance x from the bottom of

the reaction vessel, viz.,

$$v = v_\ell \frac{x}{\ell} \tag{A-2}$$

where v_ℓ is the velocity at $x = \ell$ = the length of the chamber. But

$$v_\ell = \frac{\dot{m}_\ell}{\rho_\ell A}$$

where ρ_ℓ and A are, respectively, the gas density and cross-sectional area of the reaction vessel and $\dot{m}_\ell$ is the mass flow rate at $x = \ell$. The heat transfer rate from the particles to the gas in the volume A dx at x is

$$d\dot{Q} = hA\Delta T\,dx \ \text{cal/sec} \tag{A-3}$$

where ΔT is taken to be the effective difference in the temperature between the bead surface and the surrounding gas $\left[\text{i.e., } \Delta T = T_d(a,t) - T\right]$. Combining Eqs. A-1, A-2, and A-3 and substituting the representative values A = 85 cm^2, ℓ = 13 cm, d = 0.24 cm, f = 0.5, $T_o = 300^\circ K$, B = 0.007,* v_ℓ = 32 cm/sec for Ar, v_ℓ = 100 cm/sec for He, and v_ℓ = 28 cm/sec for CO_2, into the resulting equation yields, after integration over the length ℓ of the chamber, the results

$$\dot{Q} = \begin{cases} 7.4\,\Delta T \text{ cal/sec for Ar,} \\ 16.6\,\Delta T \text{ cal/sec for He,} \\ 6.5\,\Delta T \text{ cal/sec for } CO_2. \end{cases} \tag{A-4}$$

---

* The value B = 0.007 applies to limestone. Furnas[11] used particles of iron ore, coal, coke, and limestone and found that the values of B ranged from 0.014 for iron ore to about 0.005 for coke.

From Eq. 17 we find that the rate of heat addition necessary to maintain the system isothermal is

$$\dot{Q} = \frac{p_o V}{t^*}(1-b_o)\exp\left(-\frac{t}{t^*}\right)$$

$$= \begin{cases} 58\exp\left(-\frac{t}{t^*}\right) & \text{cal/sec for Ar,} \\ 200\exp\left(-\frac{t}{t^*}\right) & \text{cal/sec for He,} \\ 25\exp\left(-\frac{t}{t^*}\right) & \text{cal/sec for } CO_2, \end{cases} \qquad \text{(A-5)}$$

for typical experiments at $T_o = 300^\circ K$ in which $p_o = 1$ atm, $V = 555\ cm^3$, $t^* = 0.19$ and $b = 0.19$ for Ar, $t^* = 0.06$ and $b = 0.1$ for He, and $t^* = 0.22$ and $b = 0.6$ for CO_2. Since the rate of heat addition necessary to maintain the system isothermal is the maximum rate of heat transfer, we may obtain upper limits for ΔT by equating Eqs. A-4 and A-5;

$$\Delta T < \begin{cases} (58/7.4)\exp(-t/t^*)\ ^\circ C \text{ for Ar,} \\ (200/16.6)\exp(-t/t^*)\ ^\circ C \text{ for He,} \\ (25/6.5)\exp(-t/t^*)\ ^\circ C \text{ for } CO_2. \end{cases}$$

Taking the averages of both sides of the above inequalities over the period of time t_f for typical experiments, and denoting the time average of ΔT by $\overline{\Delta T}$, we find that

$$\overline{\Delta T} < \begin{cases} 2^\circ C \text{ for Ar,} \\ 4^\circ C \text{ for He,} \\ 1^\circ C \text{ for } CO_2; \end{cases} \qquad \text{(A-6)}$$

the test durations were

$$t_f = \begin{cases} 0.60 \text{ sec for Ar,} \\ 0.15 \text{ sec for He,} \\ 0.60 \text{ sec for } CO_2, \end{cases}$$

and correspond, approximately, to the duration of sonic conditions in the nozzle throat. The values obtained in Eq. A-6 are constant, to within about one degree, for initial chamber temperatures in the range 230°K to 390°K.

Equation A-6 is an expression for the time average of the temperature difference between the bead surface and the gas. But we are actually interested in the temperature drop of the gas during the course of a run, i.e., in the quantity $(T_o - T)$ which may be written as

$$(T_o - T) = \left[T_o - T_d(a,t)\right] + \left[T_d(a,t) - T\right]. \qquad (A-7)$$

Two phenomena determine the value of the first term, viz., the surface temperature of the bead decreases (a) because of energy loss by convection to the gas and (b) because of endothermic desorption of gas from the bead. These two effects will be assumed to be additive, i.e., we write

$$\left[T_o - T_d(a,t)\right] = \Delta T_h + \Delta T_d \qquad (A-8)$$

where the first term is associated with heat loss by convection and the second term with the heat of desorption.

An upper limit to ΔT_h may be obtained by solving the thermal diffusion equation in a spherical bead using as boundary condition a constant rate of energy loss from each bead of

$$\dot{q} = \frac{1}{t_f} \int_0^{t_f} \frac{\dot{Q}}{N} \, dt \qquad \text{(A-9)}$$

where $\dot{Q}$ is given by Eq. A-5 and N represents the total number of beads in the chamber. Since Eq. A-5 corresponds to the maximum rate of energy loss for maintaining isothermal gases, we obtain an upper limit for ΔT_h. We find from Eq. A-9, for $N \simeq 7.6 \times 10^4$ (with m_b = 696g, ρ_b = 1.25g/cm^3, and a = 0.12 cm) that

$$\dot{q} = \begin{cases} 2.3 \times 10^{-4} \text{ cal/sec for Ar,} \\ 9.6 \times 10^{-4} \text{ cal/sec for He,} \\ 1.1 \times 10^{-4} \text{ cal/sec for } CO_2. \end{cases} \qquad \text{(A-10)}$$

The solution of the heat transfer problem outlined above is[13]

$$\Delta T_h = \frac{\dot{q}}{4\pi a^2} \left\{ \frac{3t}{\rho c_p a} + \frac{a}{5k} - \frac{2a}{k} \sum_{n=1}^{\infty} \left[\frac{\exp\left(- \frac{k\alpha_n^2 t}{\rho c_p a^2} \right)}{\alpha_n^2} \right] \right\} \qquad \text{(A-11)}$$

where ρ, c_p, a, and k are, respectively, the density, heat capacity, radius, and thermal conductivity of the bead, and the quantities α_n are the positive roots of the characteristic equation $\tan(\alpha_n) = \alpha_n$. For a = 0.12 cm, k = 0.00035 cal/cm-sec-°C,[14] ρ = 2.2g/cm^3, c_p = 0.22 cal/g-°C,[14] and t = 0.6 sec for Ar and CO_2 and t = 0.15 sec for He, Eq. A-11 leads to the result

$$\Delta T_h \simeq \begin{cases} 0.1 \text{ °C for Ar,} \\ 0.2 \text{ °C for He,} \\ 0.05 \text{ °C for } CO_2. \end{cases} \qquad \text{(A-12)}$$

The drop in surface temperature of the bead ΔT_d associated with the heat of desorption depends on the rates and heats of the desorption process. If very little gas is adsorbed and desorbed from the solid, as in the experiments with He, then ΔT_d will be approximately zero. If significant adsorption occurs, we must investigate the relative magnitude of gaseous diffusion compared to surface diffusion (see Appendix B) before an estimate of ΔT_d can be made. It is clear that any estimate of ΔT_d will be very crude; however, if it is assumed that desorption occurs uniformly within the bead, ΔT_d may be estimated using

$$m_b c_p \Delta T_d = \frac{m_d Q_d}{W} \tag{A-13}$$

where m_b and c_p are, respectively, the total mass and the heat capacity of the beads, Q_d is the molar heat of adsorption, m_d is the mass of gas desorbed during the test duration t_f of an experiment, and W is the molecular weight of the gas. The values of m_d may be estimated using the experimentally determined values of $b_o = \dot{m}_d t^* / m_o$ given in Tables I, II, and III and in Fig. 59, i.e.,

$$m_d \simeq b_o \left(\frac{m_o t_f}{t^*} \right) . \tag{A-14}$$

The heats of adsorption are,[15,16] approximately,

$$Q_d \simeq \begin{cases} 6600 \text{ cal/mole for } CO_2 \text{ at } -40^\circ C, \\ 5100 \text{ cal/mole for } CO_2 \text{ at } 120^\circ C, \\ 3000 \text{ cal/mole for Ar at } 0^\circ C, \\ 140 \text{ cal/mole for He at } 4^\circ K. \end{cases} \tag{A-15}$$

Substituting Eq. A-14 and Eq. A-15 together with p_o = 1 atm, m_b = 696g, c_p = 0.22 cal/g-°C, and

$$t^* = \begin{cases} 0.24 \text{ sec for } CO_2 \text{ at } -40^\circ C, \\ 0.19 \text{ sec for } CO_2 \text{ at } 120^\circ C, \\ 0.20 \text{ sec for Ar at } 0^\circ C, \\ 0.06 \text{ sec for He at } 0^\circ C, \end{cases}$$

into Eq. A-13 we obtain

$$\Delta T_d \simeq \begin{cases} 2^\circ C \quad \text{for } CO_2 \text{ at } -40^\circ C, \\ 0.6^\circ C \text{ for } CO_2 \text{ at } 120^\circ C, \\ 0.4^\circ C \text{ for Ar at } 0^\circ C, \\ 0^\circ C \quad \text{for He at } 0^\circ C. \end{cases}$$

Measurements of the temperature decrease of the gas-silica gel system after the completion of each run, using a number of thermocouples at various locations in the chamber, indicated that the temperature drop for CO_2 was about 3°C at an initial temperature of 115°C and about 10°C at an initial temperature of -36°C. For Ar and He, on the other hand, the temperature decrease was found to be about one °C at all initial temperatures. These measurements suggest that the effects of the heats of desorption are not large.

The experimental measurements of chamber pressure as a function of time for the CO_2-, Ar-, and He-quartz sand systems agree well with the theoretical curve for an isothermal system without mass addition (see Fig. 58). In other words, systems for which very little desorption occurs are nearly isothermal, in accord with the results

derived in Eqs. A-6 and A-12.

The analysis and experimental data indicate (a) that the temperature of the beads is approximately constant and equal to T_o during a run and (b) that heat transfer rates are sufficiently high to maintain the system effectively isothermal. It is apparent that a really quantitative analysis of the heat transfer problem requires solution of the complete set of equations describing the system, subject to the applicable boundary conditions.

APPENDIX B

DETERMINATION OF THE OVERALL RATE OF DESORPTION OF GAS FROM HIGHLY POROUS SPHERES

It is assumed that the desorption of gas from a highly porous sphere obeys the spherically symmetric diffusion equation. In particular, we assume that the radius of the average pore in the solid is small compared to the mean free path in the gas but large compared to the dimensions of a molecule so that Knudsen or free molecule flow occurs in the gas.*

Since the surface concentration of adsorbed molecules depends on the pressure, a pressure gradient in the gas phase will, in general, give rise to a concentration gradient in the adsorbed phase. We assume that flow of gas in a porous solid occurs by diffusion in the gas phase (Knudsen diffusion) and by surface diffusion in the adsorbed phase.[3,18] The assumption that the pore radius is large compared to the dimensions of a molecule implies that the thickness of the adsorbed layer remains negligibly small compared to the pore diameter. A schematic

---

* Assuming that the pores are cylindrical and have a small radius compared to the mean free path of the gas molecules, the Knudsen diffusion coefficient may be approximated, according to the kinetic theory of gases,[17] by the relation

$$D_g = \frac{2}{3} a_p \bar{v}$$

where a_p is a radius of the cylindrical pores, $\bar{v}=(8R_gT/\pi)^{1/2}$ is the average molecular velocity of a perfect gas according to kinetic theory, and T represents the absolute temperature of the gas. The ratio a_p/λ (where λ is the mean free path at S. T. P.) for silica gel with pore radius a_p 2×10^{-7}cm[14] is estimated to be about 4×10^{-2}. It can be seen that D_g depends on molecular weight but not on molecular size. If the pore radius is not large compared to the dimensions of a molecule, the flow must depend on molecular size and Knudsen diffusion no longer applies.

diagram of a typical pore in a highly porous spherical particle is shown in Fig. B-1.

The diffusion equations may be written as

$$\frac{\partial \rho_g}{\partial t} = \frac{D_g}{r^2} \frac{\partial}{\partial r} \left(r^2 \frac{\partial \rho_g}{\partial r} \right) + \dot{G} \qquad \text{(B-1a)}$$

and

$$\frac{\partial \rho_a}{\partial t} = \frac{D_a}{r^2} \frac{\partial}{\partial r} \left(r^2 \frac{\partial \rho_a}{\partial r} \right) - \dot{G} \qquad \text{(B-1b)}$$

where ρ_a is the mass of adsorbed gas per unit volume of adsorbent, ρ_g is the mass of the gaseous phase per unit volume of adsorbent, D_g and D_a are, respectively, the Knudsen diffusion coefficient and the apparent surface diffusion coefficient, and $\dot{G}$ represents the rate of mass transfer per unit volume from the adsorbed phase to the gas phase within the porous solid (thus $\dot{G}$ is positive for desorption and negative for adsorption). In Eqs. B-1a and B-1b it has been assumed (a) that D_g and D_a are independent of concentration, (b) that the porosity ε, defined as the pore volume divided by the total volume of the sphere, is independent of r, (c) that the pore radius a_p is uniform throughout the sphere, and (d) that the adsorbed molecules on the pore walls are limited to a monolayer. Adding Eqs. B-1a and B-1b, we obtain

$$\frac{\partial}{\partial t} (\rho_a + \rho_g) = \frac{D_g}{r^2} \frac{\partial}{\partial r} \left(r^2 \frac{\partial \rho_g}{\partial r} \right) + \frac{D_a}{r^2} \frac{\partial}{\partial r} \left(r^2 \frac{\partial \rho_a}{\partial r} \right) \qquad \text{(B-2)}$$

thus eliminating $\dot{G}$ from the equations.

In the following analysis, we assume (for justification, see the remarks following Eq. B-13) that the adsorbed phase and the gas are

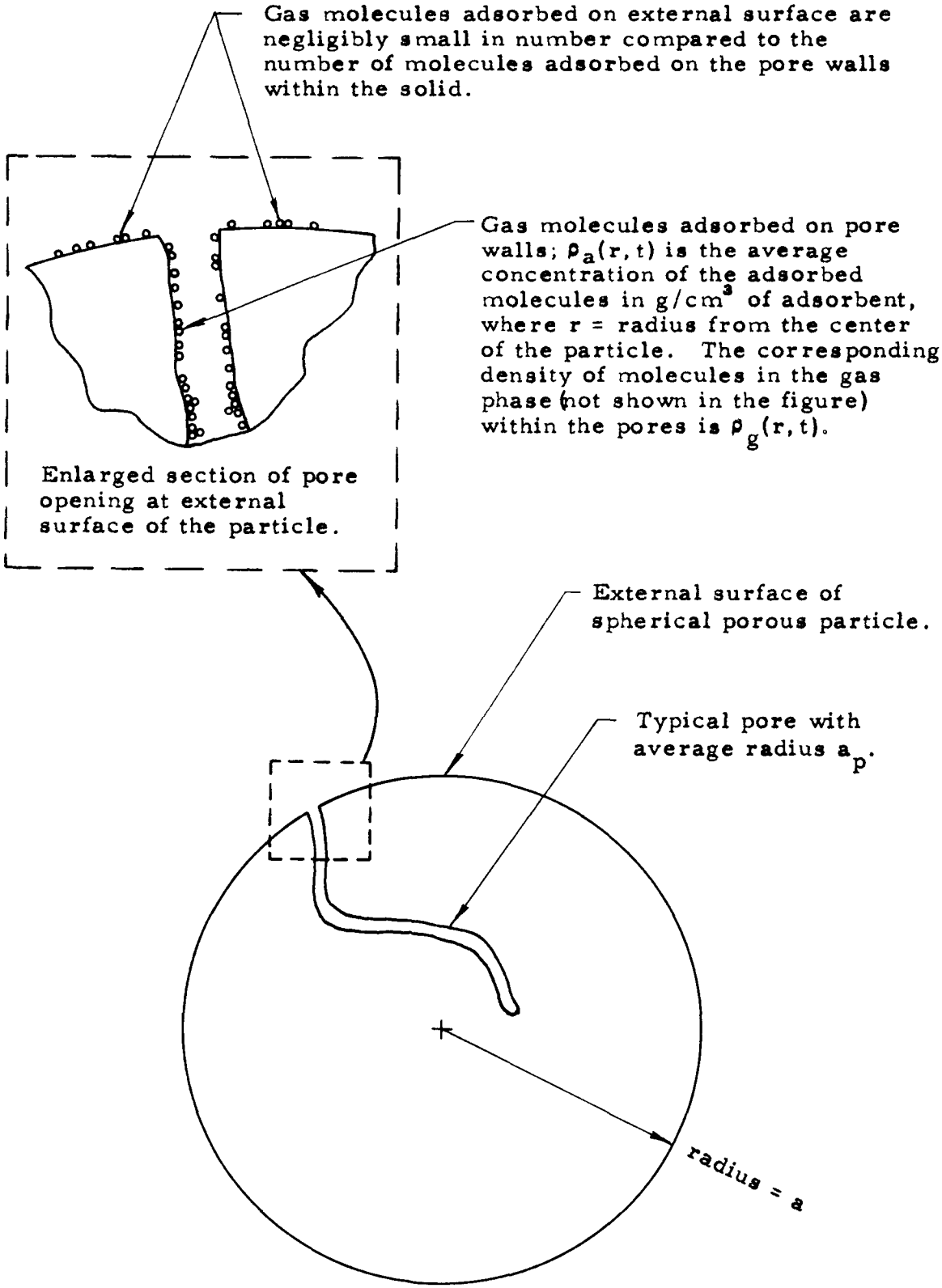

Fig. B-1. Schematic diagram of a typical pore in a highly porous spherical particle of radius a.

in equilibrium at all times and that the relation

$$\rho_a(r,t) = A\,\rho_g(r,t) + B \qquad (B-3)$$

applies. Here A = (constant) $\left[\exp(Q/RT)\right]$ is a function of the temperature with Q representing the molar heat of adsorption; B is also a function of the temperature.

Combining Eqs. B-2 and B-3, under isothermal conditions, yields the result

$$\frac{\partial \rho_g}{\partial t} = \frac{D}{r^2}\,\frac{\partial}{\partial r}\left(r^2\,\frac{\partial \rho_g}{\partial r}\right) \qquad (B-4)$$

where

$$D \equiv \frac{D_g + AD_a}{1+A} \quad .$$

The applicable boundary conditions are

$$\rho_g(r,0) = \varepsilon\rho_o \text{ and } \rho_g(a,t) = \varepsilon\rho(t) \qquad (B-5)$$

where a is the radius of the sphere, ρ_o is the initial density of gas external to the sphere, and $\rho(t)$ is the variable external density of the gas. Equation B-4 may now be solved with the result[19]

$$\left[\rho_g(r,t) - \varepsilon\rho_o\right] =$$

$$-\frac{2\varepsilon D}{ra}\sum_{n=1}^{\infty}\left\{(-1)^n n\pi\left(\sin\frac{n\pi r}{a}\right)\exp(-n^2\pi^2 t/t_d)\int_0^t\left[\rho(x)-\rho_o\right]\exp(n^2\pi^2 x/t_d)\,dx\right\} \qquad (B-6)$$

where $t_d = a^2/D$. When the external concentration varies according to Eq. 8, viz.,

$$\left|\rho(t) - \rho_o\right| = -(1-b_o)\left[1-\exp\left(-\frac{t}{t^*}\right)\right]\rho_o,$$

then Eq. B-6 leads to the result

$$\left[\rho_g(r,t) - \varepsilon\rho_o\right] = \varepsilon\rho_o(1-b_o)\left\{-1 + \frac{a}{r}\,\frac{\sin\left(\sqrt{\frac{t_d}{t^*}}\,\frac{r}{a}\right)}{\sin\sqrt{\frac{t_d}{t^*}}}\left[\exp\left(-\frac{t}{t^*}\right)\right]\right.$$

$$\left. + \frac{2a}{\pi r}\sum_{n=1}^{\infty}(-1)^n\,\frac{(\sin\frac{n\pi r}{a})\,\exp(-n^2\pi^2\frac{t}{t_d})}{n(n^2\pi^2\frac{t^*}{t_d}-1)}\right\}. \qquad (B-7)$$

The rate of mass diffusion across the surface of a single sphere is

$$\dot{m} = -\left[4\pi r^2\left(D_a\frac{\partial\rho_a}{\partial r} + D_g\frac{\partial\rho_g}{\partial r}\right)\right]_{r=a}$$

or, using Eq. B-3,

$$\dot{m} = -\left[4\pi r^2\left(D_g + AD_a\right)\frac{\partial\rho_g}{\partial r}\right]_{r=a}$$

which becomes, in view of Eq. B-7

$$\dot{m} = 4\pi a(1-b_o)\,\varepsilon\rho_o(D_g+AD_a)\left\{\left(1-\sqrt{\frac{t_d}{t^*}}\cot\sqrt{\frac{t_d}{t^*}}\right)\exp\left(-\frac{t}{t^*}\right)\right.$$

$$\left. -2\sum_{n=1}^{\infty}\frac{\exp\left(-n^2\pi^2\frac{t}{t_d}\right)}{\left(n^2\pi^2\frac{t^*}{t_d}-1\right)}\right\}. \qquad (B-8)$$

By writing a Fourier series for $\cot(\sqrt{t_d/t^*})x$ and setting $x=1$, we obtain

$$\left(1 - \sqrt{\frac{t_d}{t^*}} \cot \sqrt{\frac{t_d}{t^*}}\right) = 2 \sum_{n=1}^{\infty} \frac{1}{\left(n^2\pi^2 \frac{t^*}{t_d} - 1\right)} \quad . \tag{B-9}$$

Hence Eq. B-8 may be rewritten as

$$\dot{m} = 8\pi a(1-b_o)\varepsilon\rho_o(D_g + AD_a) \sum_{n=1}^{\infty} \left\{ \frac{\exp\left(-\frac{t}{t^*}\right) - \exp\left(-n^2\pi^2 \frac{t}{t_d}\right)}{\left(n^2\pi^2 \frac{t^*}{t_d} - 1\right)} \right\}. \tag{B-10}$$

The total rate of mass addition from N spheres is

$$\dot{m}_d = N\dot{m} = \left(\frac{m_b}{\frac{4}{3}\pi a^3 \rho_b}\right) \dot{m} \tag{B-11}$$

where m_b and ρ_b are, respectively, the total mass and the apparent density of the spheres. Substituting Eq. B-10 into Eq. B-11 we obtain the desired result, viz.,

$$\dot{m}_d = 6(1-b_o) \frac{\varepsilon\rho_o}{\rho_b} \frac{m_b}{a^2} (D_g + AD_a) \sum_{n=1}^{\infty} \left\{ \frac{\exp\left(-\frac{t}{t^*}\right) - \exp\left(-n^2\pi^2 \frac{t}{t_d}\right)}{\left(n^2\pi^2 \frac{t^*}{t_d} - 1\right)} \right\} \tag{B-12}$$

or

$$b = \left(\frac{\dot{m}_d t^*}{m_o}\right) = 6\varepsilon(1-b_o)\left(\frac{1-f}{f}\right)(1+A)\left(\frac{t^*}{t_d}\right) \sum_{n=1}^{\infty} \left\{ \frac{\exp\left(-\frac{t}{t^*}\right) - \exp\left(-n^2\pi^2 \frac{t}{t_d}\right)}{\left(n^2\pi^2 \frac{t^*}{t_d} - 1\right)} \right\} \tag{B-13}$$

where $(1-f)/f$ is equal to $\rho_o m_b / \rho_b m_o$ if f is the fractional void in the bed.

For the case where very little gas is adsorbed, we set A=0 in Eq. B-13 and $t_d \simeq a^2/D_g$. For significant adsorption but $AD_a \ll D_g$, $t_d \simeq a^2(1+A)/D_g$; finally, for $D_g \ll AD_a$, $t_d \simeq a^2(1+A)/AD_a$.

In conclusion, it is appropriate to justify the use of Eq. B-3. It has been found experimentally that the adsorption isotherms of Ar and CO_2 on silica gel are approximately linear over a wide range of pressures.[20, 21] The multimolecular adsorption theory of Brunauer, Emmett and Teller[22] provides a general equation which, under certain conditions, also yields a linear isotherm over a wide range of pressures (see, for example, ref. 23, Fig. XI-8, on p. 479). In particular, a linear isotherm is observed when the heat of adsorption in the second and succeeding layers is approximately equal to the heat of adsorption in the first layer, i.e., multilayer adsorption occurs to some extent before the bare surface is covered with a monolayer. In other words, the use of Eq. B-3 does not necessarily imply monomolecular adsorption. Direct experimental justification is provided, for example, by the fact that Eq. B-3 holds for adsorption of CO_2 on silica gel after the monolayer has been filled.[21, 24] It should be noted, however, that the theory which has been developed from Eqs. B-1a and B-1b is valid only for monomolecular adsorption.

The following limiting cases of Eq. B-13 are of some interest. For the case where $t^*/t_d \ll 1$, the discharge time is much shorter than the diffusion time. Since t^* is small, the external density drops rapidly to the value $\rho / \rho_o = b_o$ (see Eq. 8). Equation B-13 may be rewritten in the form

$$b = 6\mathcal{L}\,(1-b_o)\left(\frac{1-f}{f}\right)\,(1+A)\left[\exp(-\tau)\right]S(\tau;a) \qquad (B-14)$$

where $a = t^*/t_d$, $\tau = t/t^*$, and

$$S(\tau;a) \equiv a\sum_{n=1}^{\infty}\left\{\frac{1-\exp\left[-(a\,n^2\pi^2-1)\tau\right]}{(a\,n^2\pi^2-1)}\right\}. \qquad (B-15)$$

Differentiating $S(\tau;a)$ with respect to τ yields

$$\frac{dS}{d\tau} = a\,\exp(\tau)\sum_{n=1}^{\infty}\exp(-a\,n^2\pi^2\tau)$$

or,

$$\frac{dS}{d\tau} = a\,\exp(\tau)\left\{\sum_{n=0}^{\infty}\left[\exp(-a\,n^2\pi^2\tau)\right]-1\right\}. \qquad (B-16)$$

For very small a, we may evaluate the sum by using the Euler-Maclaurin sum formula with the result

$$\sum_{n=0}^{\infty}\exp(-a\,n^2\pi^2\tau) = \int_0^{\infty}\exp(-a\,n^2\pi^2\,\tau)\,dn + \frac{1}{2}$$

$$= \frac{1}{\pi\sqrt{a}}\left(\int_0^{\infty}\exp(-\tau\,y^2)\,dy\right) + \frac{1}{2}, \qquad (B-17)$$

whence it follows that

$$\sum_{n=0}^{\infty}\exp(-a\,n^2\pi^2\,\tau) = \frac{1}{2\sqrt{\pi a\,\tau}} + \frac{1}{2}. \qquad (B-18)$$

Substituting Eq. B-18 into Eq. B-16 we find, for sufficiently small values of $a\tau$,

$$\frac{dS}{d\tau} \simeq \frac{1}{2}\sqrt{\frac{a}{\pi}}\ \frac{\exp(\tau)}{\sqrt{\tau}}\ . \tag{B-19}$$

From Eq. B-15, it can be seen that the value of $S(\tau;a)$ at $\tau = 0$ is equal to zero; hence, we may integrate Eq. B-19 to obtain $S(\tau;a)$ as follows:

$$S(\tau;a) \simeq \frac{1}{2}\sqrt{\frac{a}{\pi}}\int_0^{\tau} \frac{\exp(t')}{\sqrt{t'}}\ dt' = \sqrt{\frac{a}{\pi}}\int_0^{\sqrt{\tau}} \exp(t^2)dt. \tag{B-20}$$

The integral in Eq. B-20 is tabulated in ref. 25. Substituting Eq. B-20 into Eq. B-14 yields the desired result

$$b \simeq 6\varepsilon\left(\frac{1-f}{f}\right)(1-b_o)(1+A)\sqrt{\frac{a}{\pi}}\ \exp(-\tau)\int_0^{\sqrt{\tau}} \exp(t^2)dt \qquad \text{for small } a\,. \tag{B-21}$$

For the case where $t^*/t_d \gg 1$, the process of mass addition by diffusion occurs very rapidly compared with the discharge rate and the density within the pores decreases nearly as rapidly as the external density, i.e., the rate of desorption is determined by the external density. For $t > 0$, Eq. B-13 then becomes, approximately,

$$b \simeq \varepsilon(1-b_o)\left(\frac{1-f}{f}\right)(1+A)\exp\left(-\frac{t}{t^*}\right)\ .$$

APPENDIX C

DERIVATION OF THE ENERGY EQUATION

Consider a vessel containing gas and beads from which gases are desorbed while gas flow occurs through a de Laval nozzle. We construct a surface S(t) bounding the volume V(t) in which the gas-bead system is contained. In this manner, we construct a thermodynamic system containing uniformly distributed sources. Applying the first law of thermodynamics, we may write the expression

$$\frac{d}{dt}\int_{V(t)} \rho\left(e + \frac{v^2}{2}\right)dV = \dot{m}_d\left[c_v T_d + \left(\frac{p}{\rho}\right)_d\right] + \int_{V(t)} \dot{q}\, dV + \int_{S(t)} \vec{v}\cdot(\sigma\,\vec{n})\,dS \qquad (C\text{-}1)$$

corresponding to the statement

> increase in energy of the system = energy supplied to the system through the boundaries or from imbedded sources + work done on the system.

Here the time derivative is the Euler time derivative following the fluid, e = internal energy per unit mass, $v^2/2$ = kinetic energy per unit mass, $\dot{m}_d c_p T_d$ represents the rate of energy addition from the uniformly distributed sources at the temperature T_d associated with desorption of gas at the temperature T_d, $\vec{v}$ = velocity of the gas, $\dot{q}$ = rate of heat addition per unit volume of gas, σ = stress tensor (with components $\sigma_{ij} = -p\,\delta_{ij} + \tau_{ij}$, where τ_{ij} = ijth component of the viscous stress tensor and $-p\,\delta_{ij}$ = ijth component of the pressure tensor), and $\vec{n}$ = outward directed normal to S(t). Using the general relation[26]

$$\frac{d}{dt}\int_{V(t)} \rho f(x,t)\, dV = \int_{V(t)} \rho \frac{df(x,t)}{dt}\, dV$$

we obtain the identity

$$\frac{d}{dt}\int_{V(t)} \rho\left(e + \frac{v^2}{2}\right)dV = \int_{V(t)} \rho \frac{d}{dt}\left(e + \frac{v^2}{2}\right) dV .$$

Furthermore, using the continuity equation $\partial\rho/\partial t + \nabla.(\rho\vec{v}) = 0$ and noting that $d/dt = \partial/\partial t + \vec{v}.\nabla$, we find that

$$\int_{V(t)} \rho \frac{d}{dt}\left(e + \frac{v^2}{2}\right) dV = \int_{V(t)} \left\{ \frac{\partial}{\partial t}\left[\rho\left(e + \frac{v^2}{2}\right)\right] + \nabla.\left[\rho\vec{v}\left(e + \frac{v^2}{2}\right)\right]\right\} dV$$

$$= \int_{V(t)} \frac{\partial}{\partial t}\left[\rho\left(e + \frac{v^2}{2}\right)\right] dV + \int_{S(t)} \rho\left(e + \frac{v^2}{2}\right)\vec{v}\,.\,\hat{n}\, dS$$

where Gauss's theorem has been applied. Neglecting shearing stresses, Eq. C-1 becomes, therefore,

$$\int_{V(t)} \left\{ \frac{\partial}{\partial t}\left[\rho\left(e + \frac{v^2}{2}\right)\right] - \dot{q}\right\} dV = \dot{m}_d c_p T_d - \int_{S(t)} p\vec{v}\,.\,\hat{n}\, dS$$

$$- \int_{S(t)} \rho\left(e + \frac{v^2}{2}\right)\vec{v}\,.\,\hat{n}\, dS. \qquad (C-2)$$

It is now convenient to choose S(t) as the surface bounding the chamber volume V . We may then integrate the term appearing on the left-hand side of Eq. C-2 over the uniform container. Thus, we find

for the integral the result

$$\frac{\partial}{\partial t}(m\, c_v T) - \dot{Q}$$

if m denotes the total mass of free gas in the container at any time and $\dot{Q}$ represents the total rate of heat addition to the volume V . It is apparent that $\vec{v} = 0$ everywhere on S(t) except where mass is leaving from the chamber. Hence

$$\int_{S(t)} p\vec{v} \cdot \hat{n}\, dS = \int_{S(t)} \frac{p}{\rho}(\rho \vec{v}) \cdot \hat{n}\, dS = \dot{m}_e \left(\frac{p}{\rho}\right)_e = \dot{m}_e R_g T_e$$

for ideal gases where the subscript e identifies the uniform conditions at the exit plane and $\dot{m}_e$ represents the mass flow rate out of the control volume V (which equals the mass discharge rate through the de Laval nozzle). Similarly,

$$\int_{S(t)} \rho\left(e + \frac{v^2}{2}\right)\vec{v} \cdot \hat{n}\, dS = \left(e + \frac{v^2}{2}\right)_e \dot{m}_e = \left(c_v T + \frac{v^2}{2}\right)_e \dot{m}_e = c_v T \dot{m}_e$$

since the translational energy per unit mass at the exit plane of the volume V is negligibly small compared with the internal energy per unit mass at the same location.

Introducing the preceding relations into Eq. C-2, we obtain the desired result, viz.,

$$\frac{\partial}{\partial t}(mc_v T) = \dot{Q} + \dot{m}_d c_p T_d - \dot{m}_e c_p T .$$

REFERENCES FOR PART II

1. P. P. Wegener, The Physics of Fluids 2, 264 (1959).
2. S. Brunauer, The Adsorption of Gases and Vapors, Vol. 1: Physical Adsorption, pp. 454-471, Princeton University Press, Princeton, N. J., 1945.
3. G. Damköhler, Z. phys. Chem. A174, 222 (1935).
4. P. C. Carman and F. A. Raal, Proc. Roy. Soc. 209A, 38 (1951).
5. H. H. Heitland, The Reviews of Scientific Instruments 32, 1203 (1961).
6. I. F. Homfray, Z. phys. Chem. 74, 129 (1910).
7. S. Brunauer, ref. 2, p. 382.
8. W. Kälberer and C. Schuster, Z. phys. Chem. A141, 270 (1929).
9. W. Kälberer and H. Mark, Z. phys. Chem. A139, 151 (1928).
10. P. C. Carman, Flow of Gases Through Porous Media, p. 120, Academic Press, Inc., New York, N. Y., 1956.
11. C. C. Furnas, Ind. Eng. Chem. 22, 721 (1930).
12. T. E. W. Schumann, J. Franklin Inst. 208, 305 (1929).
13. H. S. Carslaw and J. C. Jaeger, Conduction of Heat in Solids, 2nd Edition, p. 242, Oxford University Press, Oxford, England, 1959.
14. C. L. Mantell, Adsorption, p. 176, McGraw-Hill Book Company, Inc., New York, N. Y., 1951.
15. S. Brunauer, ref. 2, pp. 234, 240, 263.
16. W. Kälberer and C. Schuster, ref. 8.
17. R. D. Present, Kinetic Theory of Gases, pp. 55-61, McGraw-Hill Book Company, Inc., New York, N. Y., 1958.
18. R. M. Barrer and J. A. Barrie, Proc. Roy. Soc. A213, 250 (1952).
19. H. S. Carslaw and J. C. Jaeger, ref. 13, p. 233.

20. W. A. Patrick, W. C. Preston, A. E. Owens, J. Phys. Chem. 29, 421 (1925).

21. S. Brunauer, ref. 2, pp. 16, 68-70.

22. S. Brunauer, P. H. Emmett and E. Teller, J. Am. Chem. Soc. 60, 309 (1938).

23. A. W. Adamson, Physical Chemistry of Surfaces, p. 479, Interscience Publishers, Inc., New York, N. Y., 1960.

24. S. Brunauer, ref. 2, pp. 286-291.

25. E. Jahnke and F. Emde, Tables of Functions, 4th Edition, p. 32, Dover Publications, New York, N. Y., 1945.

26. See, for example, W. Nachbar, F. Williams, and S. S. Penner, Quar. Appl. Math. 17, 43 (1959).

Table I. Values of the parameters b_o, $a = t^*/t_d$, and (1+A) obtained by fitting Eqs. 8 and 9 to the experimental data for He.

T(°K)	b_o	$a \times 10^2$	(1+ A)	$(D_g + AD_e) \times 10^3$ (cm^2/sec)	$(D_g)_{theor} \times 10^3$ (cm^2/sec)
223	0.095	8.0	0.7	12.2	14.5
237	0.112	5.0	1.0	11.2	15.0
251	0.103	5.0	1.0	11.0	15.4
268	0.088	9.0	0.7	14.4	15.9
279	0.114	5.0	1.0	12.1	16.2
296	0.110	5.8	1.1	14.5	16.7
324	0.099	8.0	0.8	16.1	17.5
337	0.112	6.0	1.0	15.7	17.8
362	0.105	6.0	0.9	14.8	18.5
389	0.105	5.0	1.0	13.6	19.1

Table II. Values of the parameters b_o, $a = t^* t_d$, and $(1+A)$ obtained by fitting Eqs. 8 and 9 to the experimental data for Ar.

T(°K)	b_o	$a \times 10^3$	$(1+A)$	$(D_g + AD_a) \times 10^3$ (cm^2/sec)	$(D_g)_{theor} \times 10^3$ (cm^2/sec)
228	0.324	0.2	50	0.7	4.6
231	0.296	0.2	43	0.6	4.7
239	0.280	0.2	41	0.6	4.7
251	0.259	1.0	17	1.2	4.9
255	0.254	1.0	16	1.1	4.9
267	0.240	2.0	11	1.6	5.0
267	0.239	1.2	14	1.2	5.0
281	0.211	7.0	5.3	2.7	5.1
288	0.189	12.0	3.8	3.4	5.2
296	0.187	10.0	3.9	3.0	5.3
296	0.193	10.0	4.0	3.0	5.3
297	0.179	12.0	3.4	3.0	5.3
312	0.189	6.0	5.0	2.4	5.4
319	0.172	20.0	2.8	4.3	5.5
319	0.169	20.0	2.6	4.0	5.5
325	0.170	20.0	2.6	4.1	5.5
333	0.165	20.0	2.6	4.1	5.6
334	0.161	18.0	2.6	3.8	5.6
345	0.162	20.0	2.5	4.1	5.7
353	0.152	20.0	2.3	3.9	5.8
353	0.142	20.0	2.2	3.6	5.8
363	0.143	20.0	2.1	3.6	5.9
370	0.142	20.0	2.2	3.7	5.9
378	0.147	20.0	2.3	3.9	6.0
379	0.142	24.0	2.0	4.0	6.0
383	0.124	28.0	1.6	4.0	6.0

Table III. Values of the parameters b_o and $a^{1/2}(1+A)$ obtained by fitting Eqs. 9 and D-21 to the experimental data for CO_2.

T(°K)	b_o	$a^{1/2}(1+A)$
237	0.684	3.0
248	0.692	3.1
260	0.669	2.9
274	0.660	2.8
294	0.600	2.1
305	0.584	2.1
306	0.593	2.0
333	0.515	1.5
351	0.461	1.2
364	0.423	1.1
378	0.379	0.9
390	0.356	0.8
390	0.367	0.8

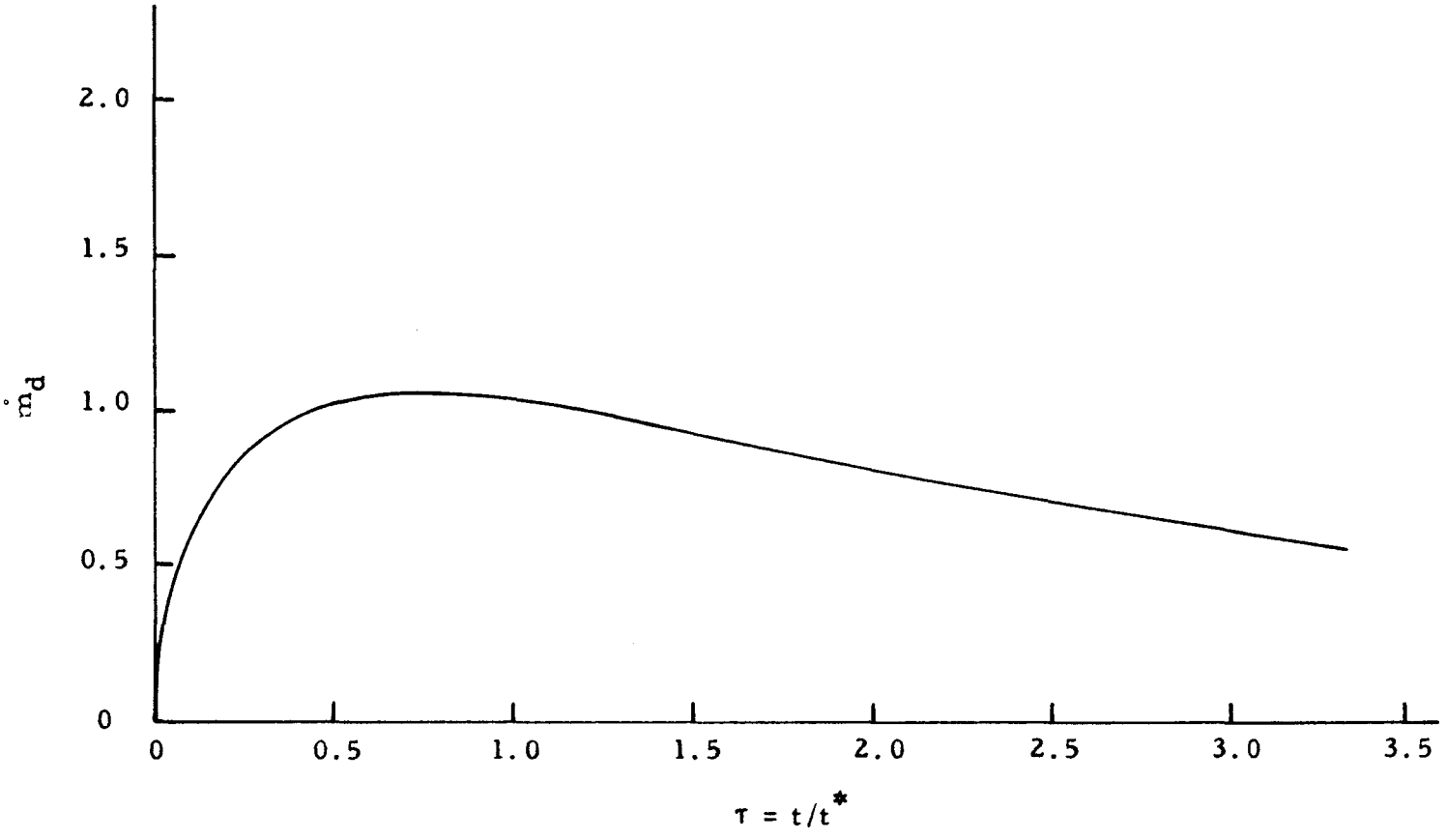

Fig. 1. The desorption rate $\dot{m}_d$ as a function of the reduced time $\tau = t/t^*$. The following values were used for the parameters in Eq. (9): $m_o = 0.89$ g, $t^* = 0.190$ sec, $f = 0.5$, $\epsilon = 0.43$, $b_o = 0.193$, $(1 + A) = 4.0$, and $t^*/t_d = 0.01$.

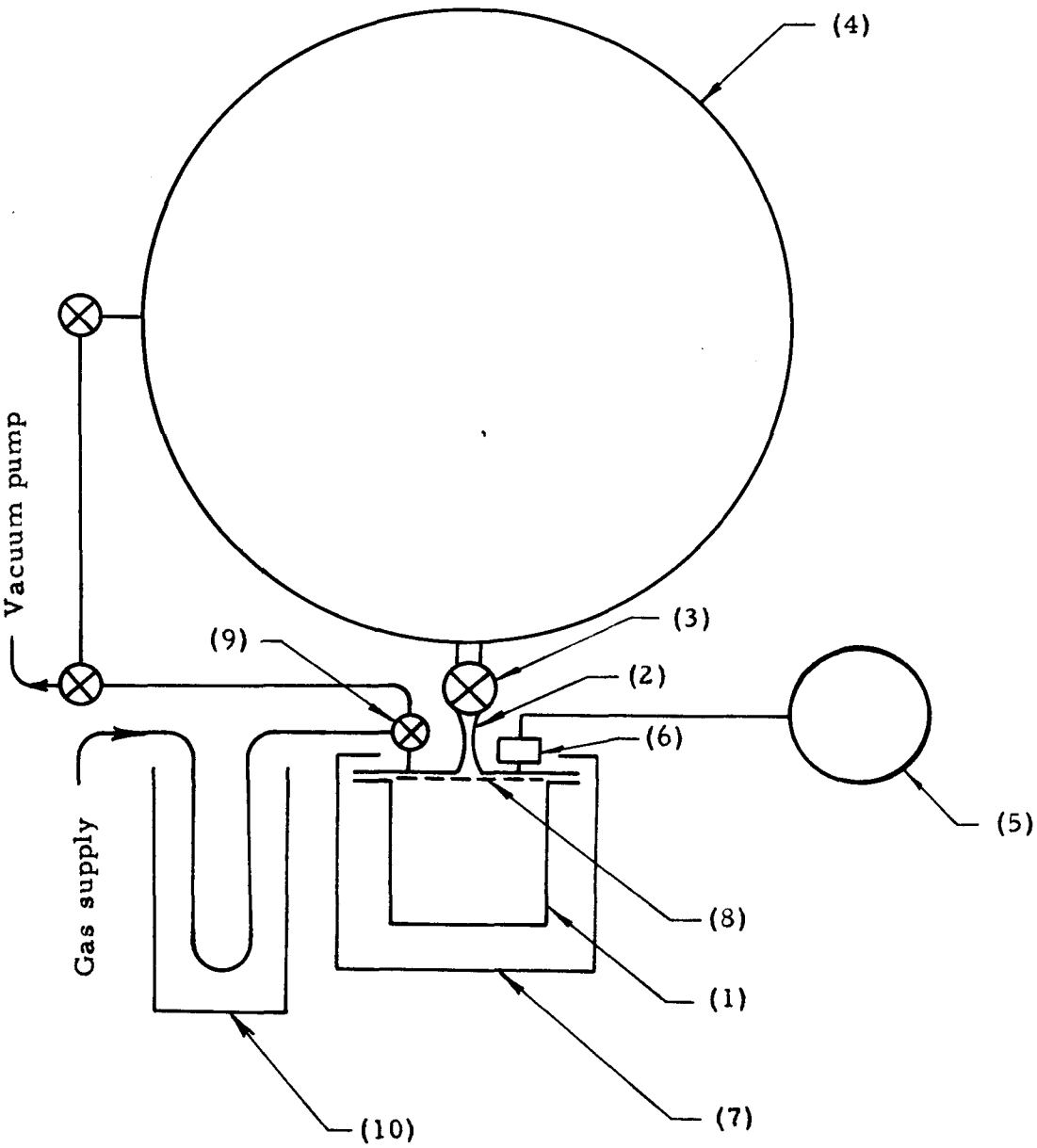

Fig. 2. Schematic diagram showing the apparatus used for experimental measurements.

(1): reaction vessel; (2): de Laval nozzle; (3): rapidly opening valve; (4): dump tank; (5): oscilloscope; (6): Strain-gage pressure transducer; (7): heating or cooling bath; (8): 100 mesh screen; (9): three-way stopcock; (10): dry ice trap for removal of water.

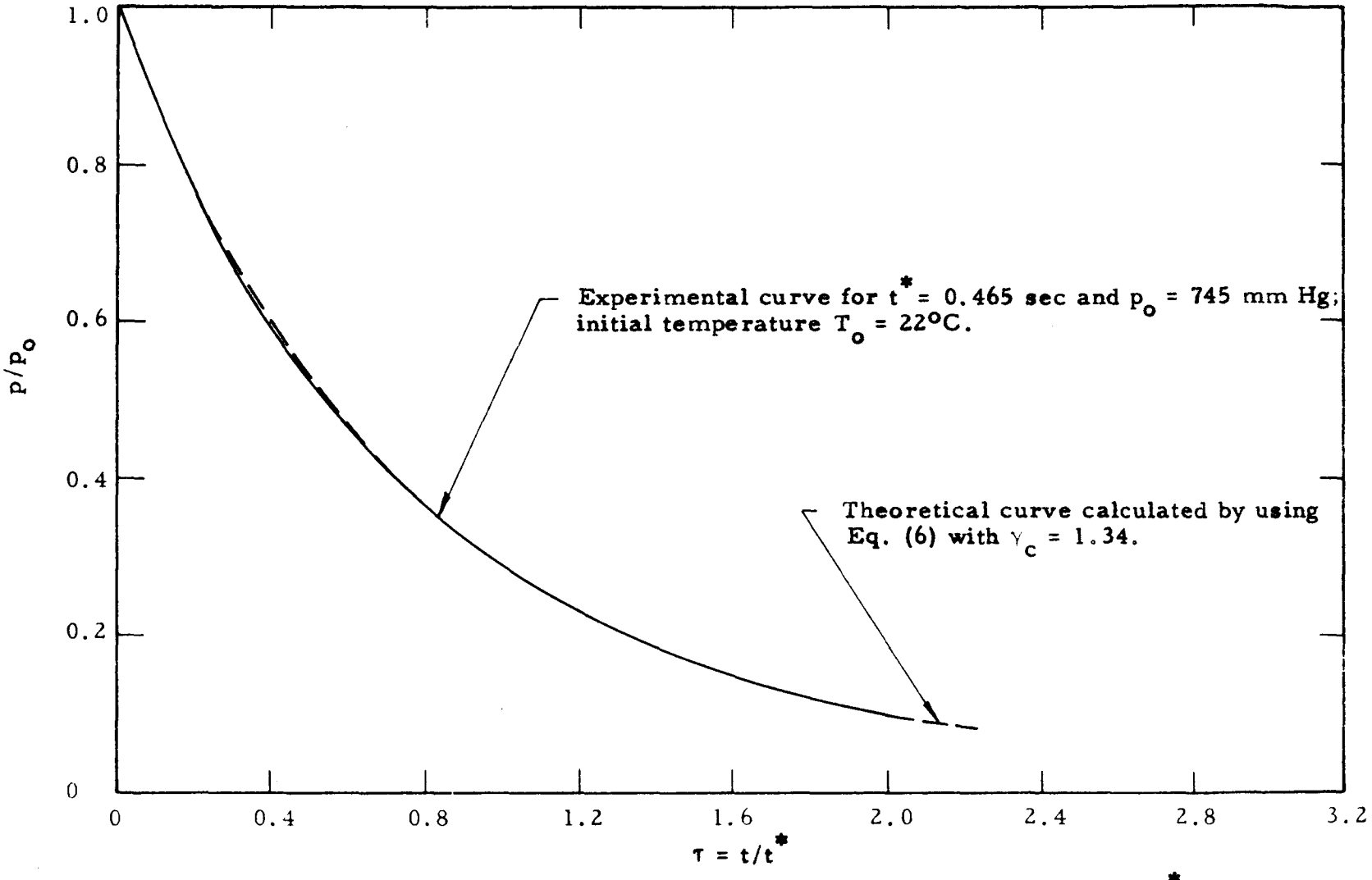

Fig. 3. The reduced pressure p/p_o as a function of the reduced time $\tau = t/t^*$ for CO_2 discharging from a vessel containing no solid adsorbent.

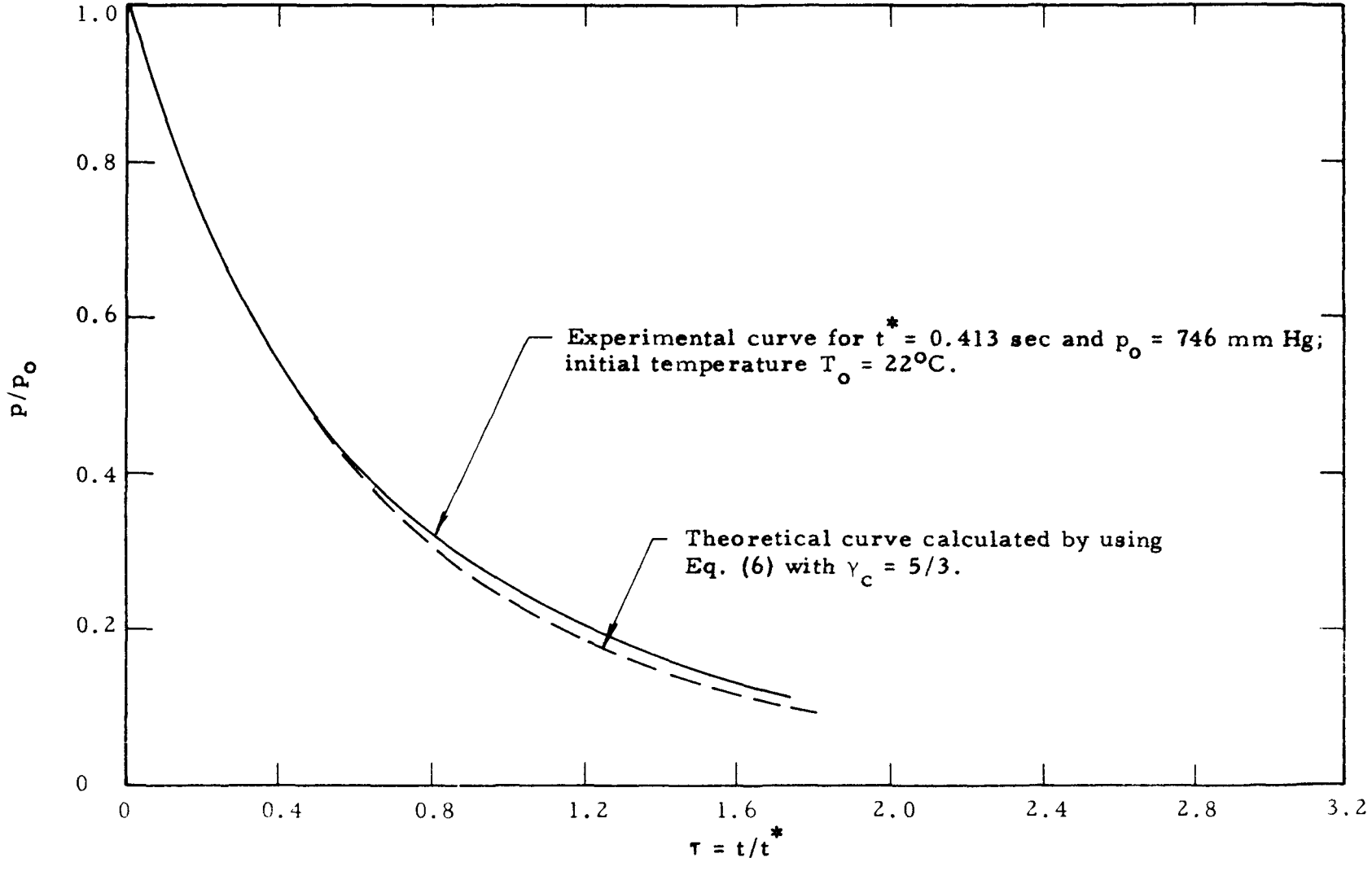

Fig. 4. The reduced pressure p/p_o as a function of the reduced time $\tau = t/t^*$ for Ar discharging from a vessel containing no solid adsorbent.

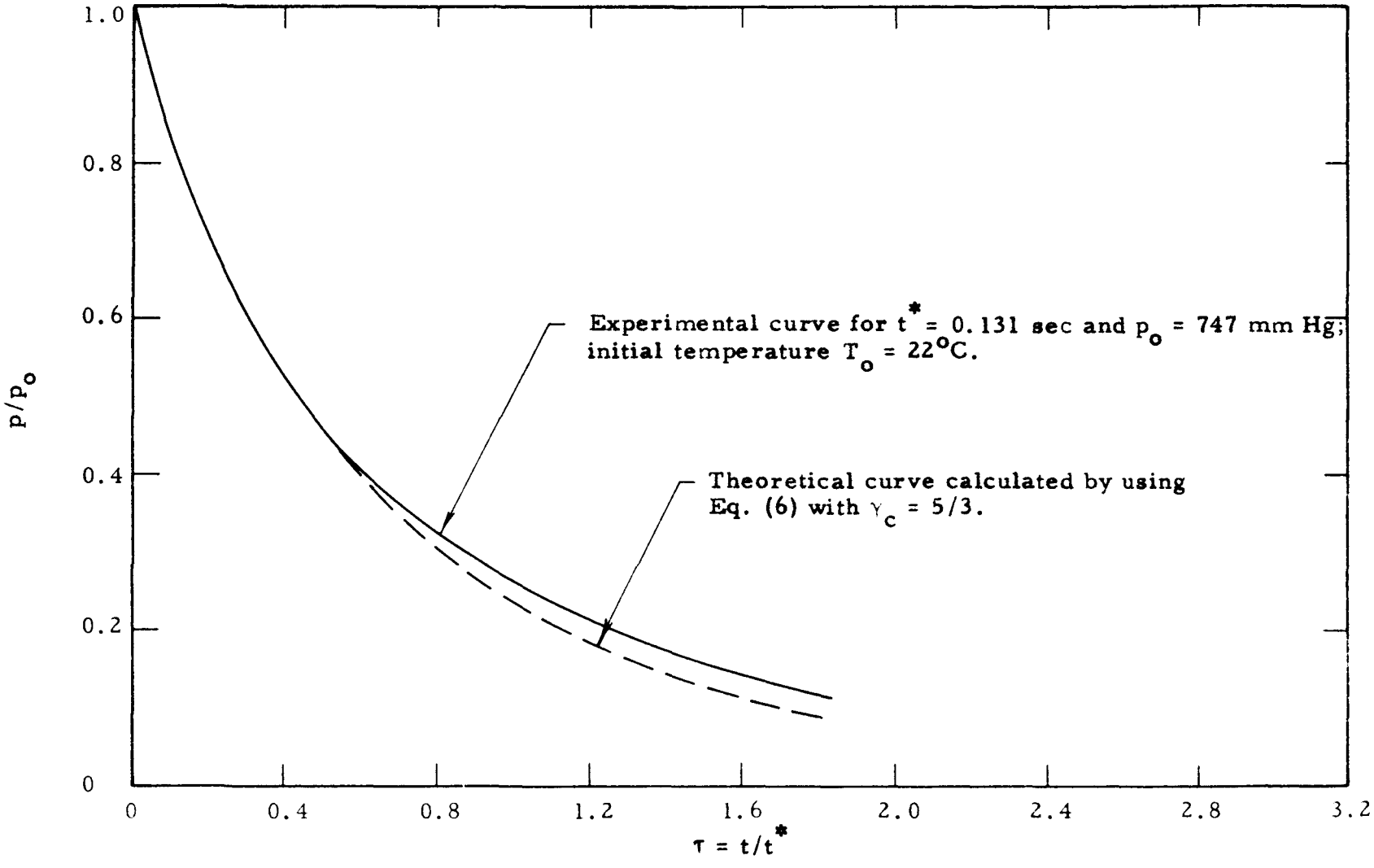

Fig. 5. The reduced pressure p/p_o as a function of the reduced time $\tau = t/t^*$ for He discharging from a vessel containing no solid adsorbent.

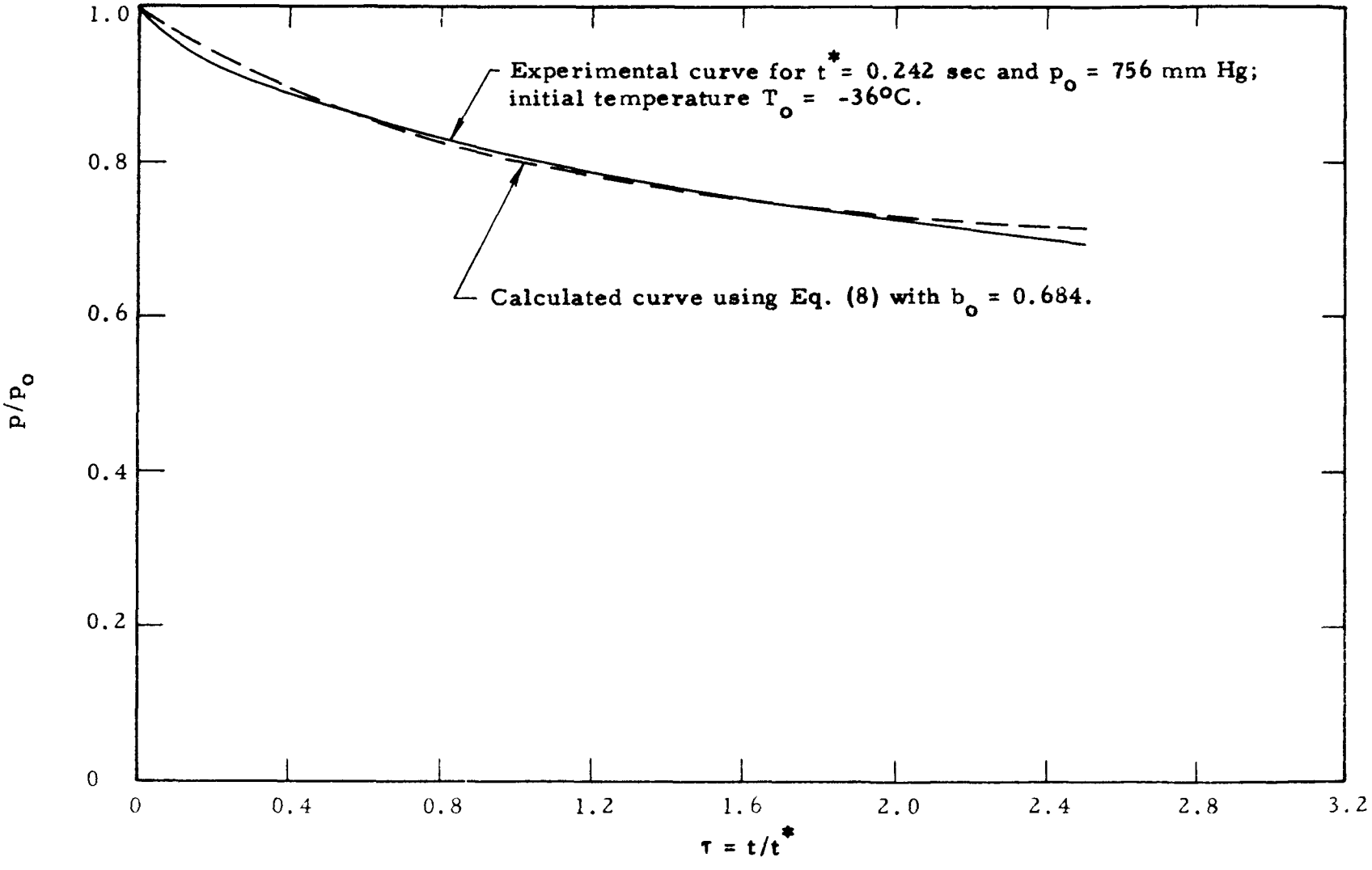

Fig. 6. The reduced pressure p/p_o as a function of the reduced time $\tau = t/t^*$ for CO_2 discharging from a vessel containing silica gel of mesh size 6-16.

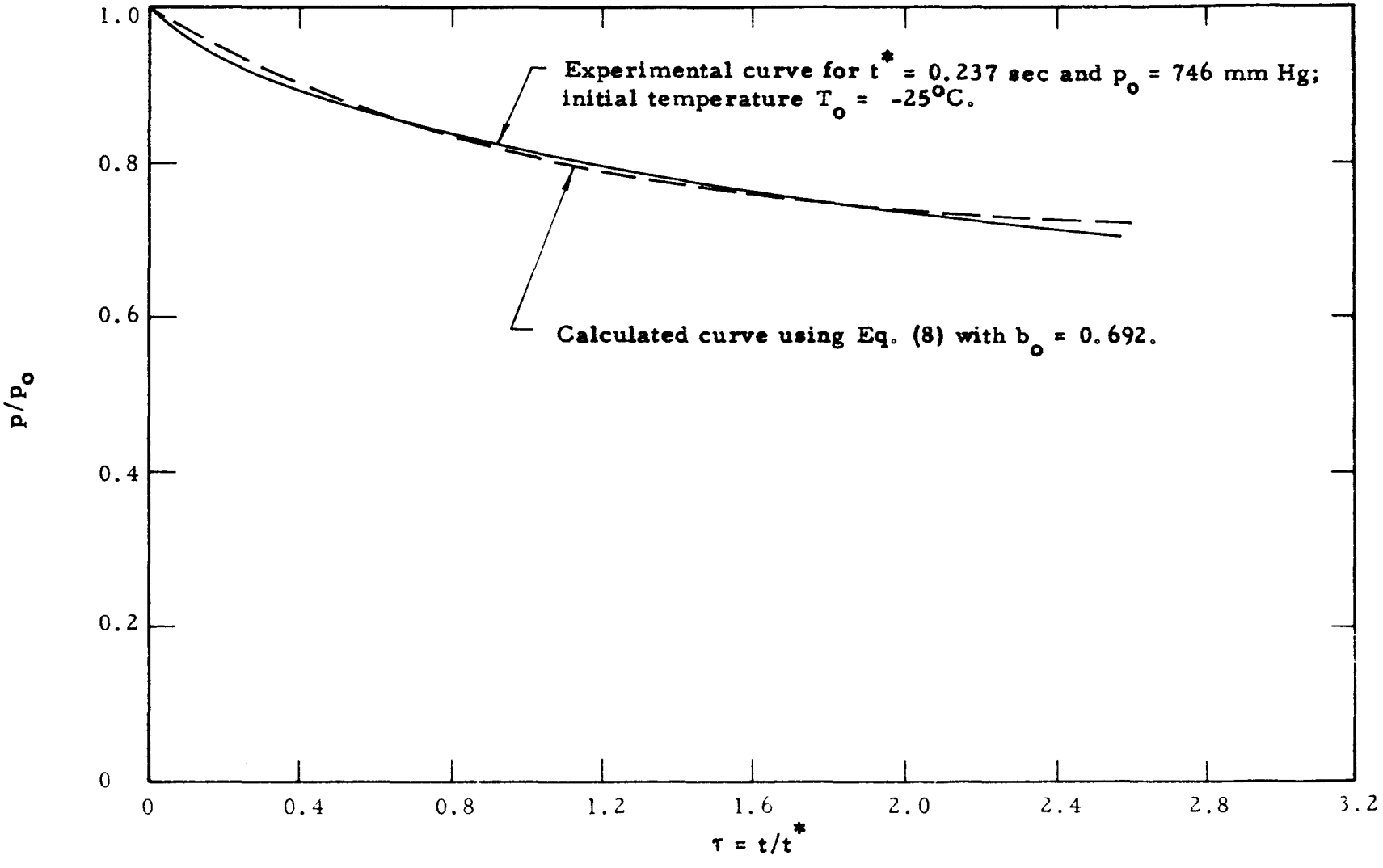

Fig. 7. The reduced pressure p/p_o as a function of the reduced time $\tau = t/t^*$ for CO_2 discharging from a vessel containing silica gel of mesh size 6-16.

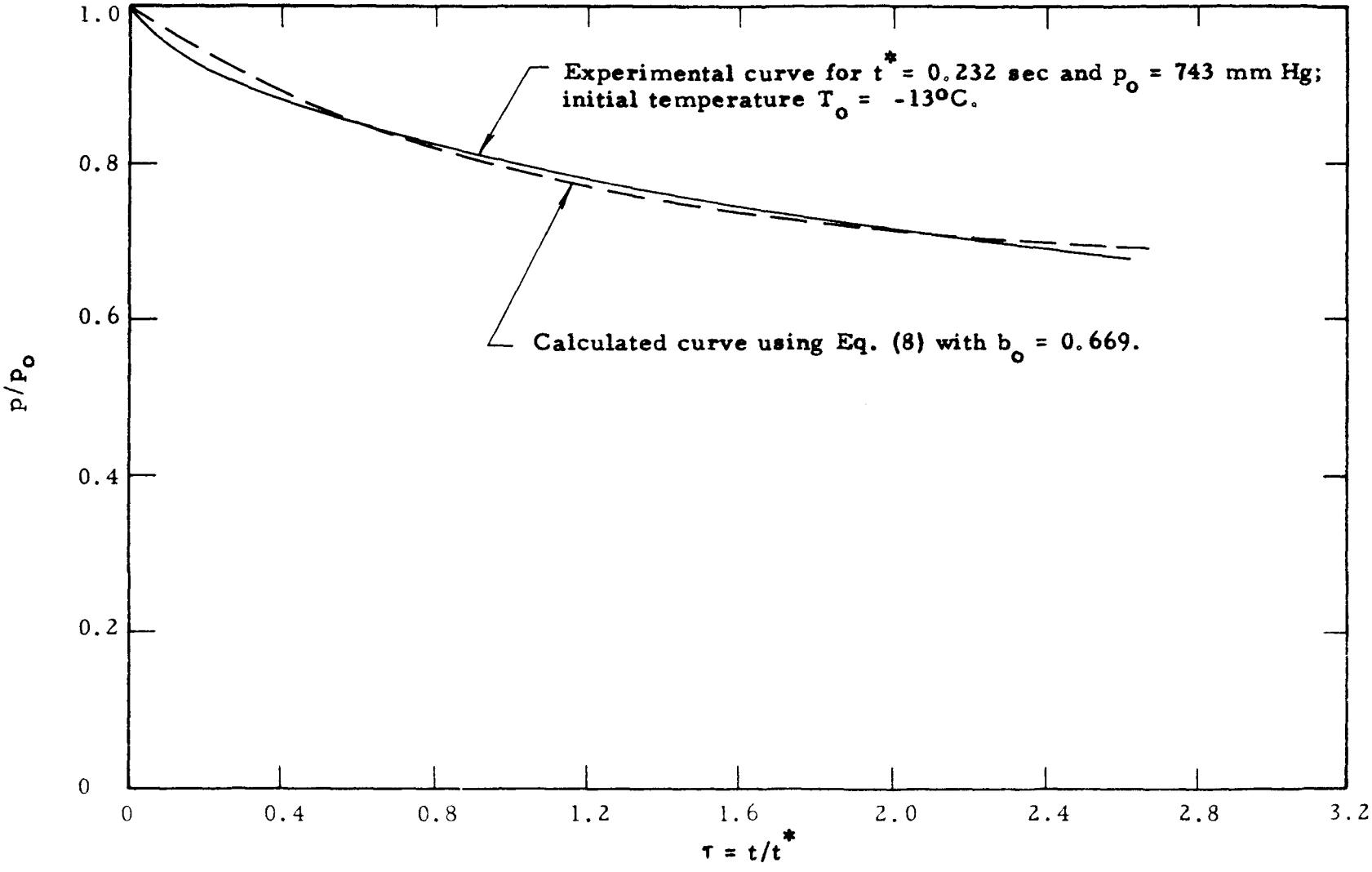

Fig. 8. The reduced pressure p/p_o as a function of the reduced time $\tau = t/t^*$ for CO_2 discharging from a vessel containing silica gel of mesh size 6-16.

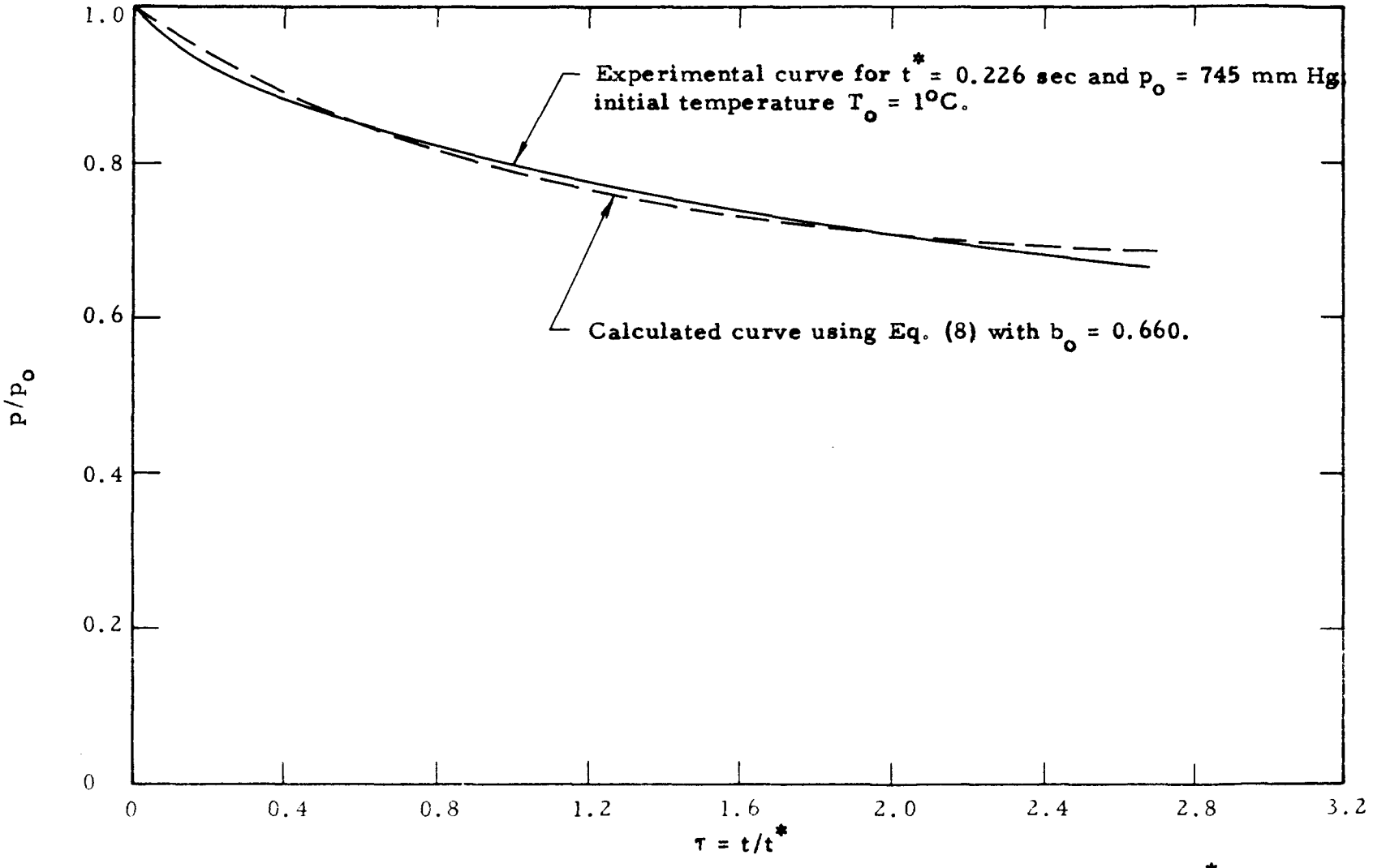

Fig. 9. The reduced pressure p/p_o as a function of the reduced time $\tau = t/t^*$ for CO_2 discharging from a vessel containing silica gel of mesh size 6-16.

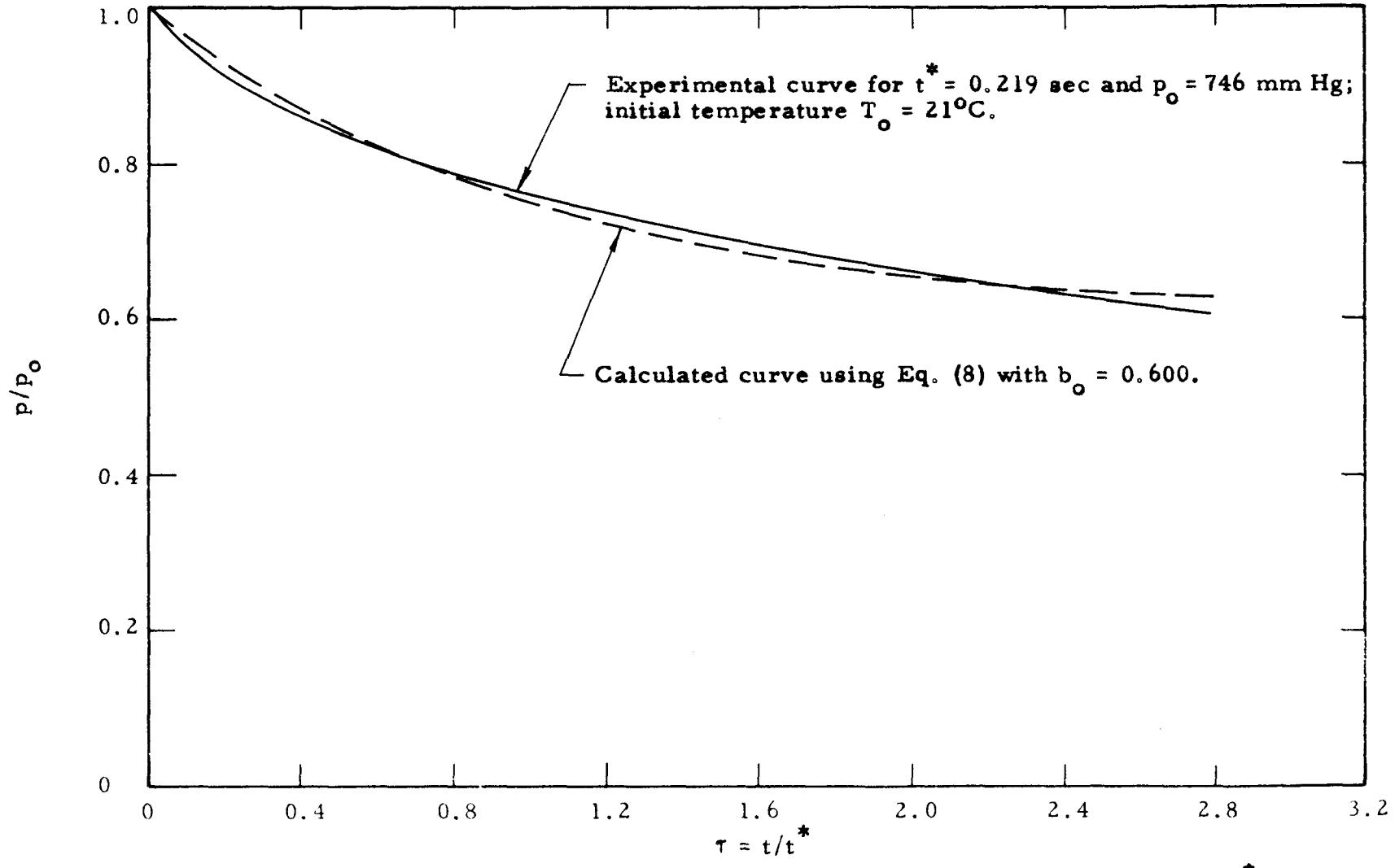

Fig. 10. The reduced pressure p/p_o as a function of the reduced time $\tau = t/t^*$ for CO_2 discharging from a vessel containing silica gel of mesh size 6-16.

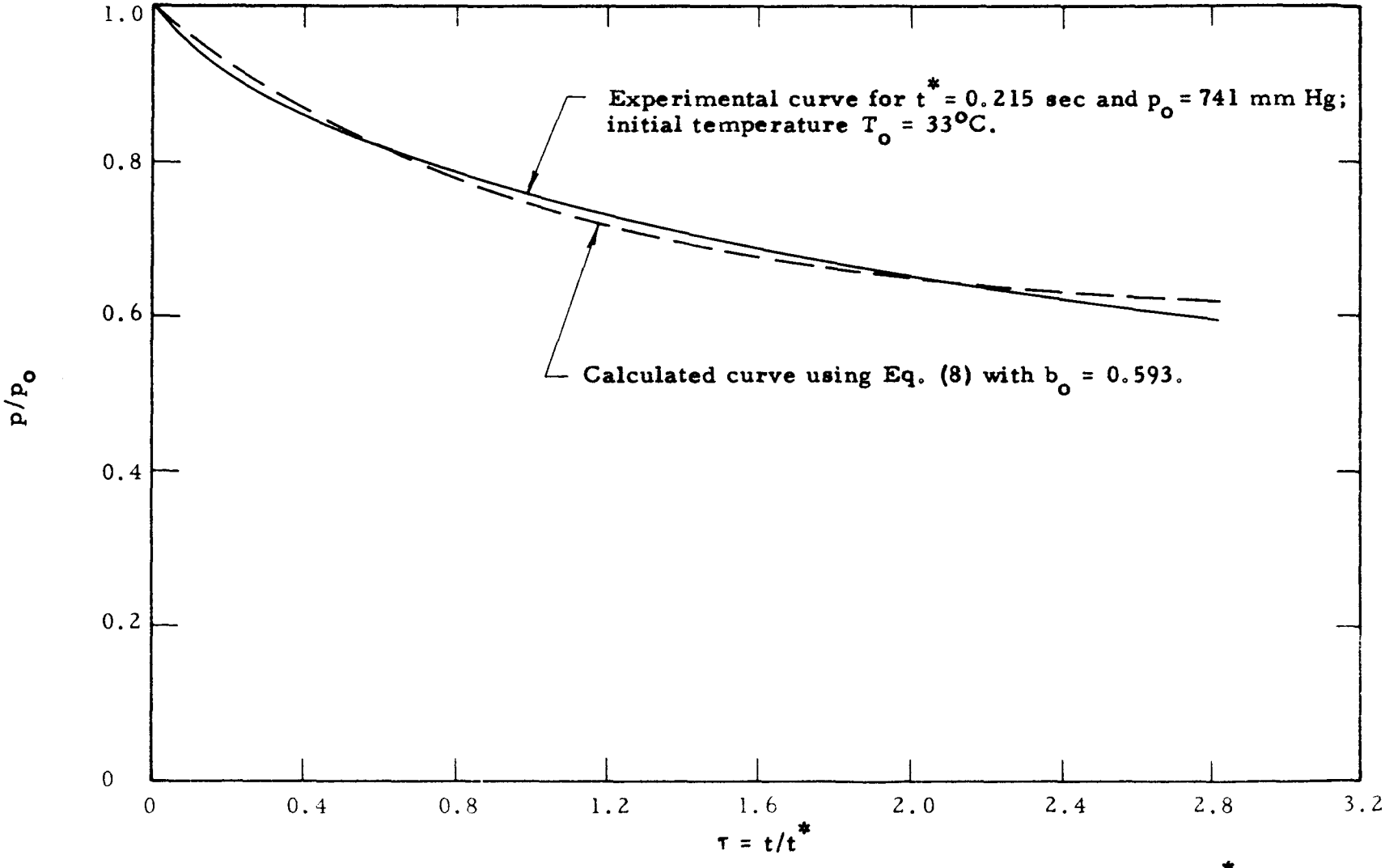

Fig. 11. The reduced pressure p/p_o as a function of the reduced time $\tau = t/t^*$ for CO_2 discharging from a vessel containing silica gel of mesh size 6-16.

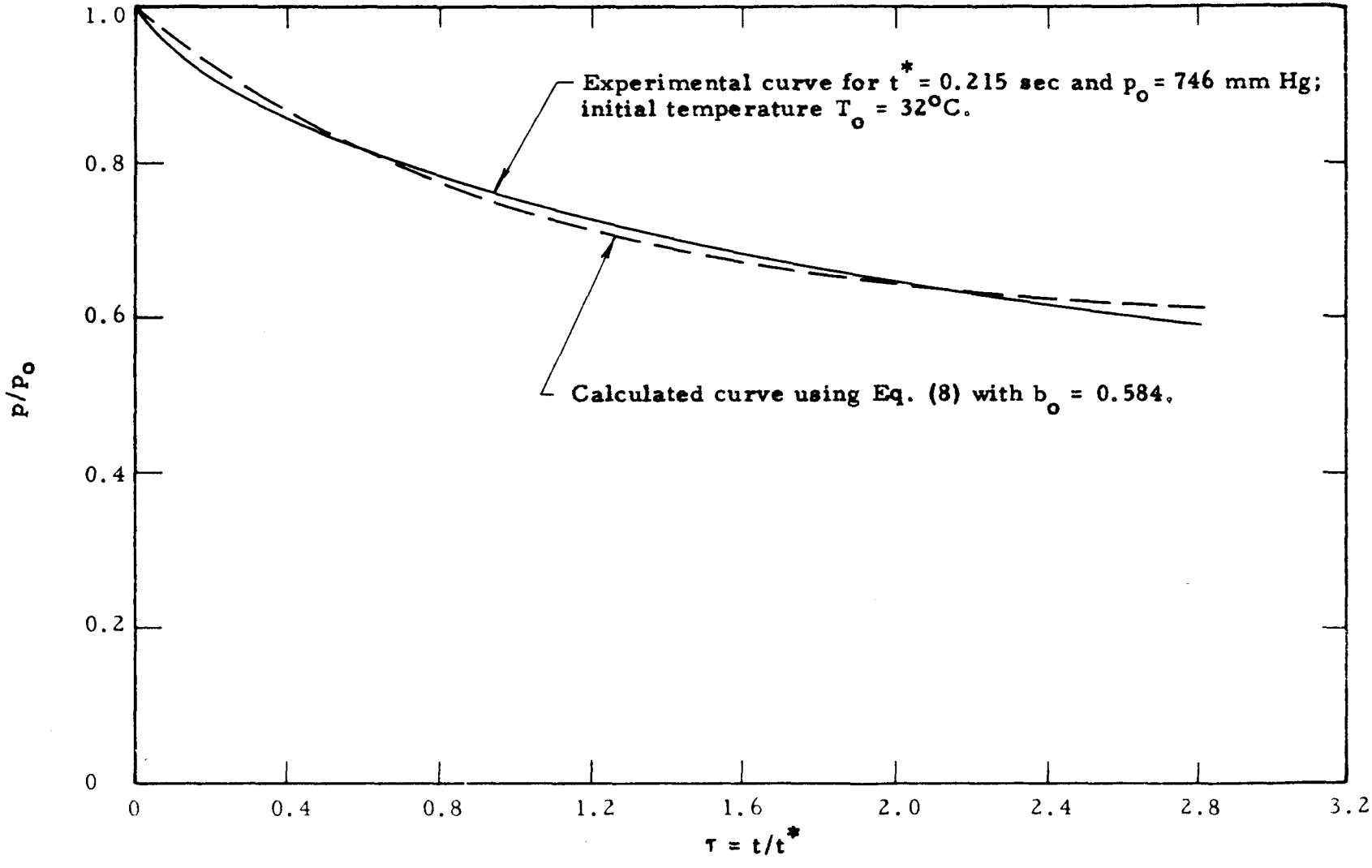

Fig. 12. The reduced pressure p/p_o as a function of the reduced time $\tau = t/t^*$ for CO_2 discharging from a vessel containing silica gel of mesh size 6-16.

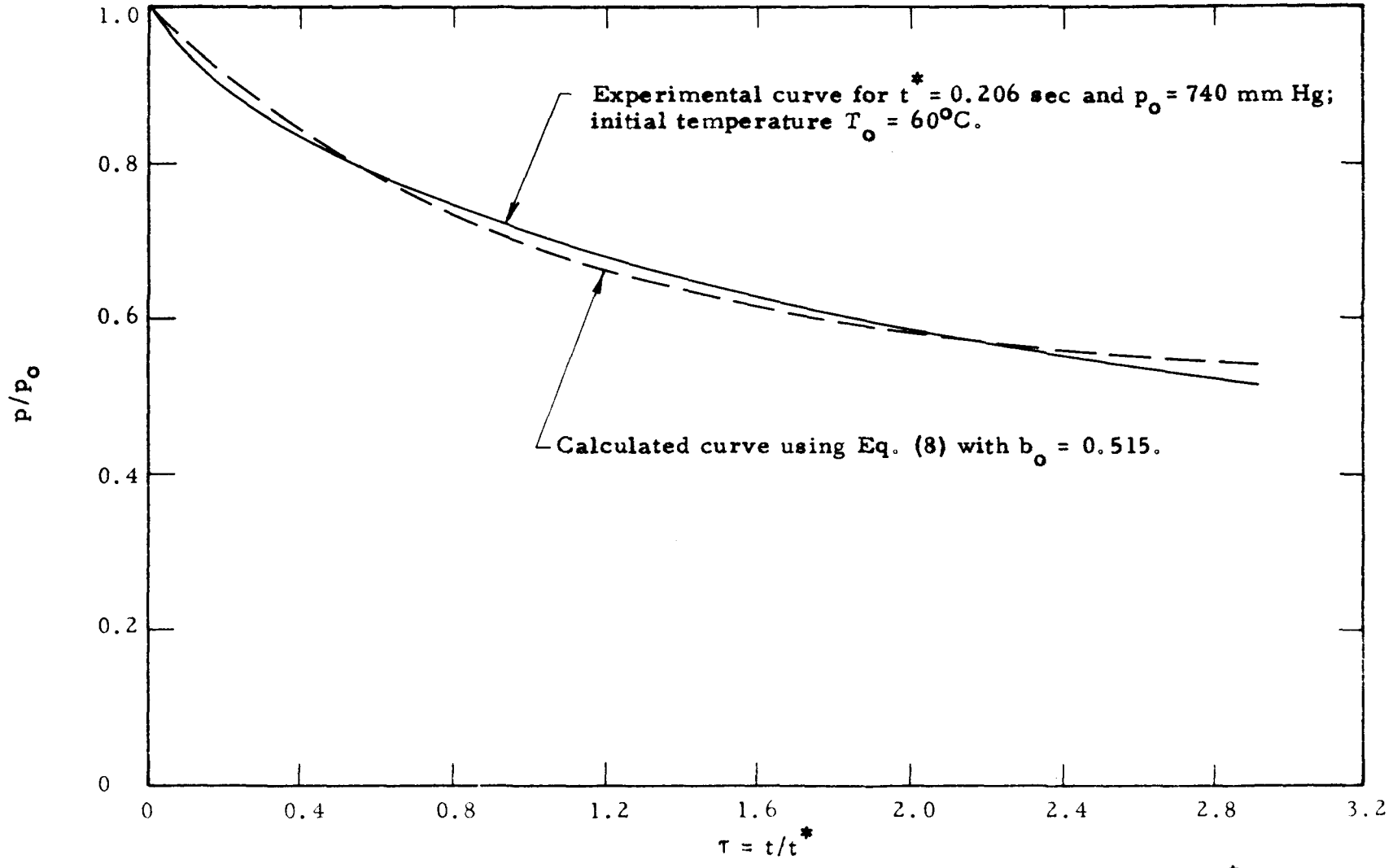

Fig. 13. The reduced pressure p/p_o as a function of the reduced time $\tau = t/t^*$ for CO_2 discharging from a vessel containing silica gel of mesh size 6-16.

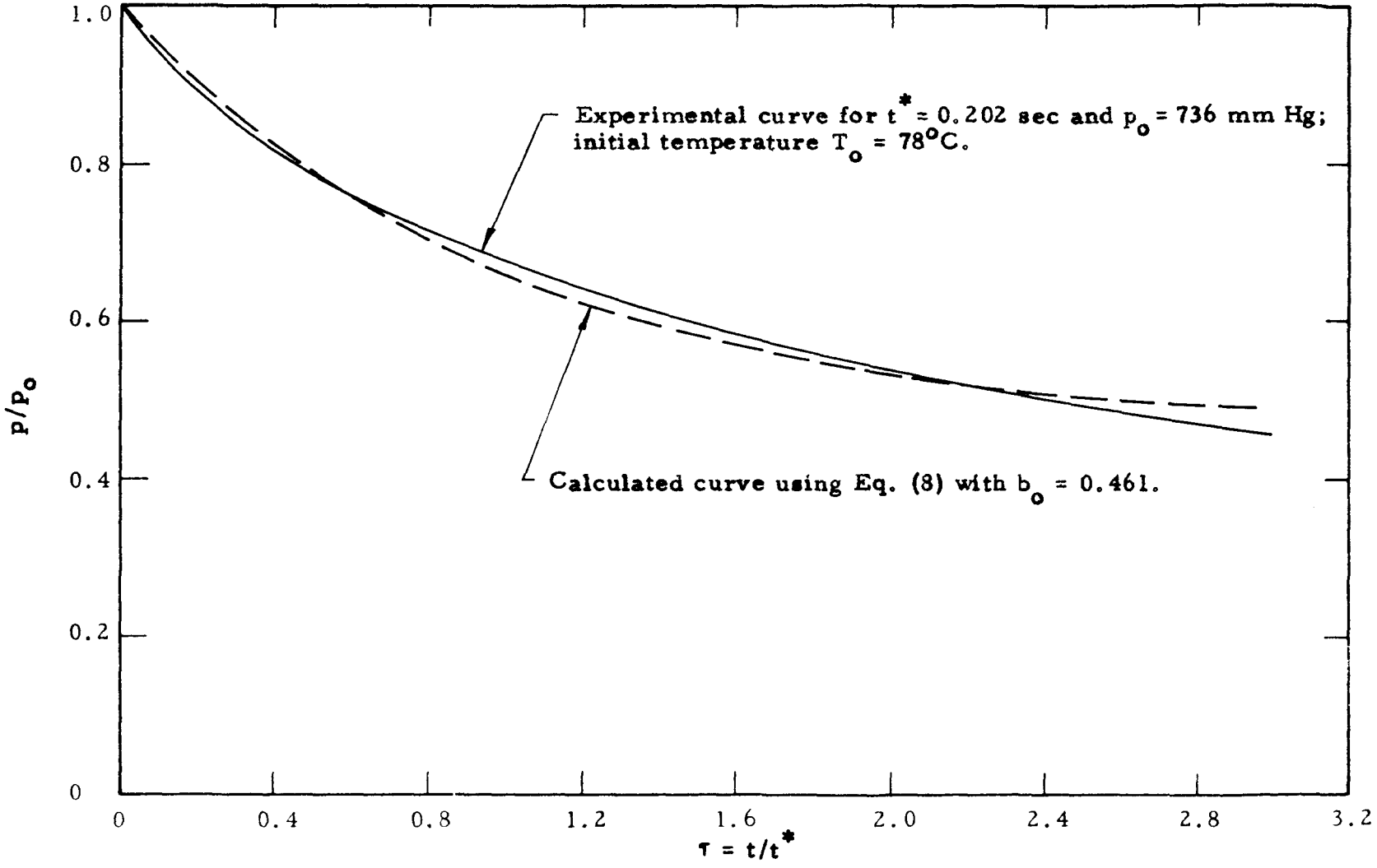

Fig. 14. The reduced pressure p/p_o as a function of the reduced time $\tau = t/t^*$ for CO_2 discharging from a vessel containing silica gel of mesh size 6-16.

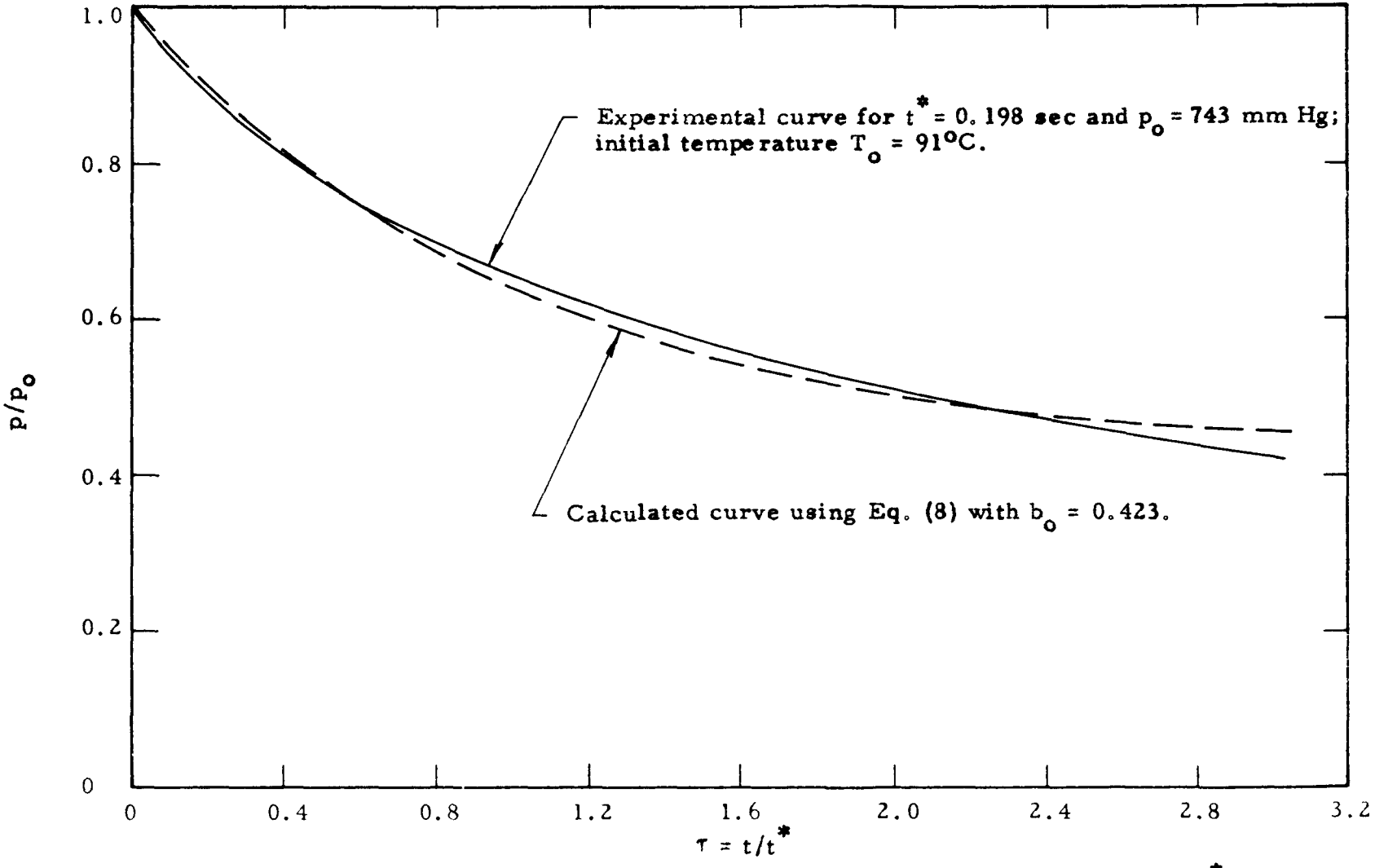

Fig. 15. The reduced pressure p/p_o as a function of the reduced time $\tau = t/t^*$ for CO_2 discharging from a vessel containing silica gel of mesh size 6-16.

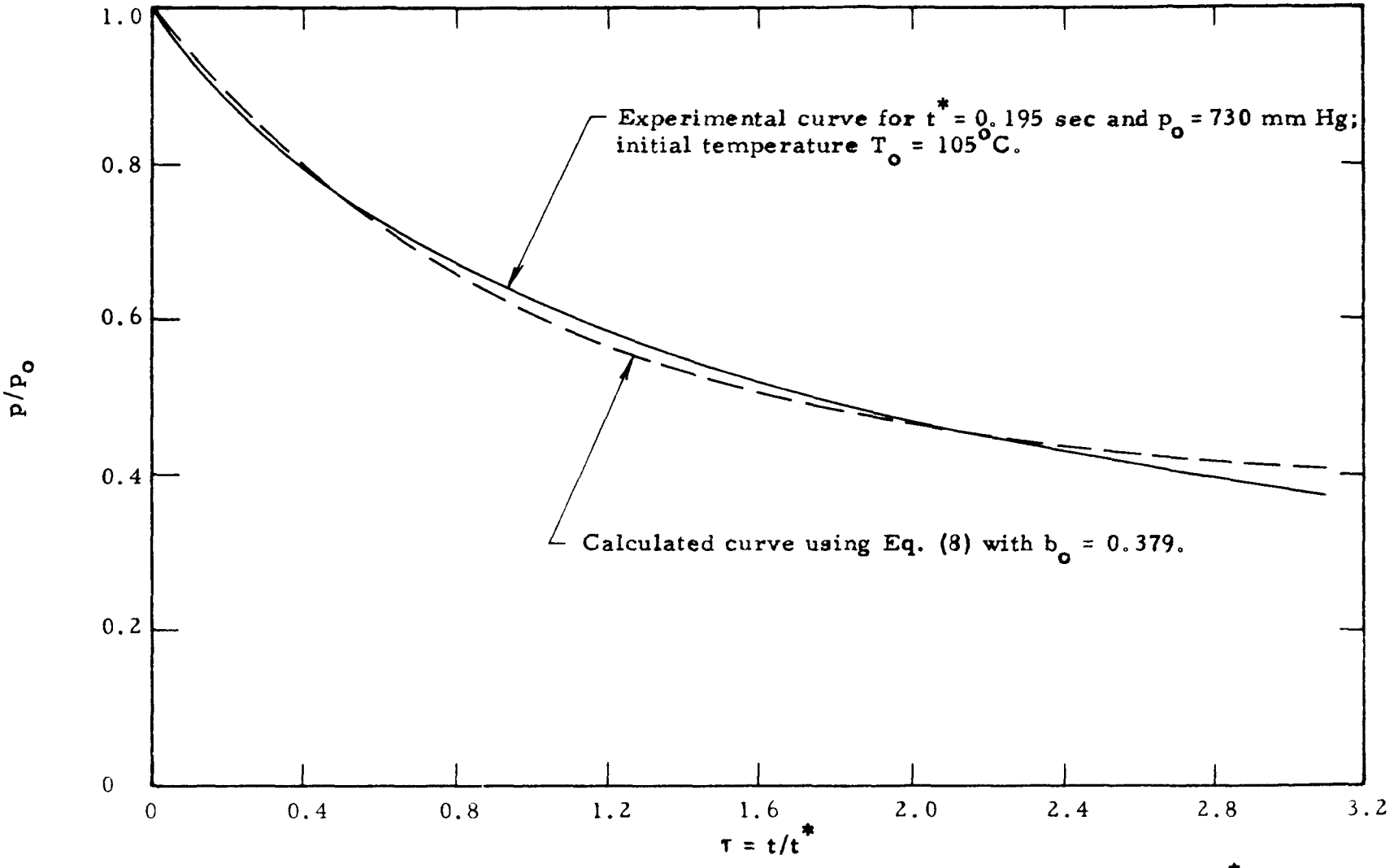

Fig. 16. The reduced pressure p/p_o as a function of the reduced time $\tau = t/t^*$ for CO_2 discharging from a vessel containing silica gel of mesh size 6-16.

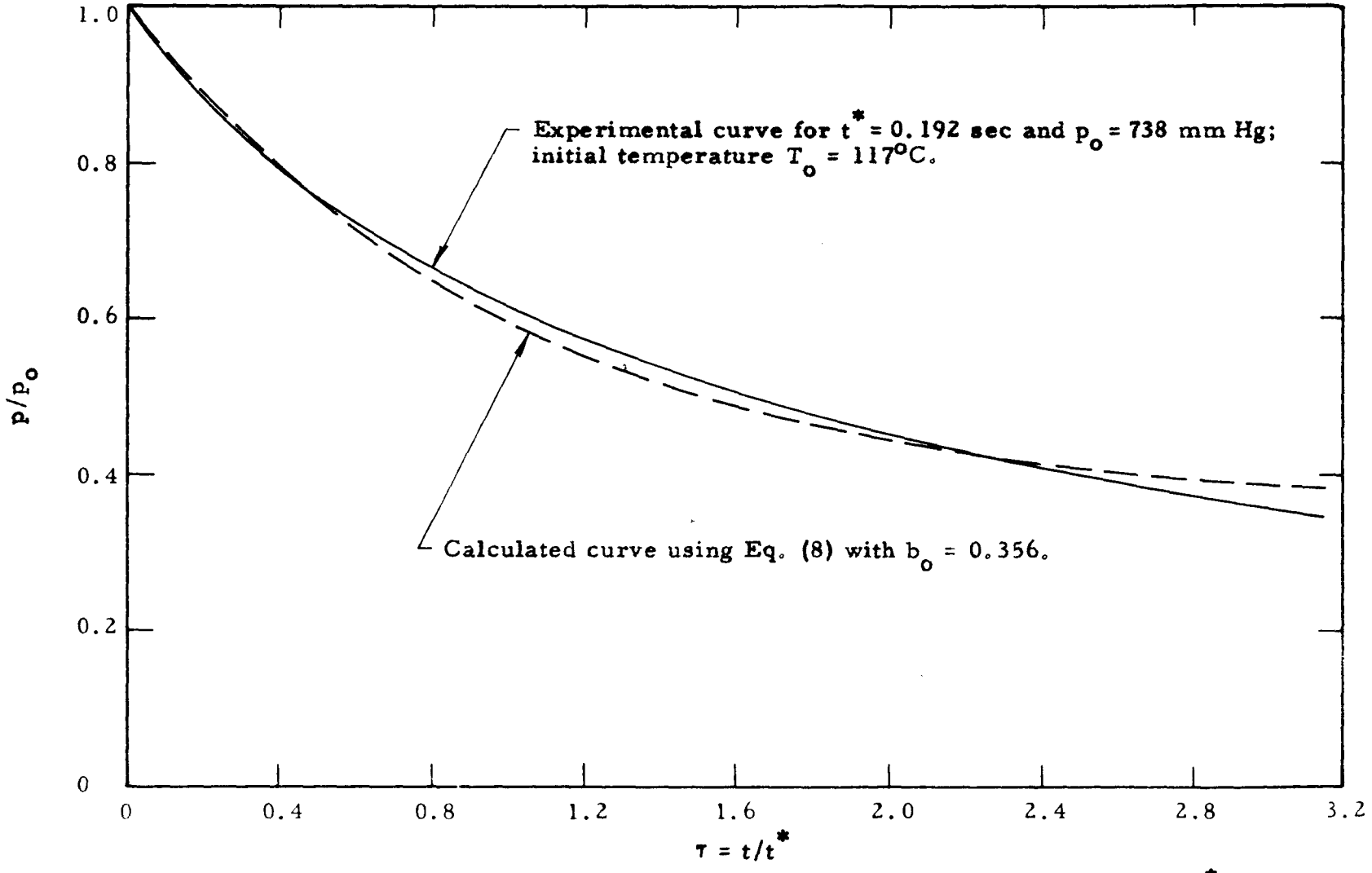

Fig. 17. The reduced pressure p/p_o as a function of the reduced time $\tau = t/t^*$ for CO_2 discharging from a vessel containing silica gel of mesh size 6-16.

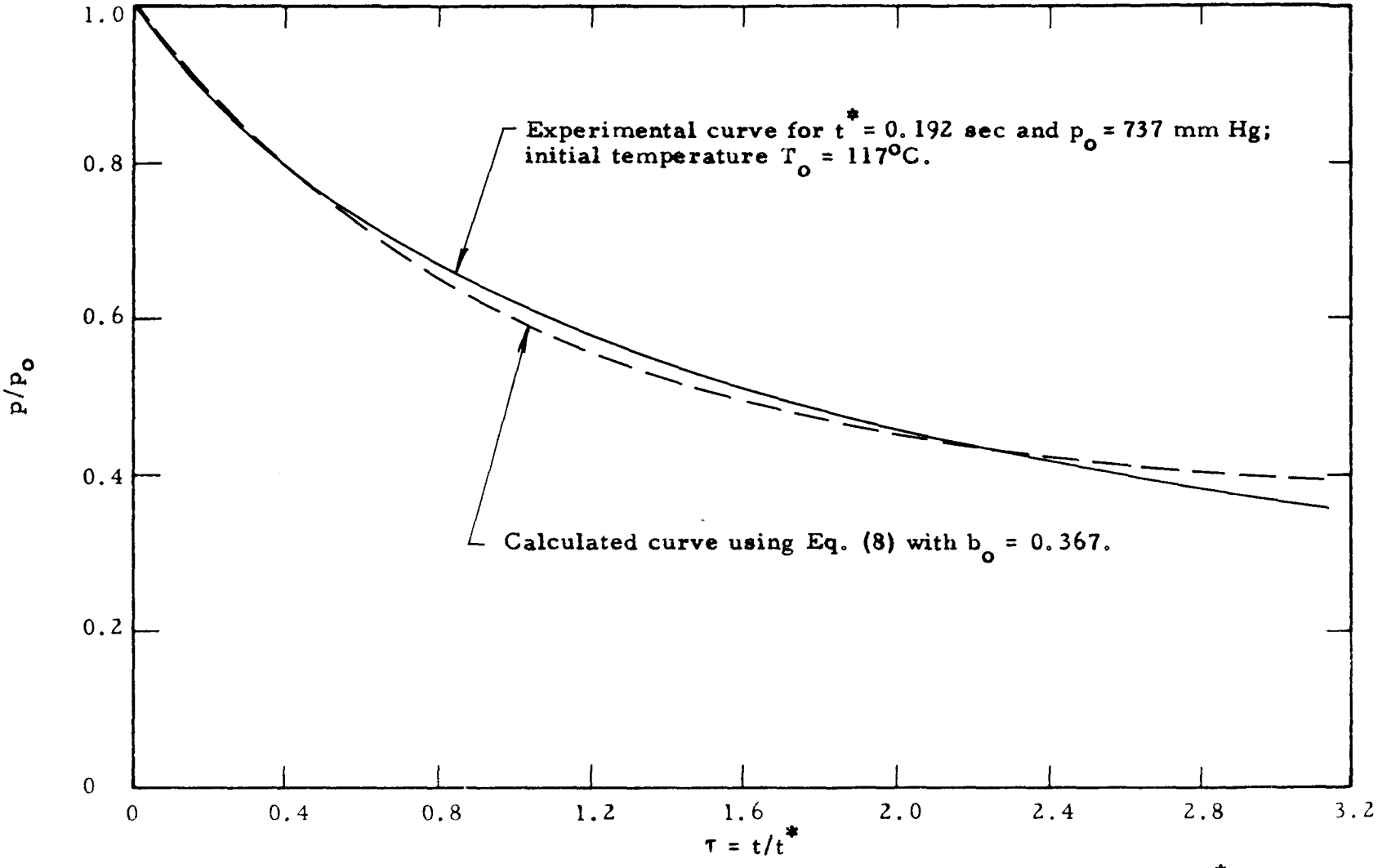

Fig. 18. The reduced pressure p/p_o as a function of the reduced time $\tau = t/t^*$ for CO_2 discharging from a vessel containing silica gel of mesh size 6-16.

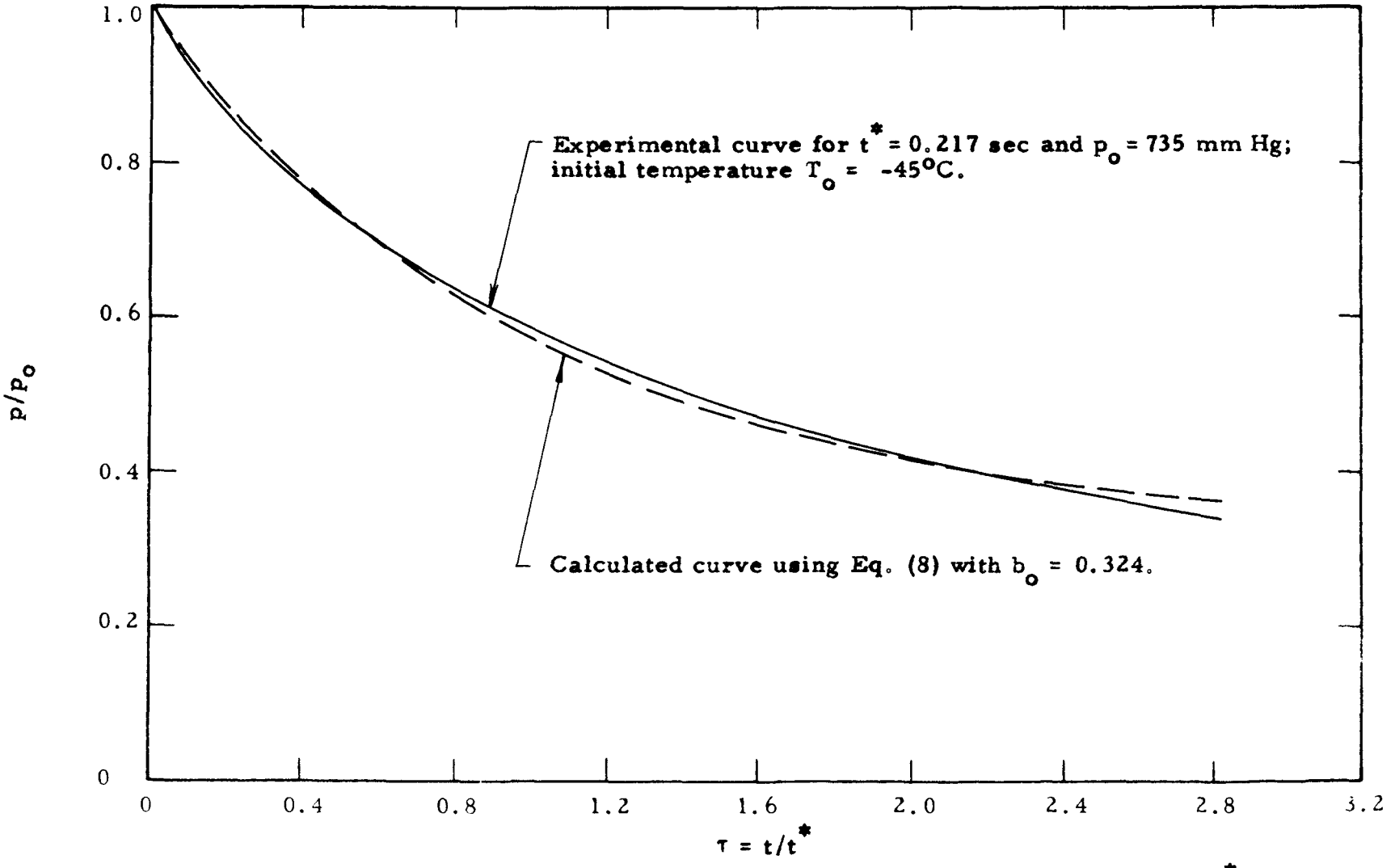

Fig. 19. The reduced pressure p/p_o as a function of the reduced time $\tau = t/t^*$ for Ar discharging from a vessel containing silica gel of mesh size 6-16.

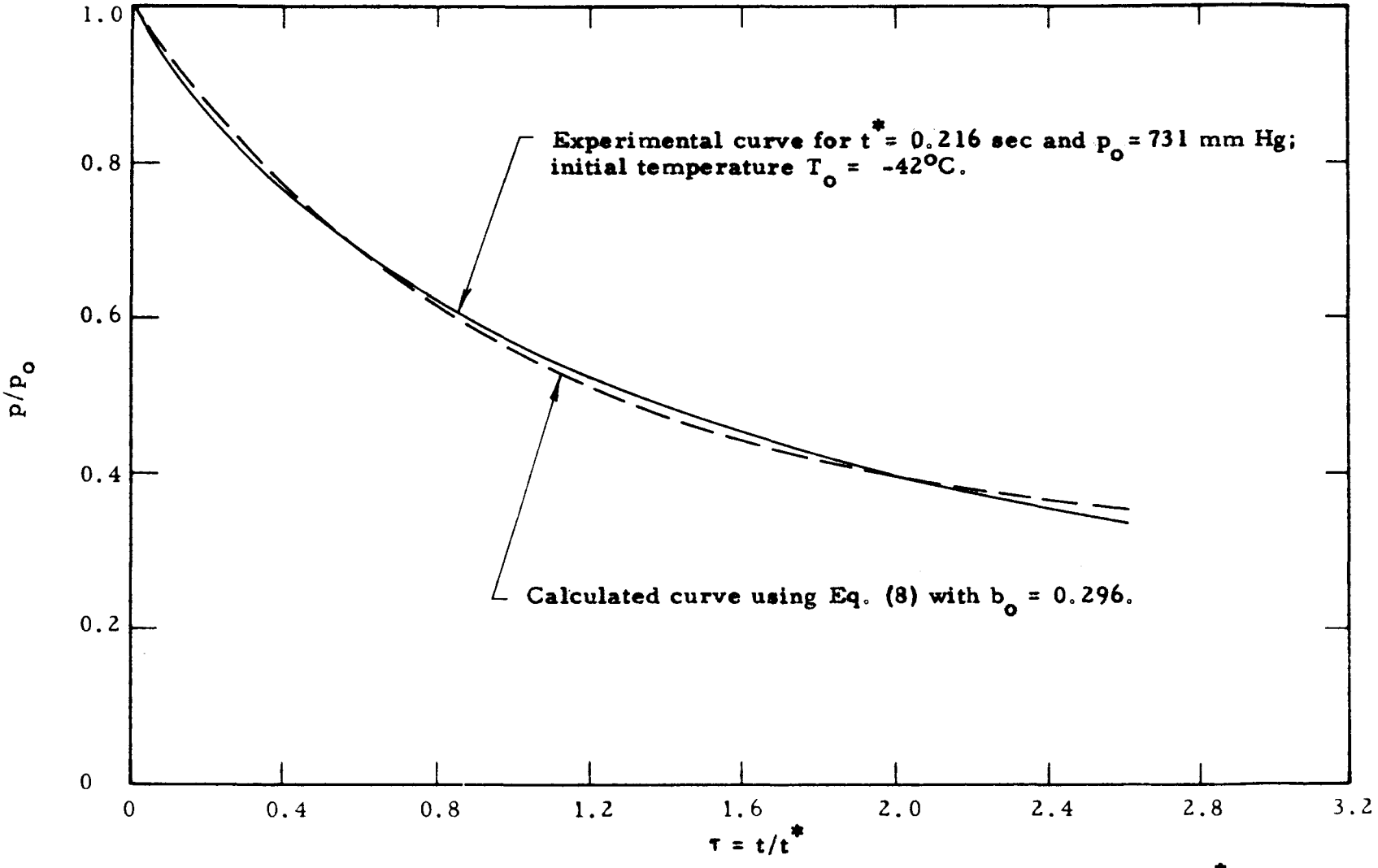

Fig. 20. The reduced pressure p/p_o as a function of the reduced time $\tau = t/t^*$ for Ar discharging from a vessel containing silica gel of mesh size 6-16.

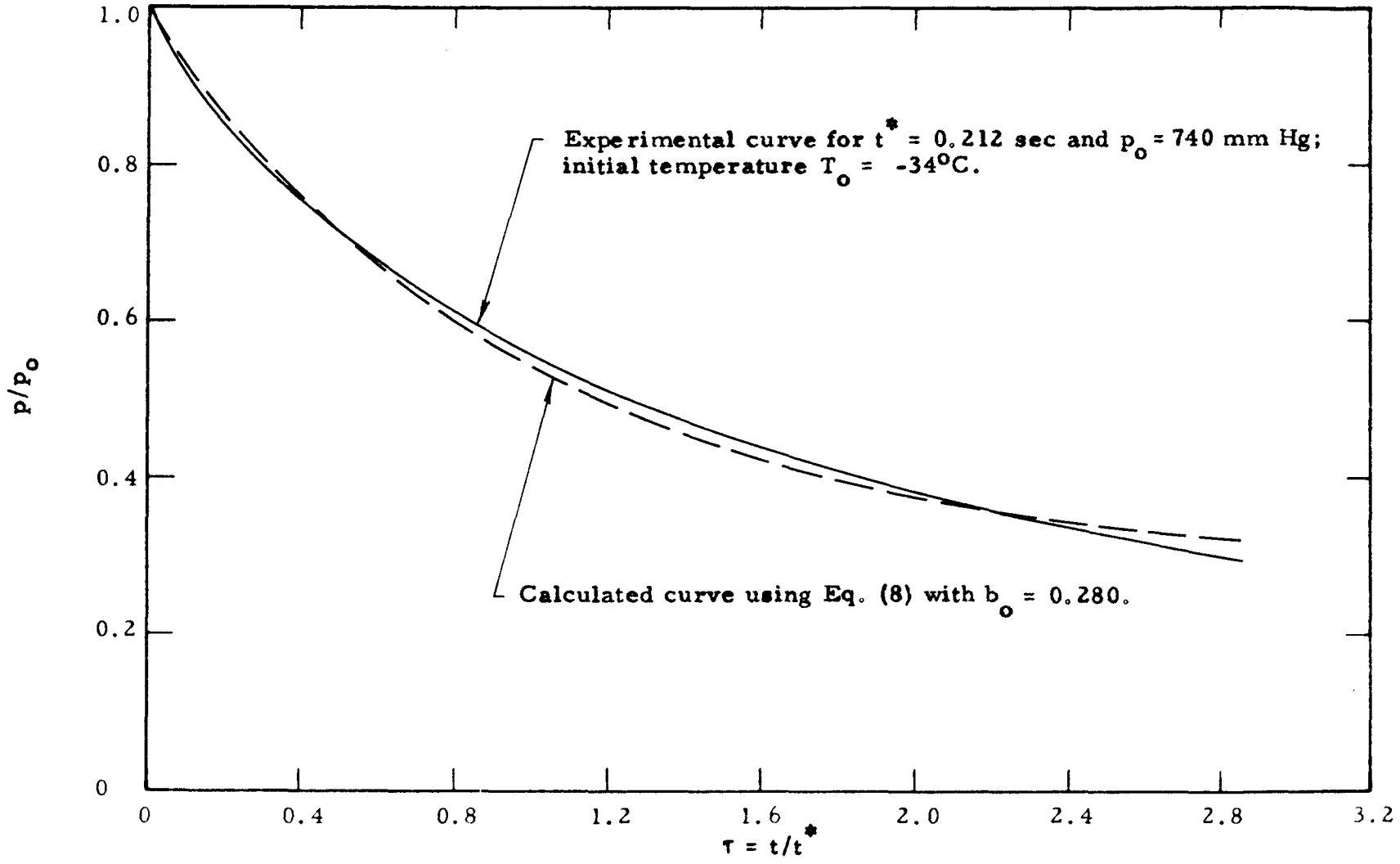

Fig. 21. The reduced pressure p/p_o as a function of the reduced time $\tau = t/t^*$ for Ar discharging from a vessel containing silica gel of mesh size 6-16.

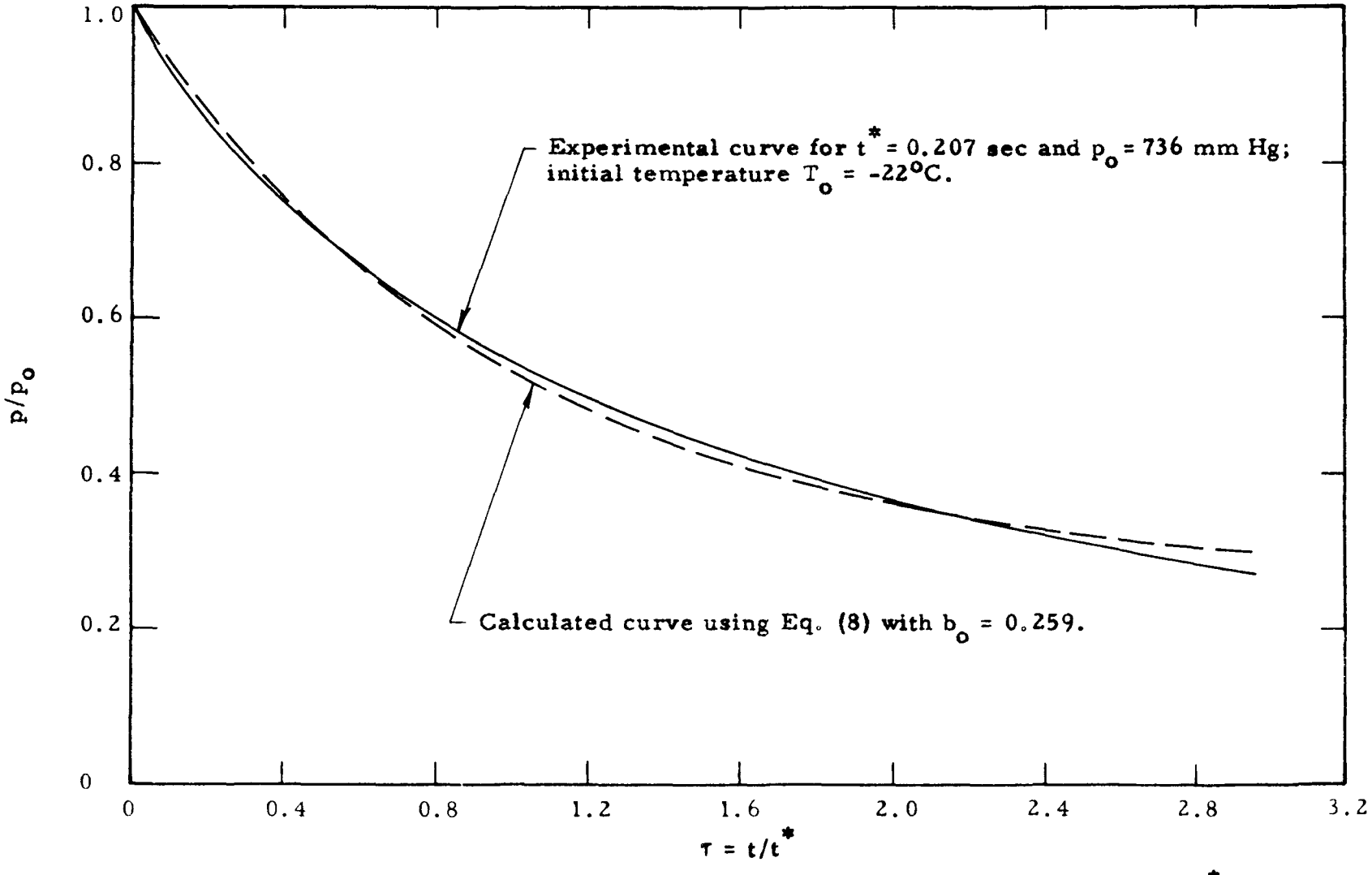

Fig. 22. The reduced pressure p/p_o as a function of the reduced time $\tau = t/t^*$ for Ar discharging from a vessel containing silica gel of mesh size 6-16.

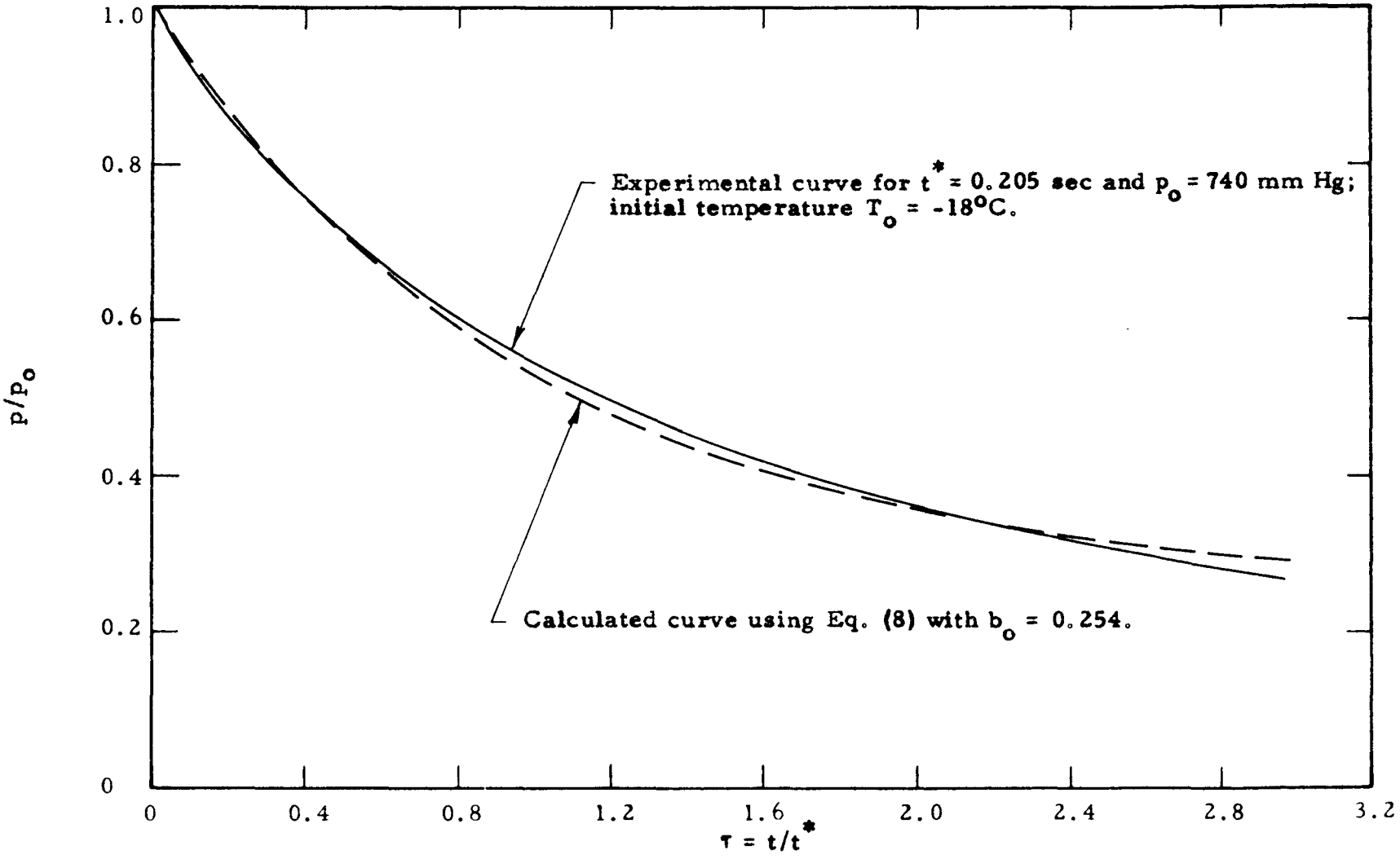

Fig. 23. The reduced pressure p/p_o as a function of the reduced time $\tau = t/t^*$ for Ar discharging from a vessel containing silica gel of mesh size 6-16.

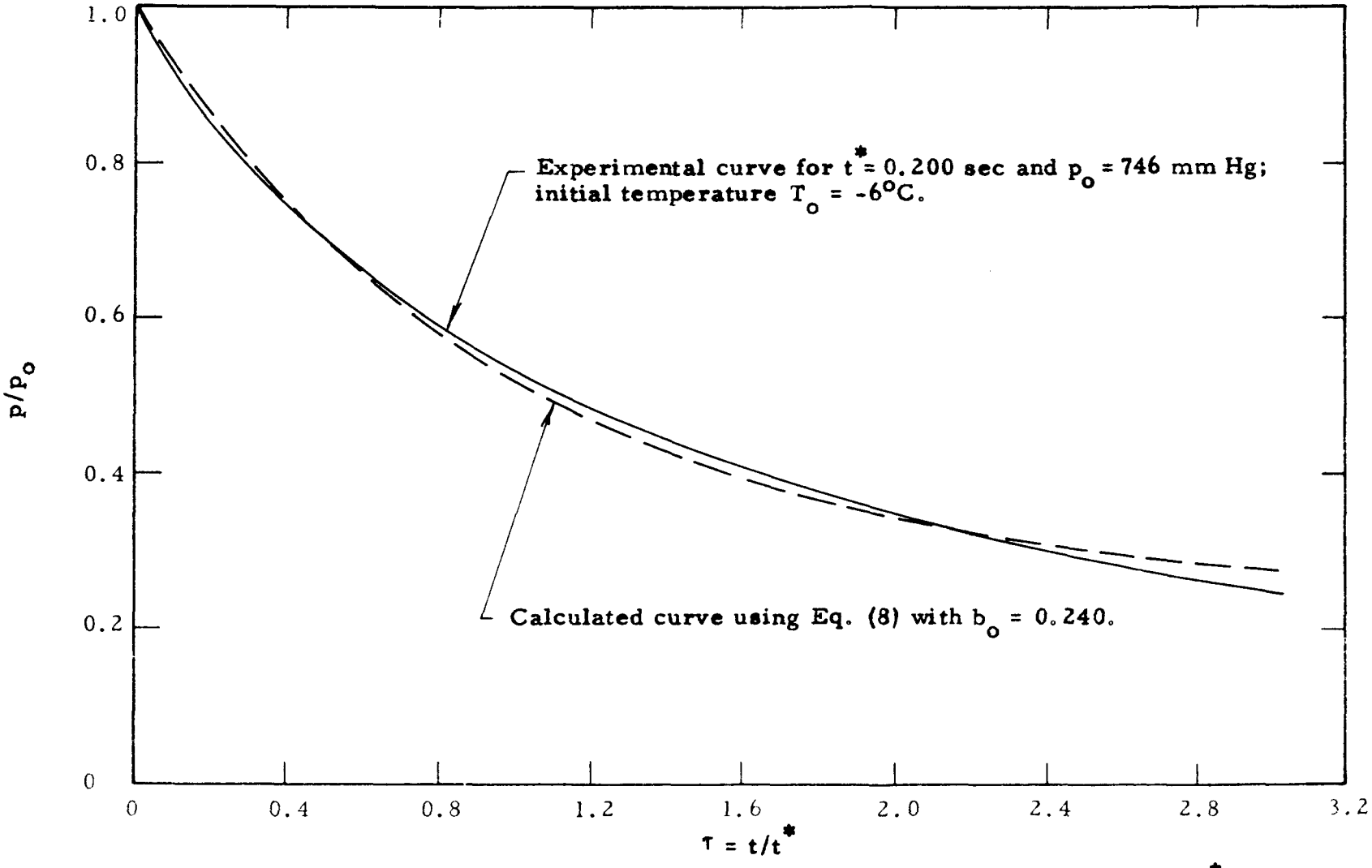

Fig. 24. The reduced pressure p/p_o as a function of the reduced time $\tau = t/t^*$ for Ar discharging from a vessel containing silica gel of mesh size 6-16.

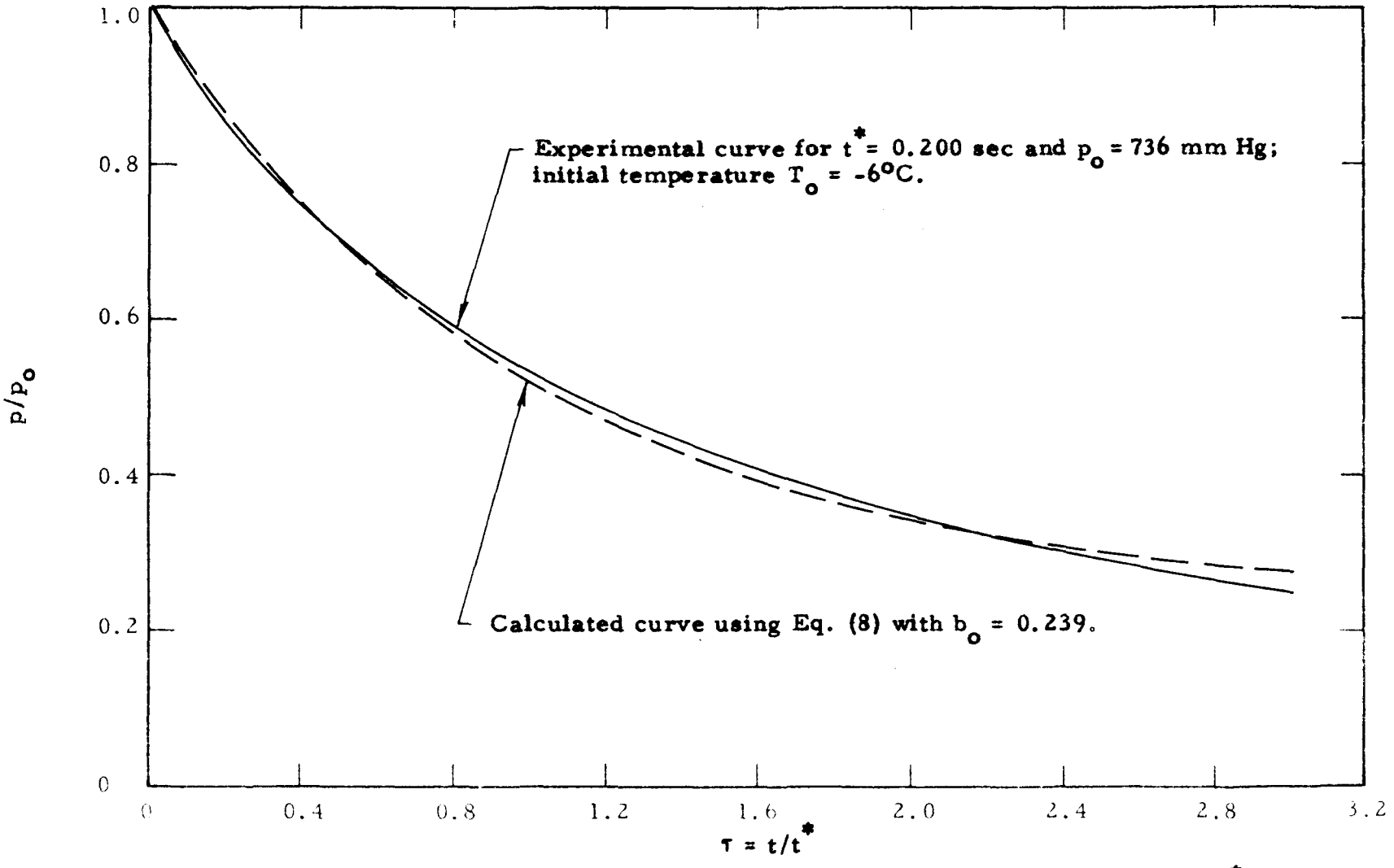

Fig. 25. The reduced pressure p/p_o as a function of the reduced time $\tau = t/t^*$ for Ar discharging from a vessel containing silica gel of mesh size 6-16.

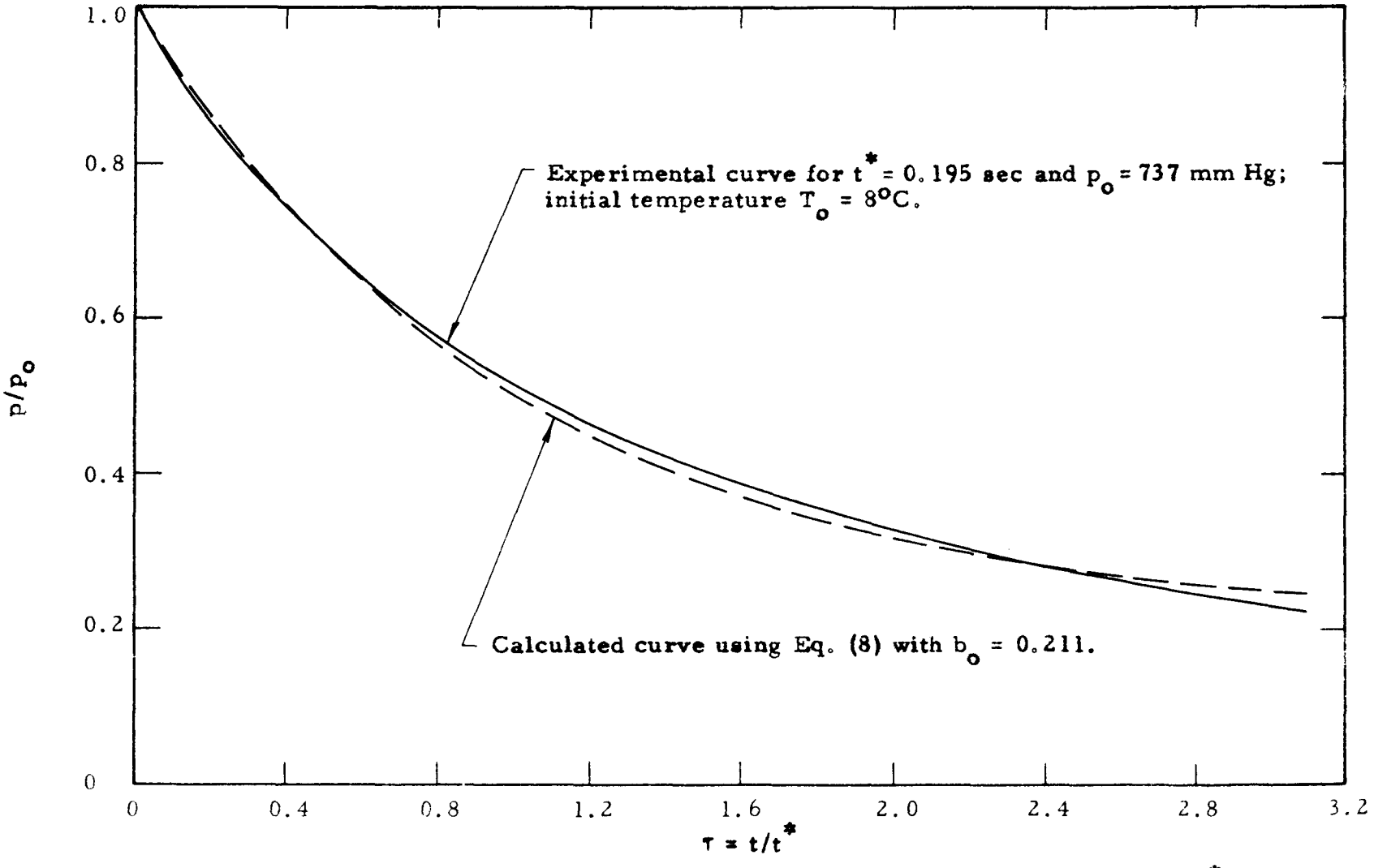

Fig. 26. The reduced pressure p/p_o as a function of the reduced time $\tau = t/t^*$ for Ar discharging from a vessel containing silica gel of mesh size 6-16.

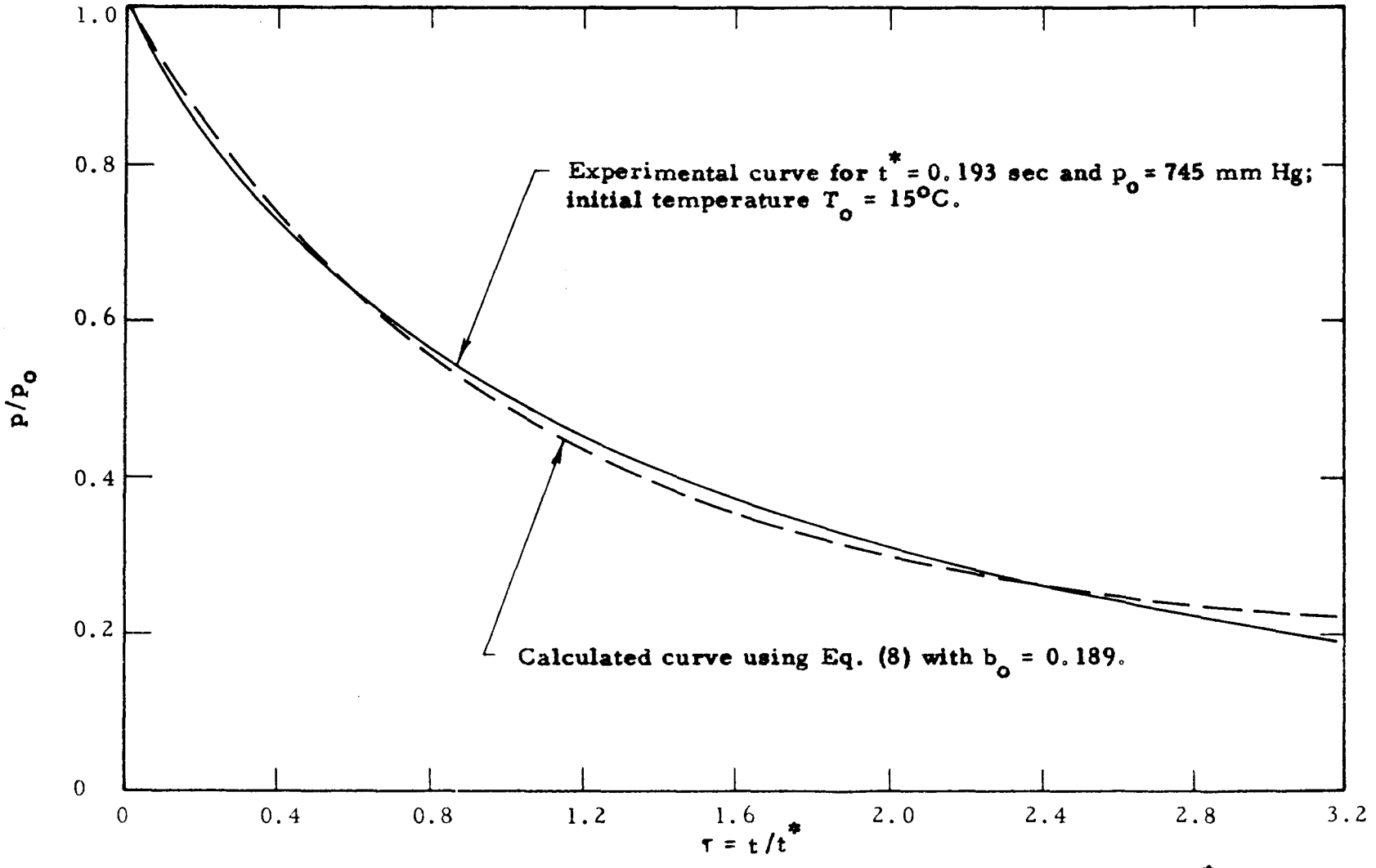

Fig. 27. The reduced pressure p/p_o as a function of the reduced time $\tau = t/t^*$ for Ar discharging from a vessel containing silica gel of mesh size 6-16.

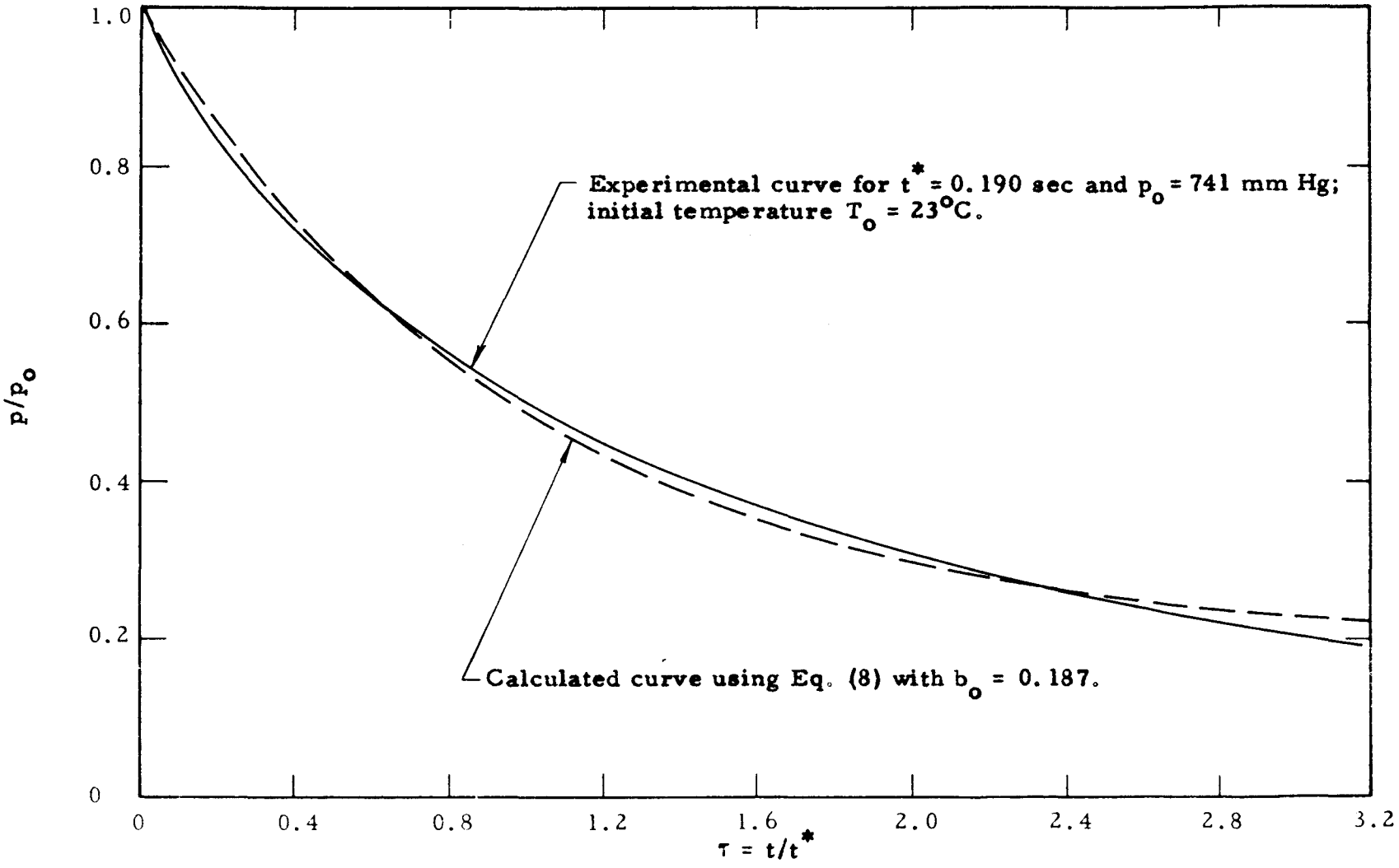

Fig. 28 The reduced pressure p/p_o as a function of the reduced time $\tau = t/t^*$ for Ar discharging from a vessel containing silica gel of mesh size 6-16.

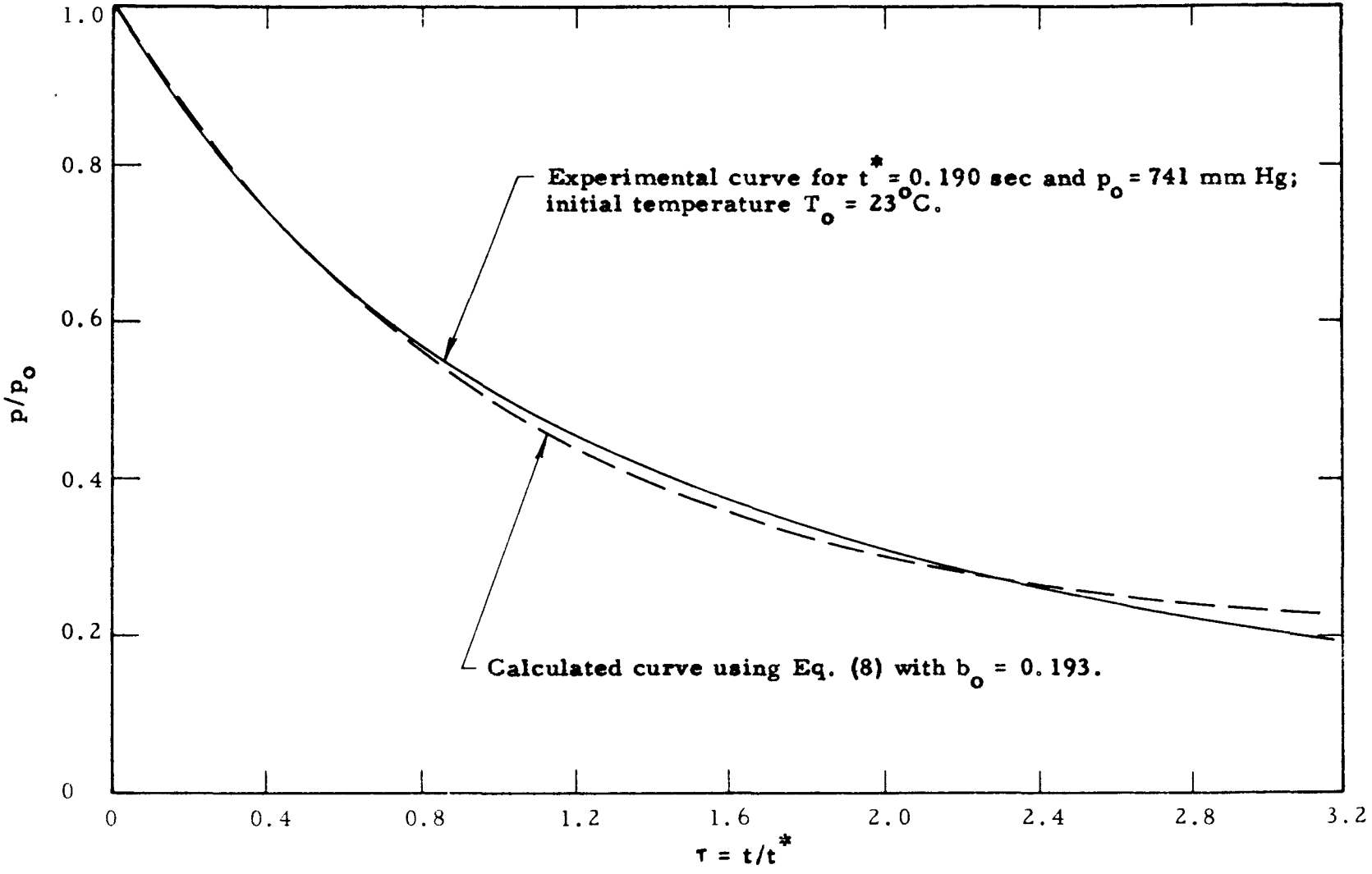

Fig. 29. The reduced pressure p/p_o as a function of the reduced time $\tau = t/t^*$ for Ar discharging from a vessel containing silica gel of mesh size 6-16.

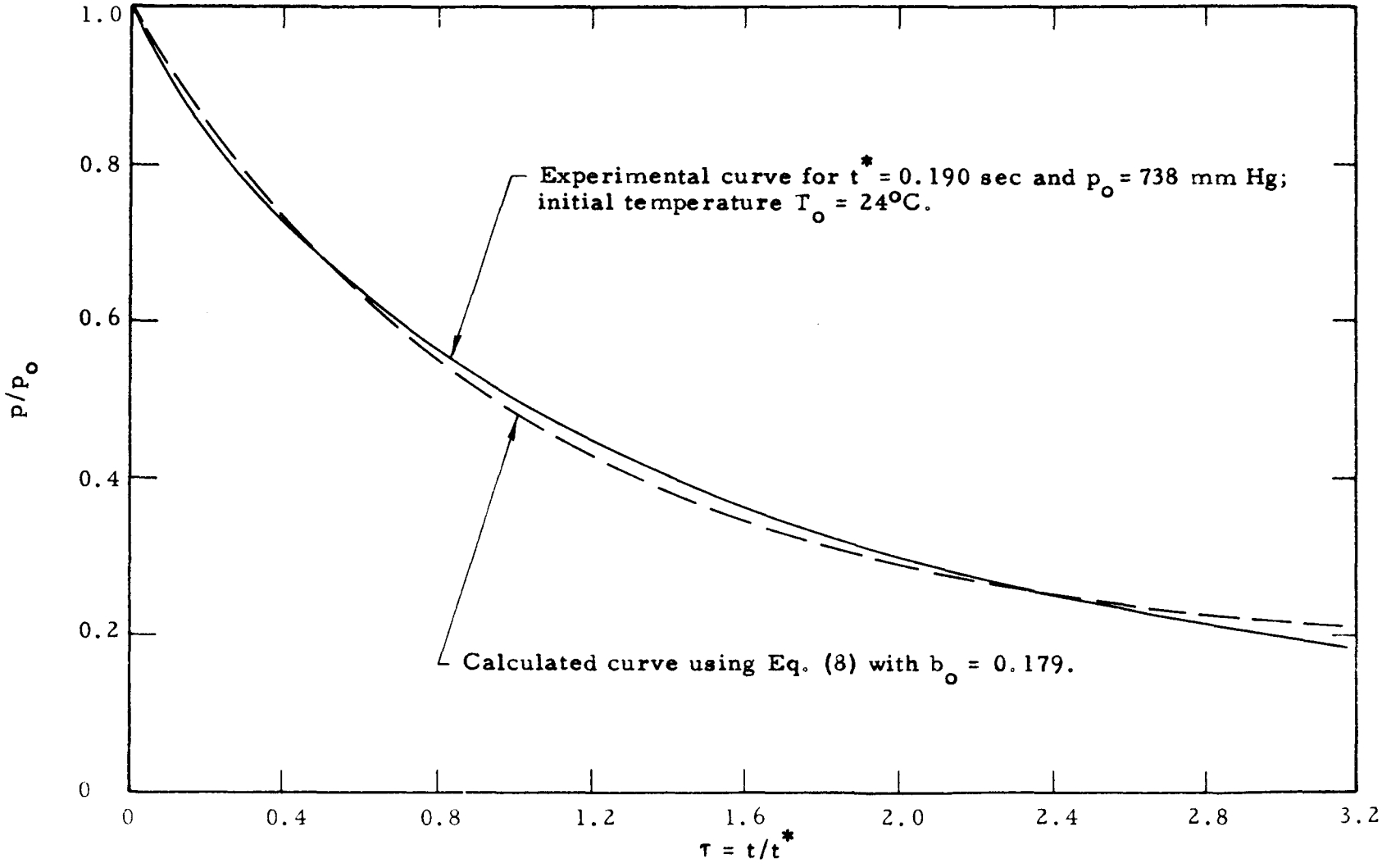

Fig. 30. The reduced pressure p/p_o as a function of the reduced time $\tau = t/t^*$ for Ar discharging from a vessel containing silica gel of mesh size 6-16.

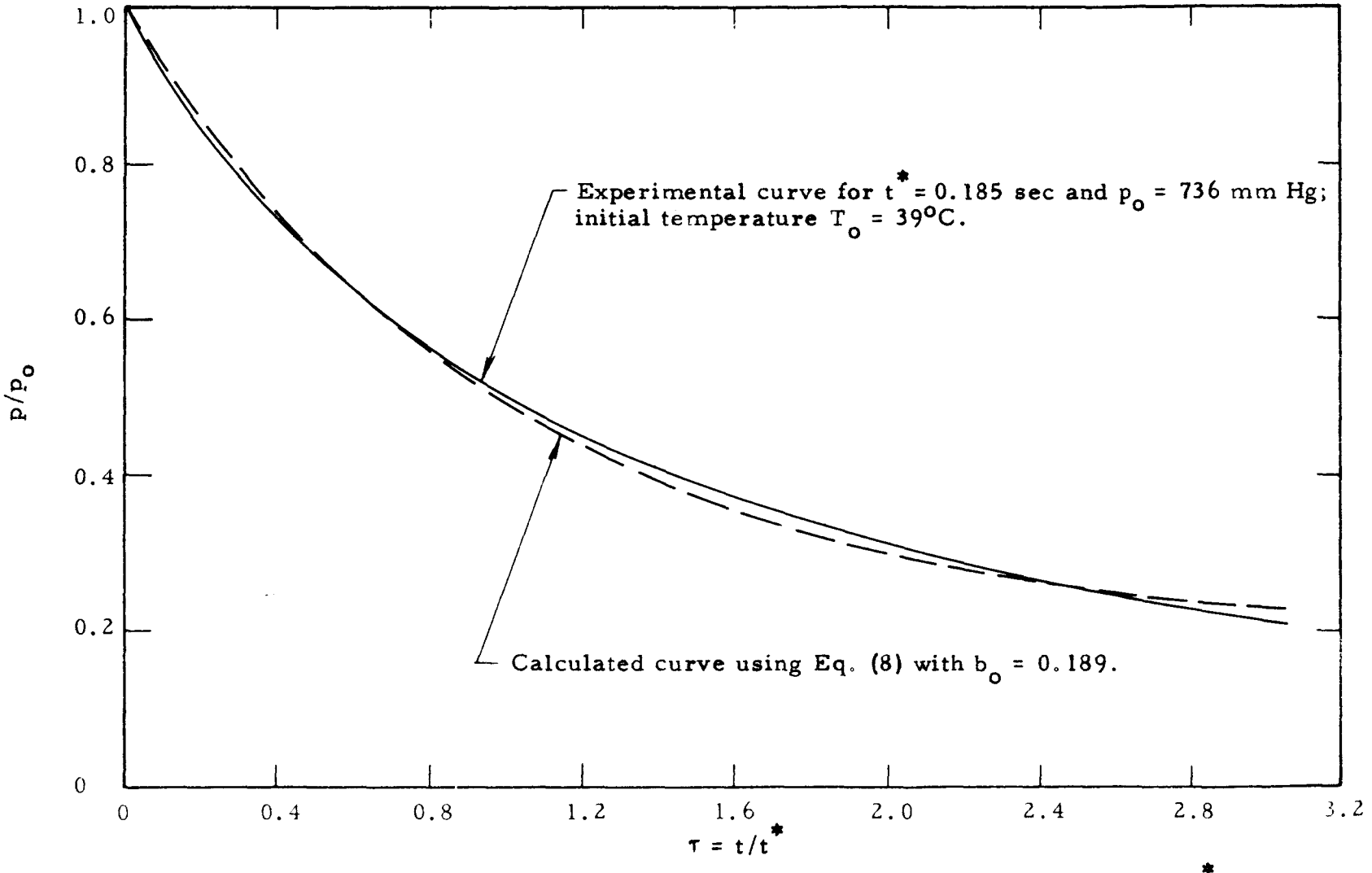

Fig. 31. The reduced pressure p/p_o as a function of the reduced time $\tau = t/t^*$ for Ar discharging from a vessel containing silica gel of mesh size 6-16.

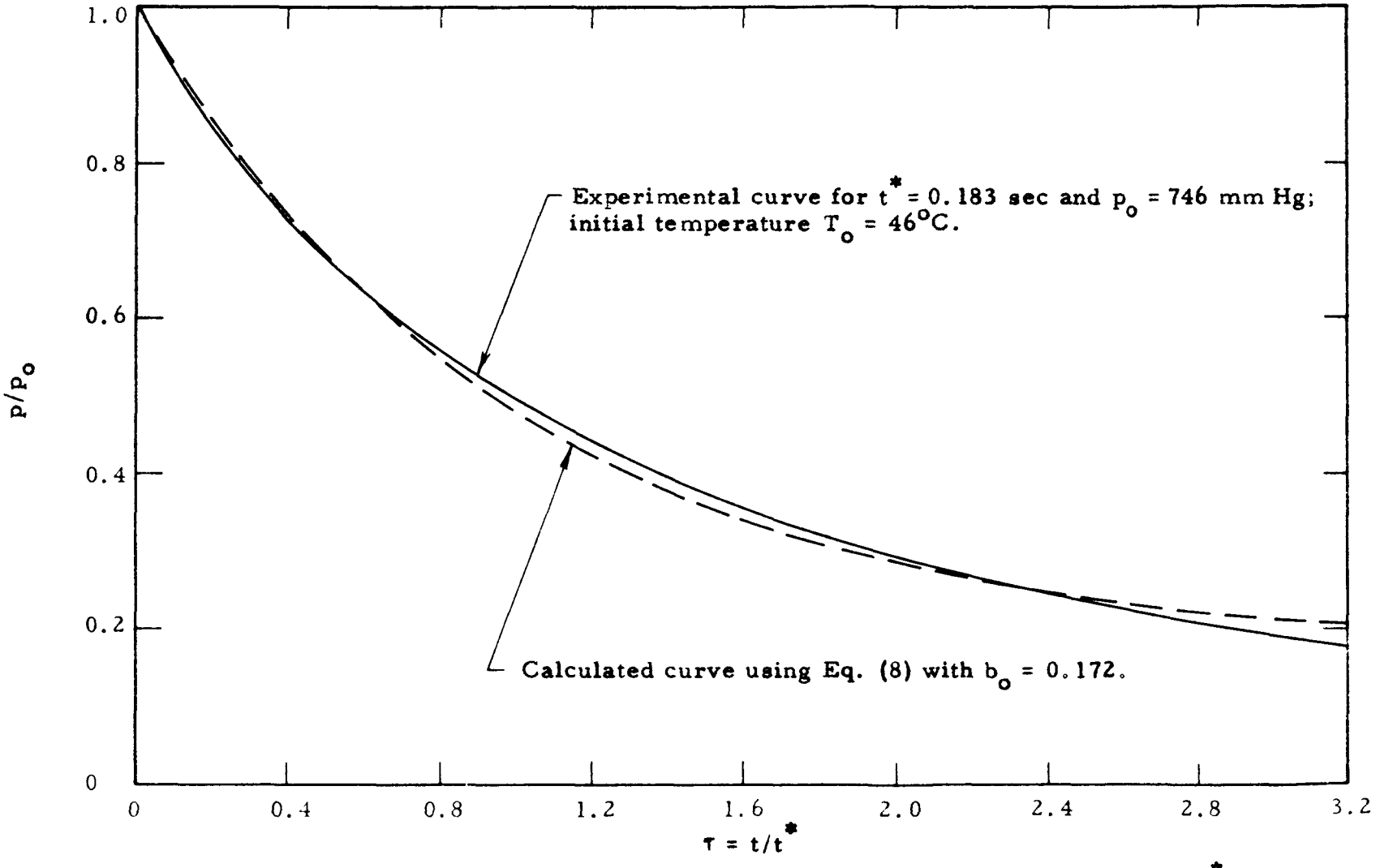

Fig. 32. The reduced pressure p/p_o as a function of the reduced time $\tau = t/t^*$ for Ar discharging from a vessel containing silica gel of mesh size 6-16.

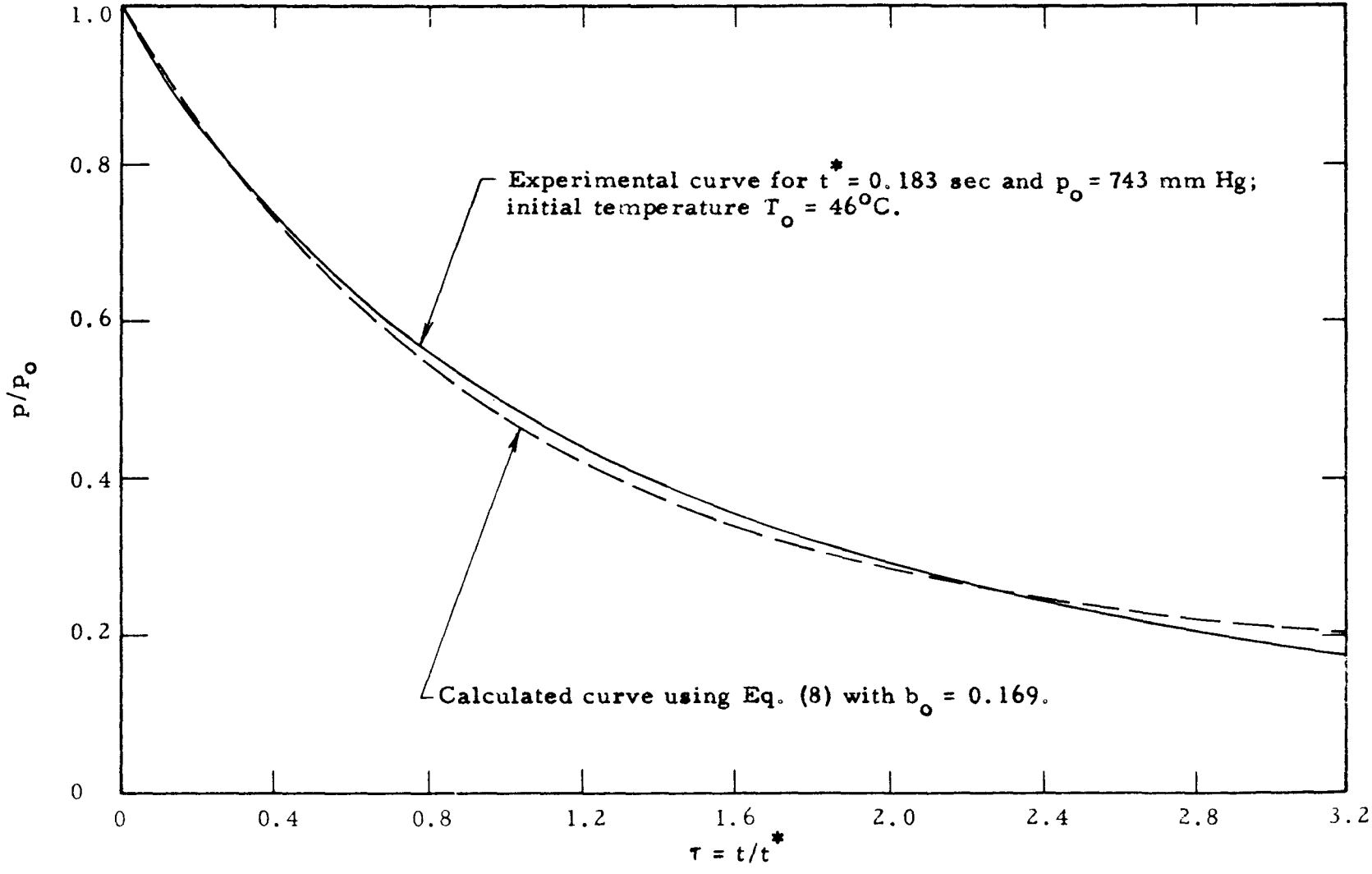

Fig. 33. The reduced pressure p/p_o as a function of the reduced time $\tau = t/t^*$ for Ar discharging from a vessel containing silica gel of mesh size 6-16.

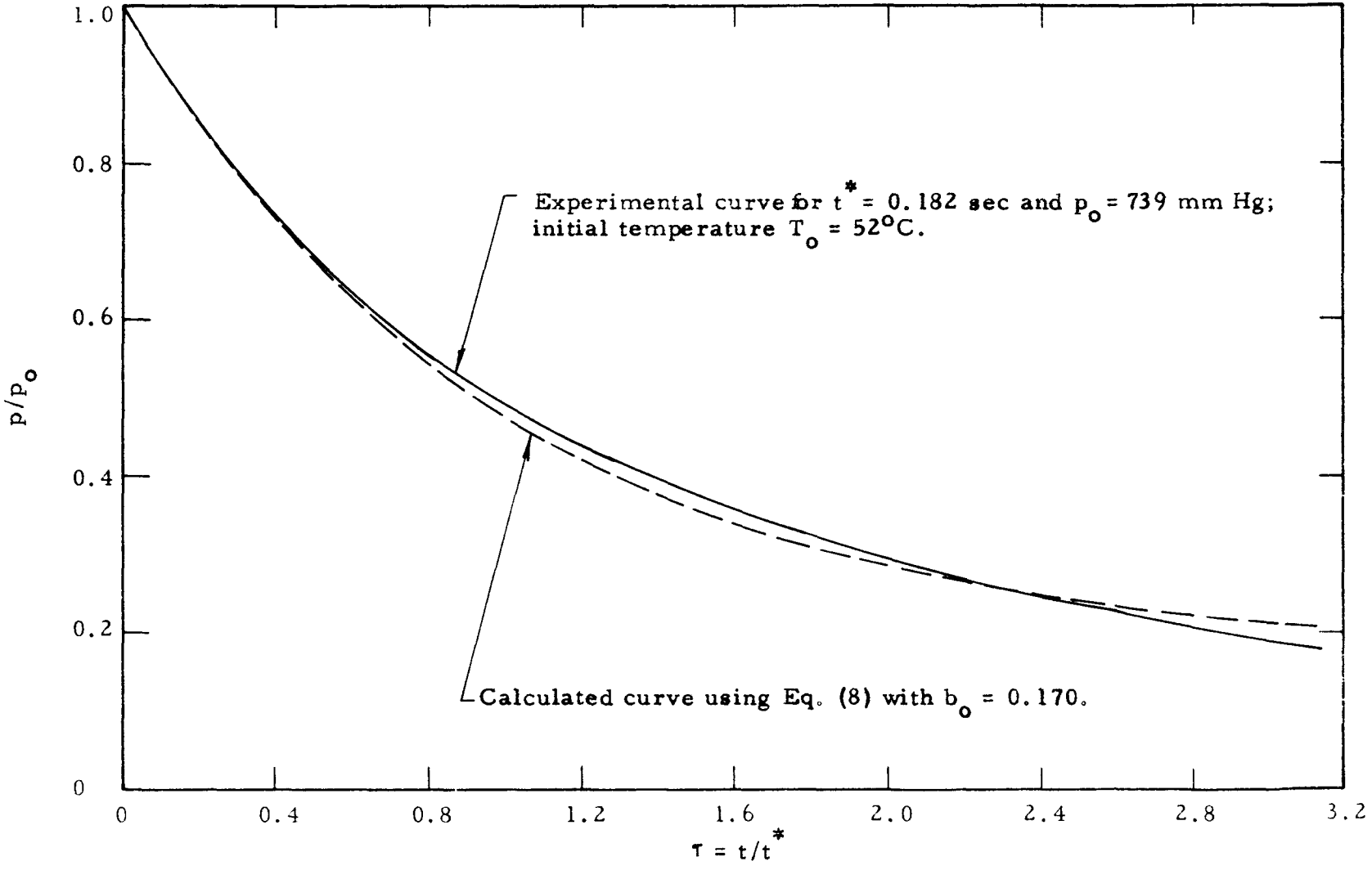

Fig. 34. The reduced pressure p/p_o as a function of the reduced time $\tau = t/t^*$ for Ar discharging from a vessel containing silica gel of mesh size 6-16.

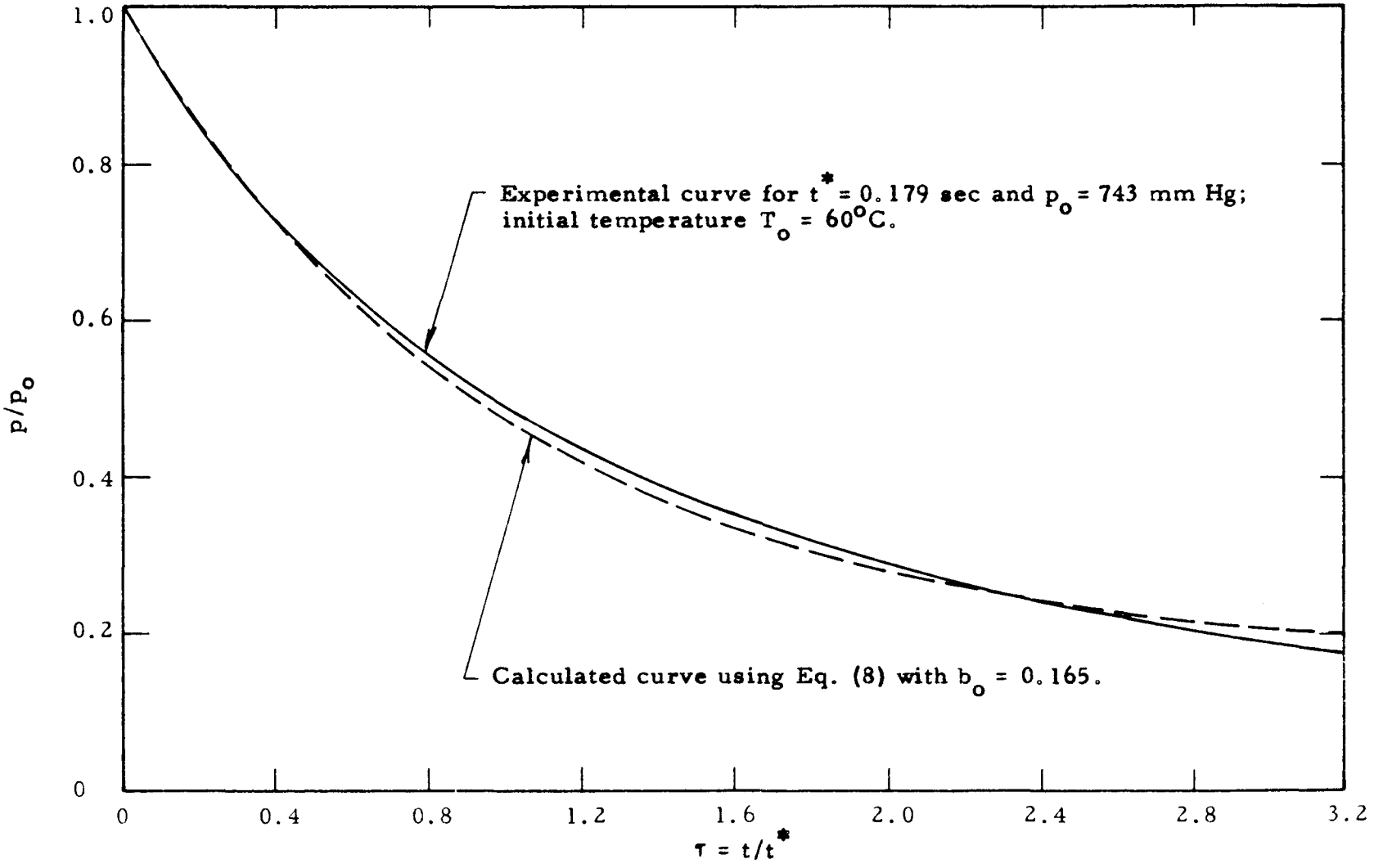

Fig. 35. The reduced pressure p/p_o as a function of the reduced time $\tau = t/t^*$ for Ar discharging from a vessel containing silica gel of mesh size 6-16.

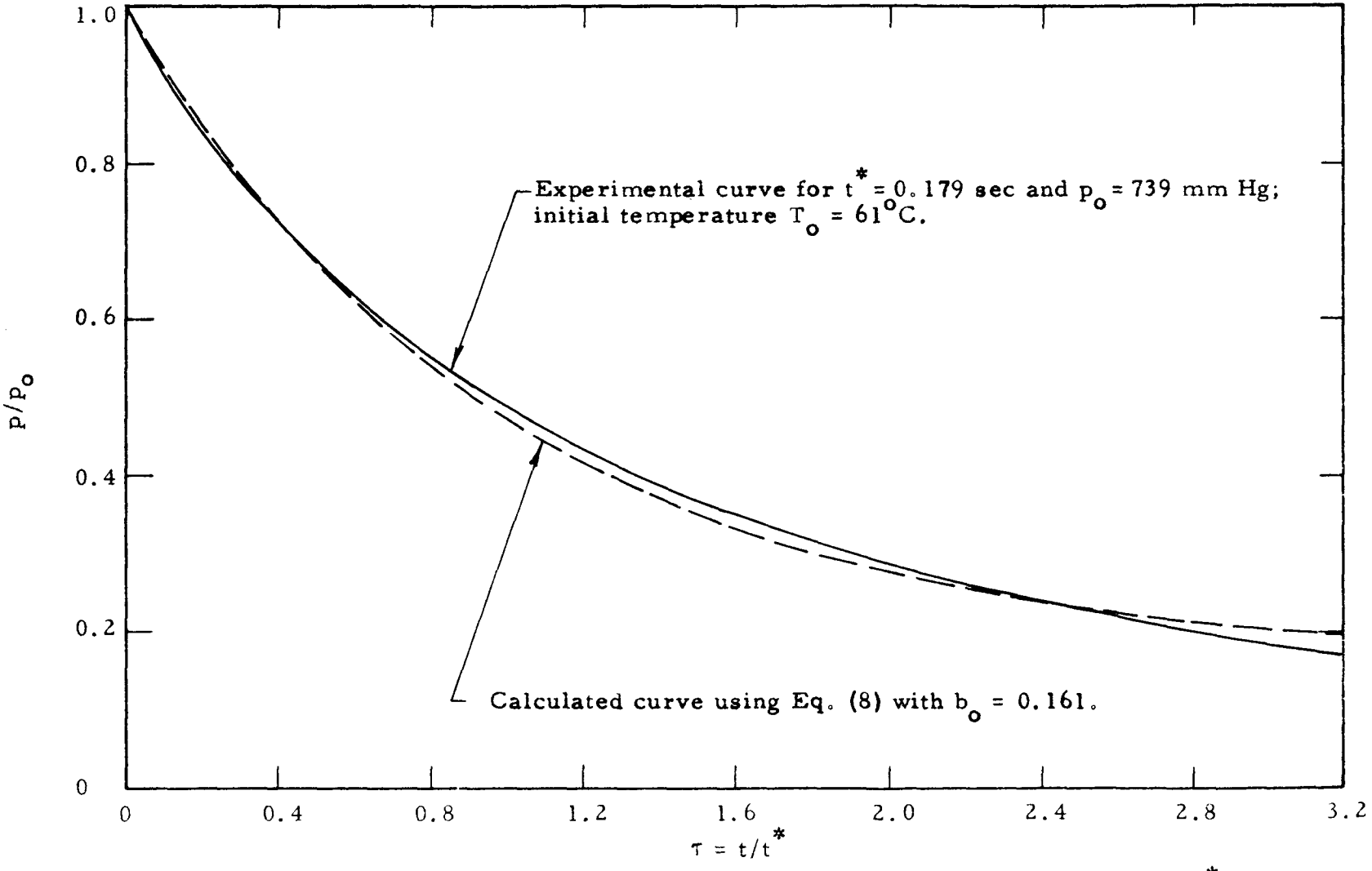

Fig. 36. The reduced pressure p/p_o as a function of the reduced time $\tau = t/t^*$ for Ar discharging from a vessel containing silica gel of mesh size 6-16.

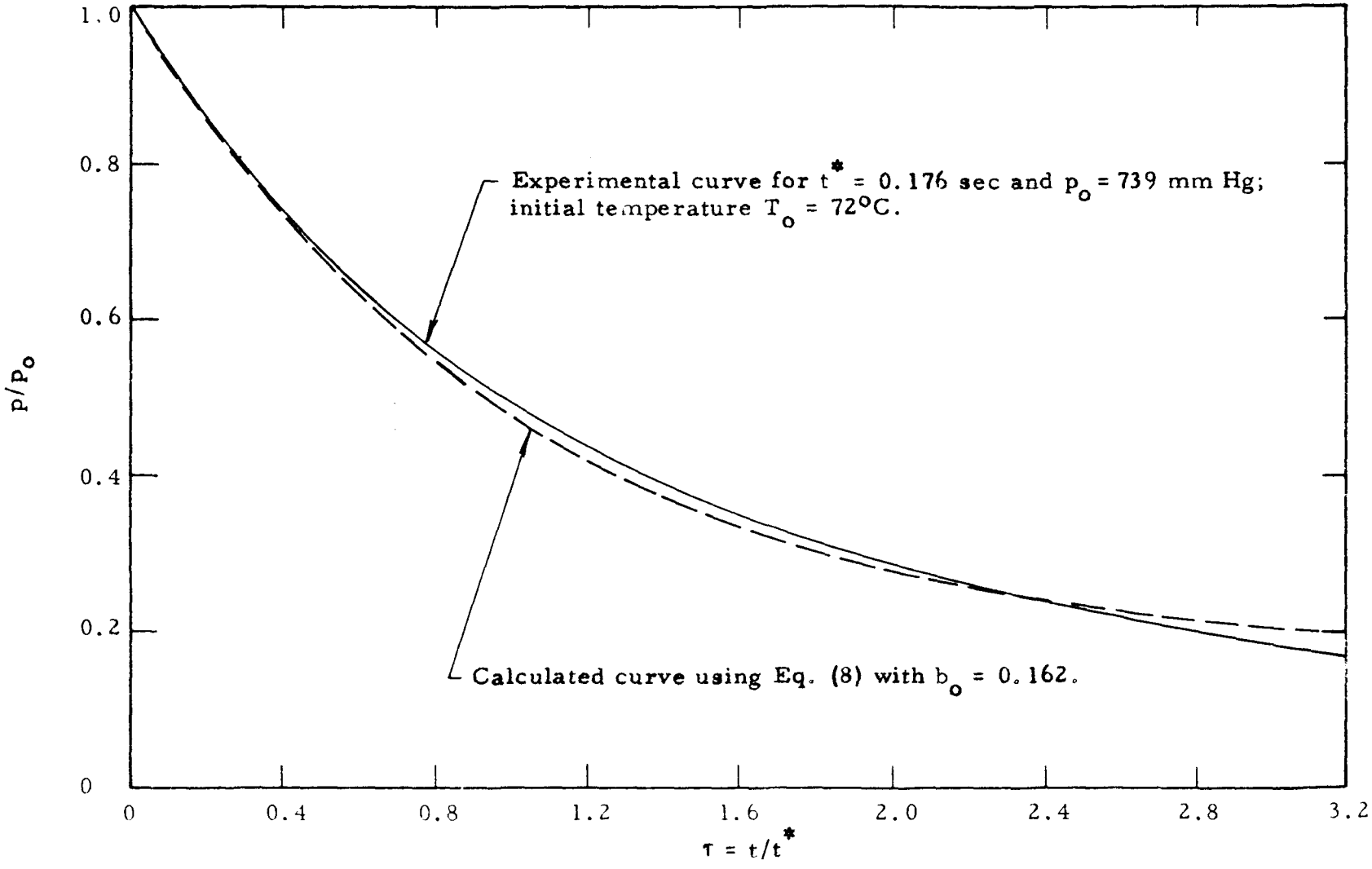

Fig. 37 The reduced pressure p/p_o as a function of the reduced time $\tau = t/t^*$ for Ar discharging from a vessel containing silica gel of mesh size 6-16.

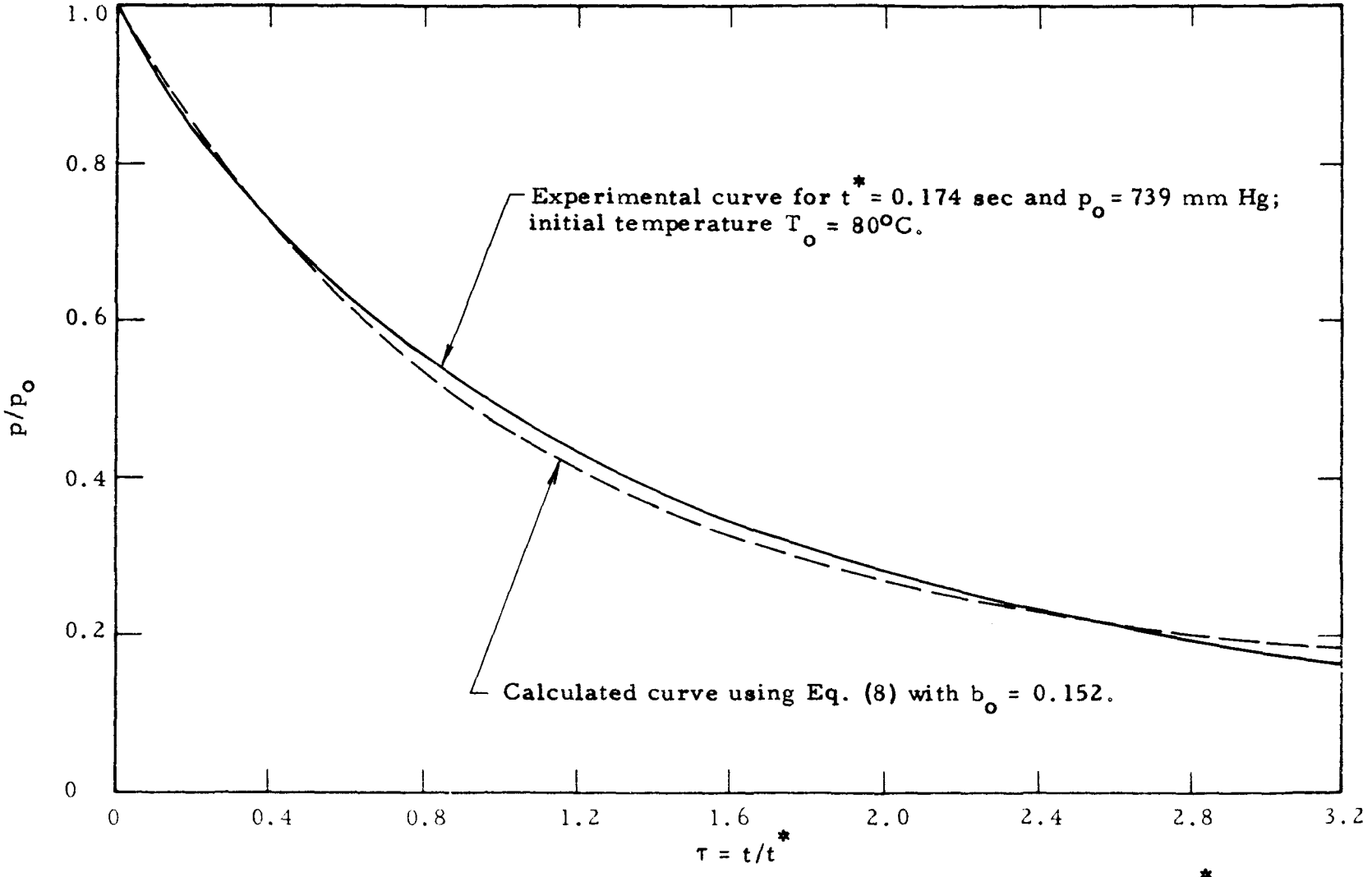

Fig. 38. The reduced pressure p/p_o as a function of the reduced time $\tau = t/t^*$ for Ar discharging from a vessel containing silica gel of mesh size 6-16.

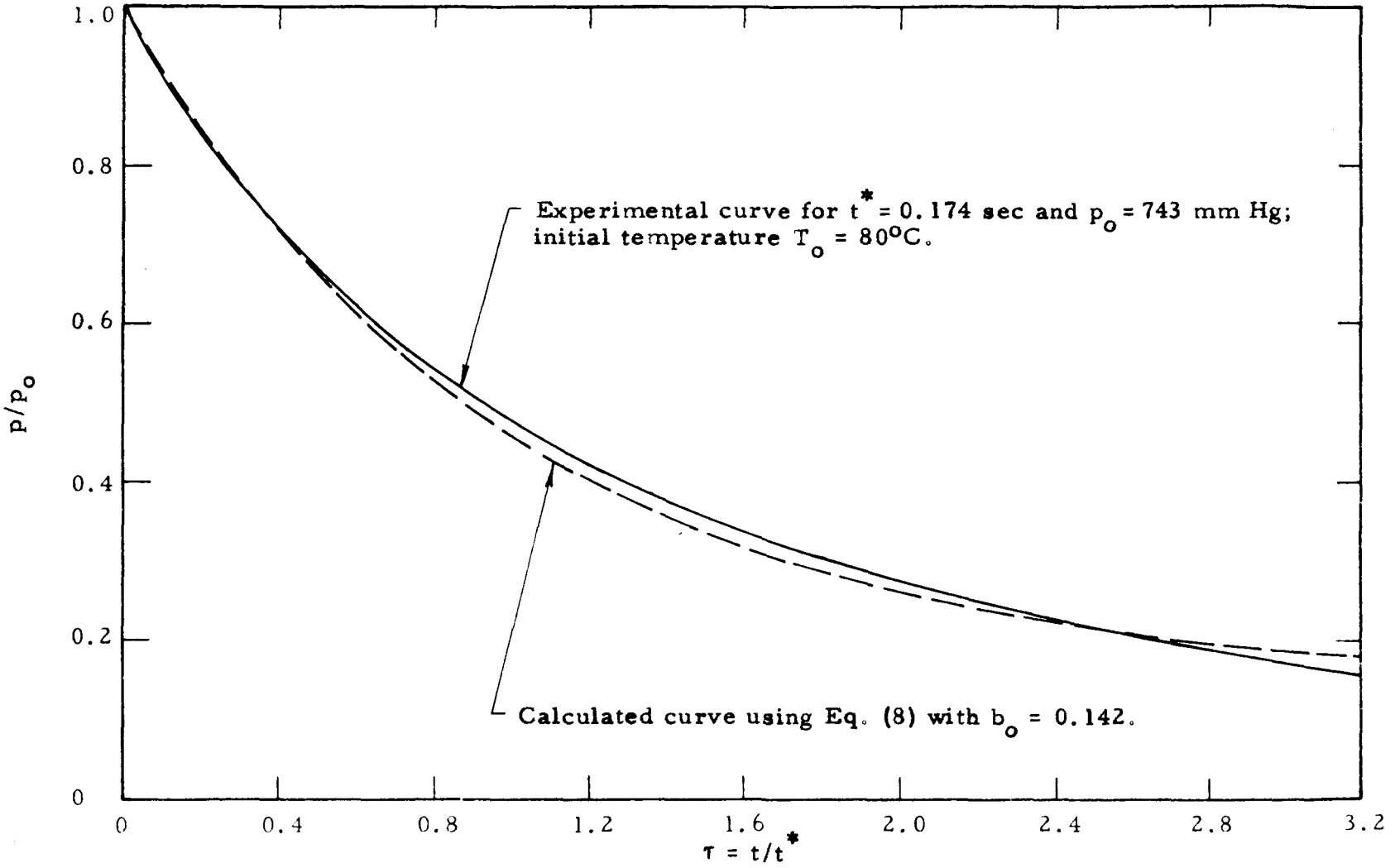

Fig. 39. The reduced pressure p/p_o as a function of the reduced time $\tau = t/t^*$ for Ar discharging from a vessel containing silica gel of mesh size 6-16.

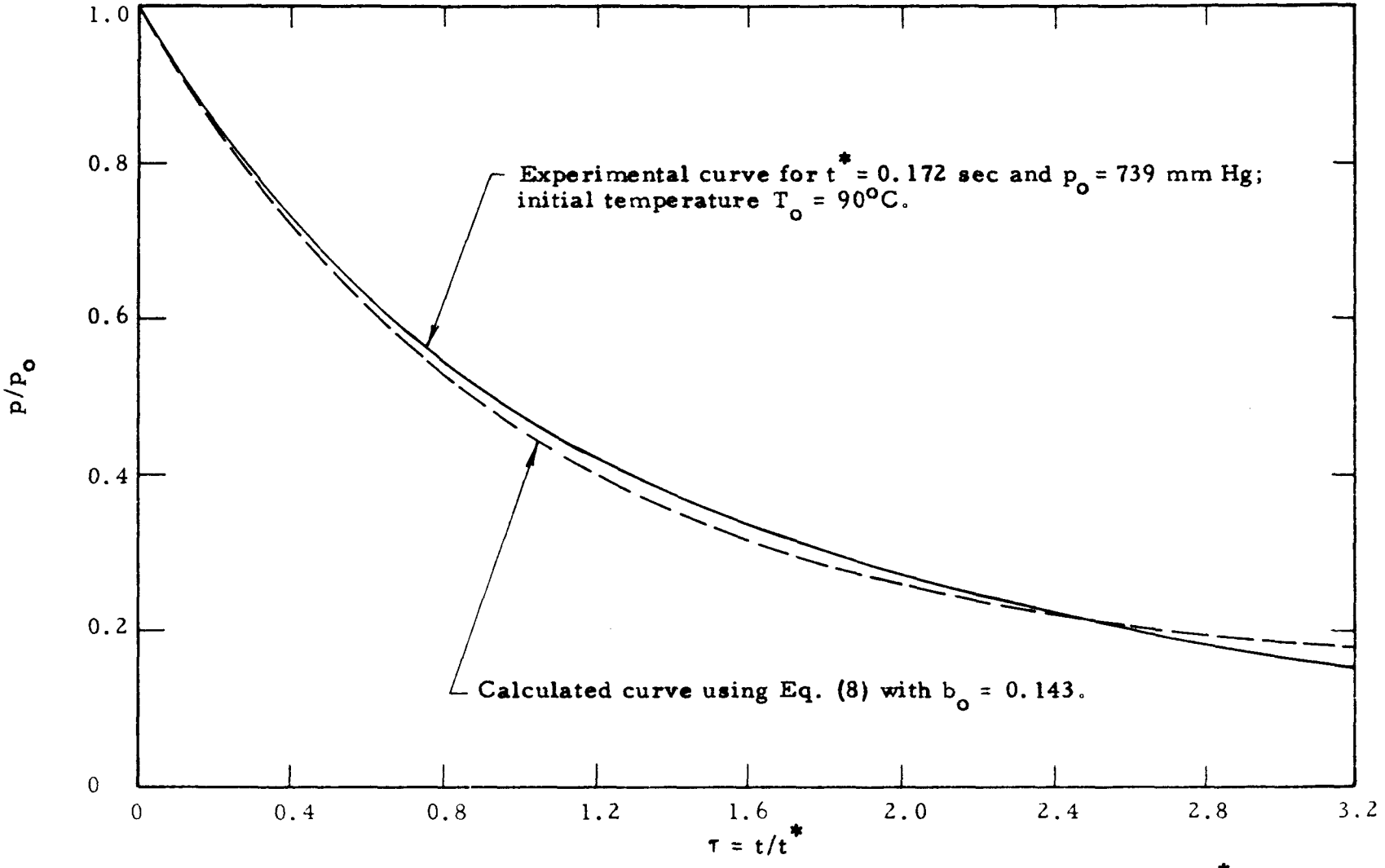

Fig. 40. The reduced pressure p/p_o as a function of the reduced time $\tau = t/t^*$ for Ar discharging from a vessel containing silica gel of mesh size 6-16.

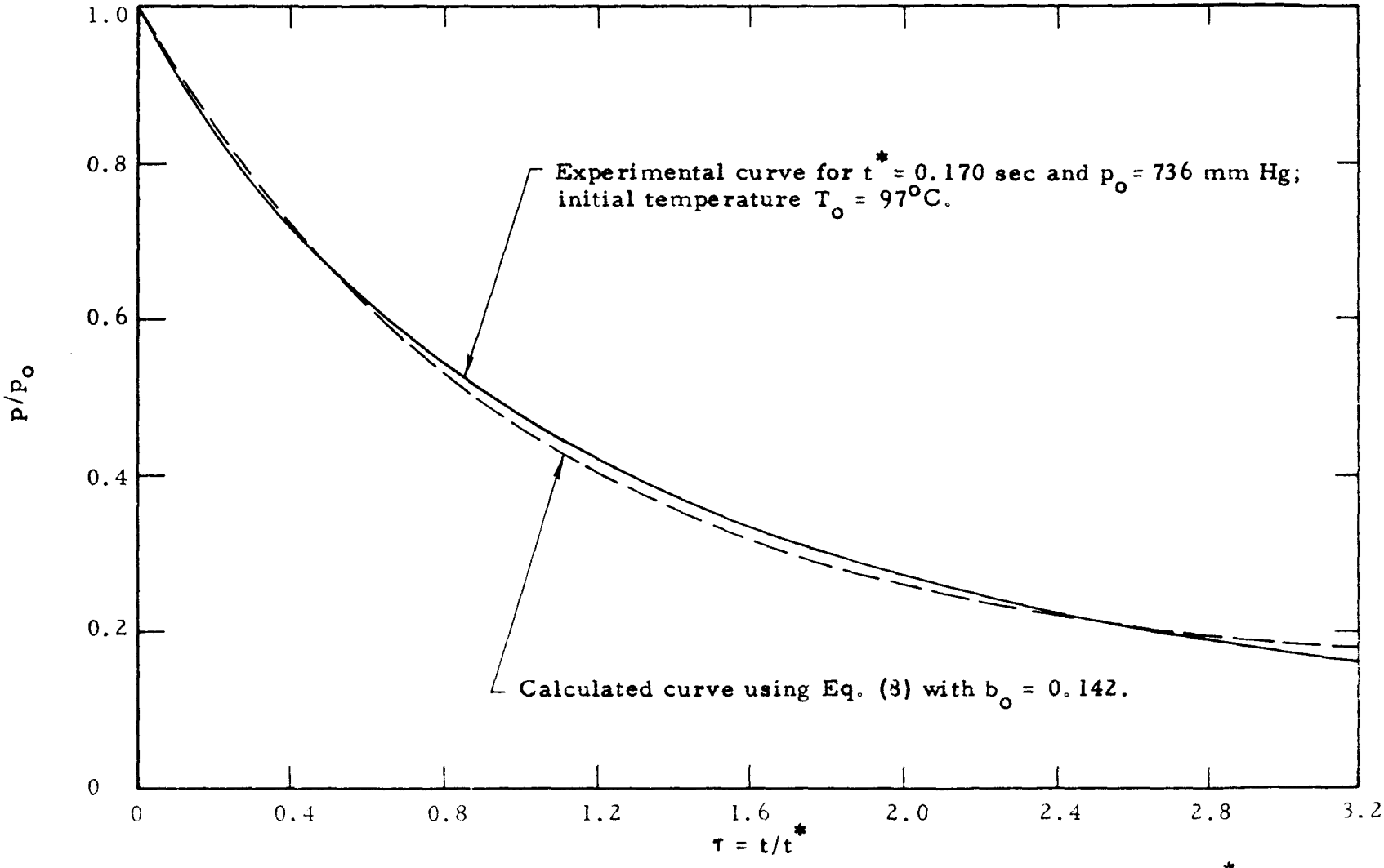

Fig. 41. The reduced pressure p/p_o as a function of the reduced time $\tau = t/t^*$ for Ar discharging from a vessel containing silica gel of mesh size 6-16.

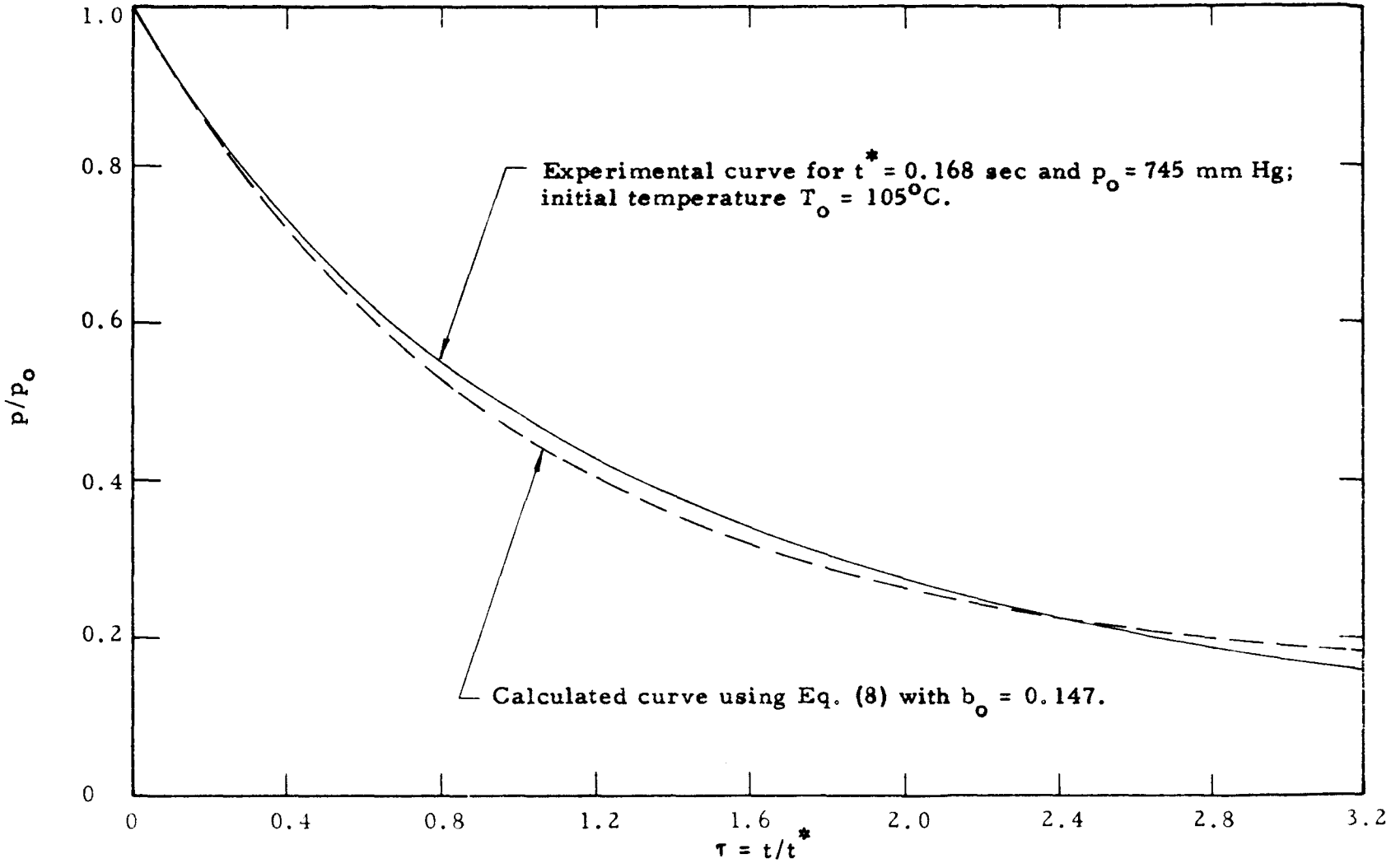

Fig. 42. The reduced pressure p/p_o as a function of the reduced time $\tau = t/t^*$ for Ar discharging from a vessel containing silica gel of mesh size 6-16.

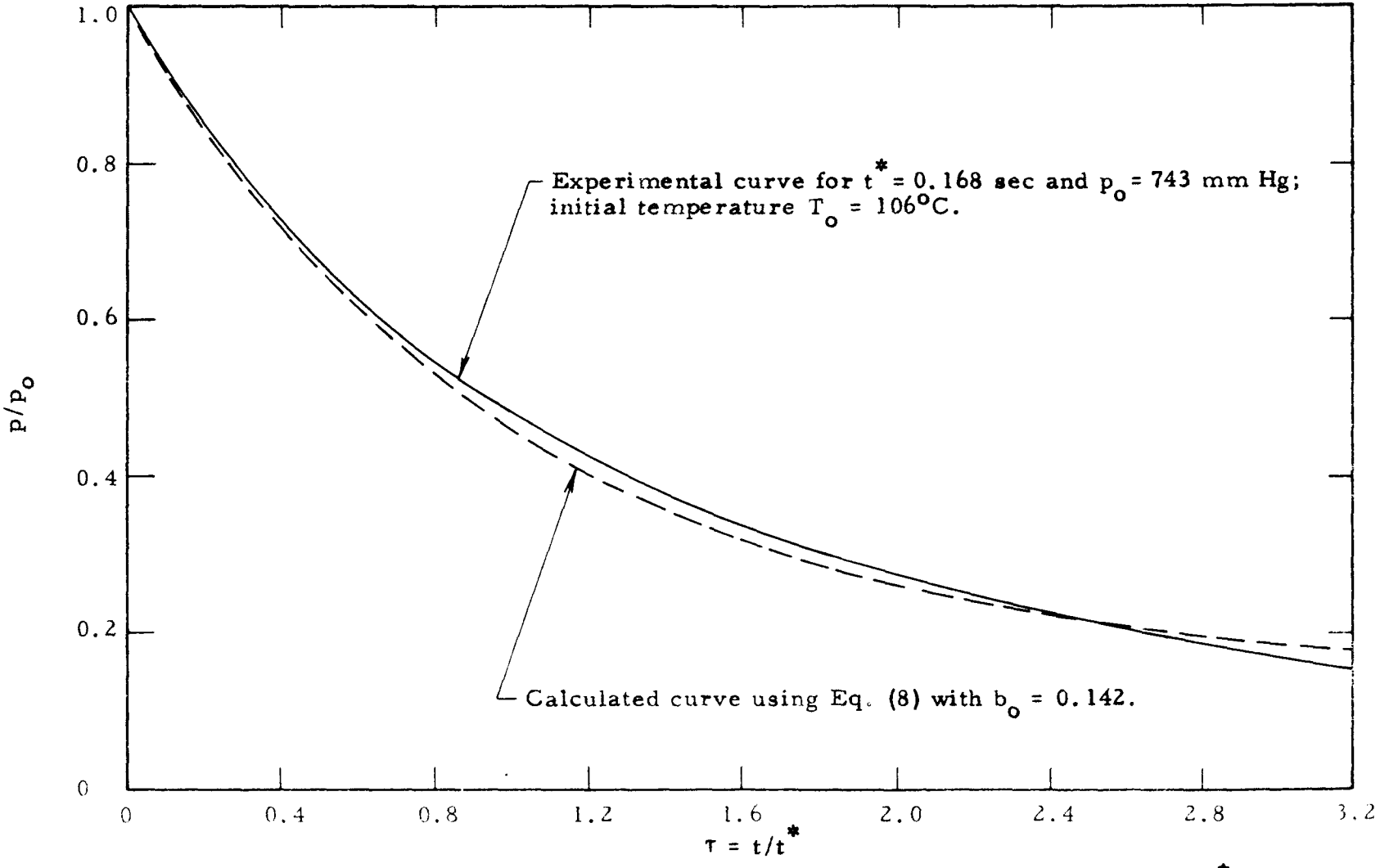

Fig. 43. The reduced pressure p/p_o as a function of the reduced time $\tau = t/t^*$ for Ar discharging from a vessel containing silica gel of mesh size 6-16.

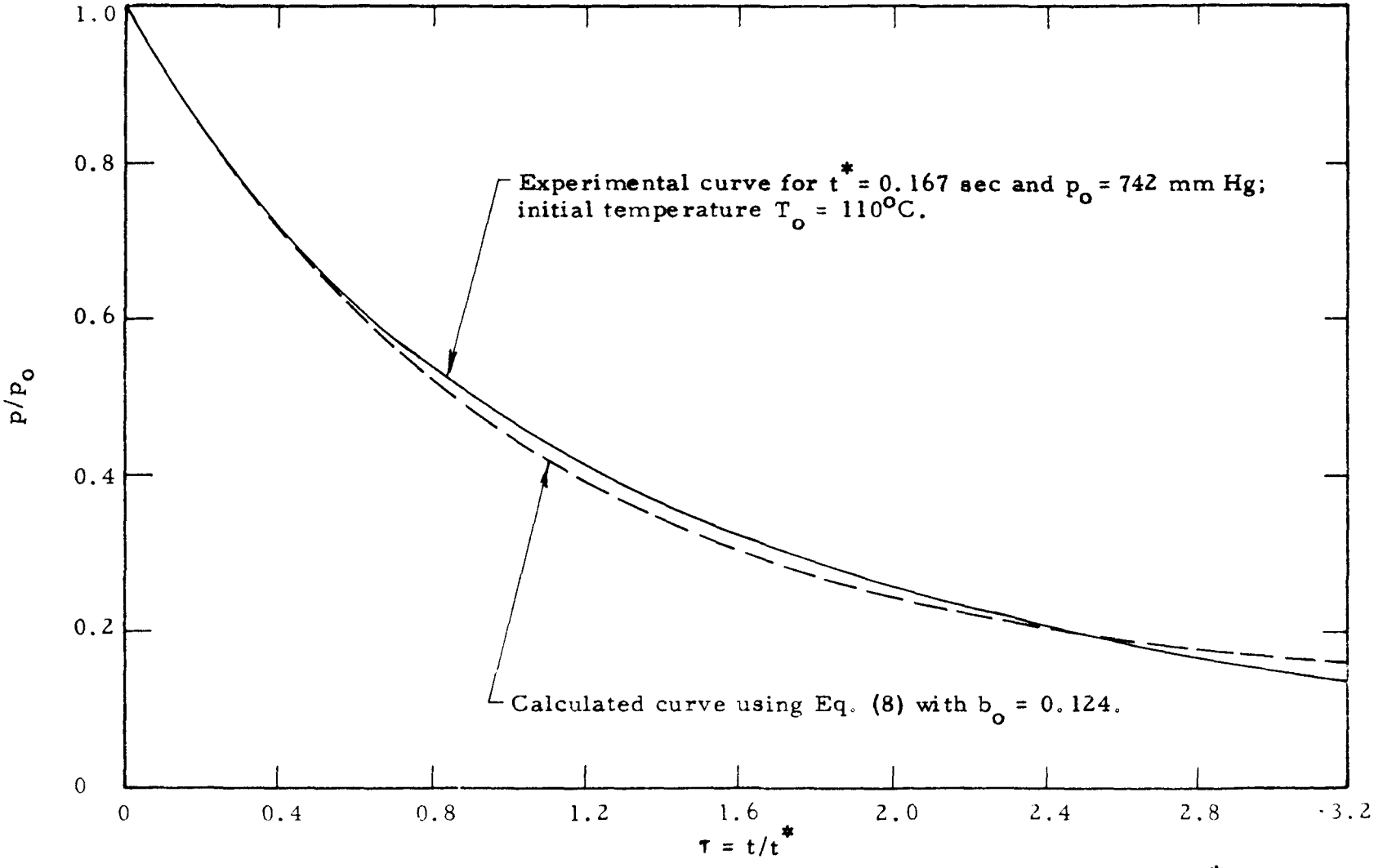

Fig. 44. The reduced pressure p/p_o as a function of the reduced time $\tau = t/t^*$ for Ar discharging from a vessel containing silica gel of mesh size 6-16.

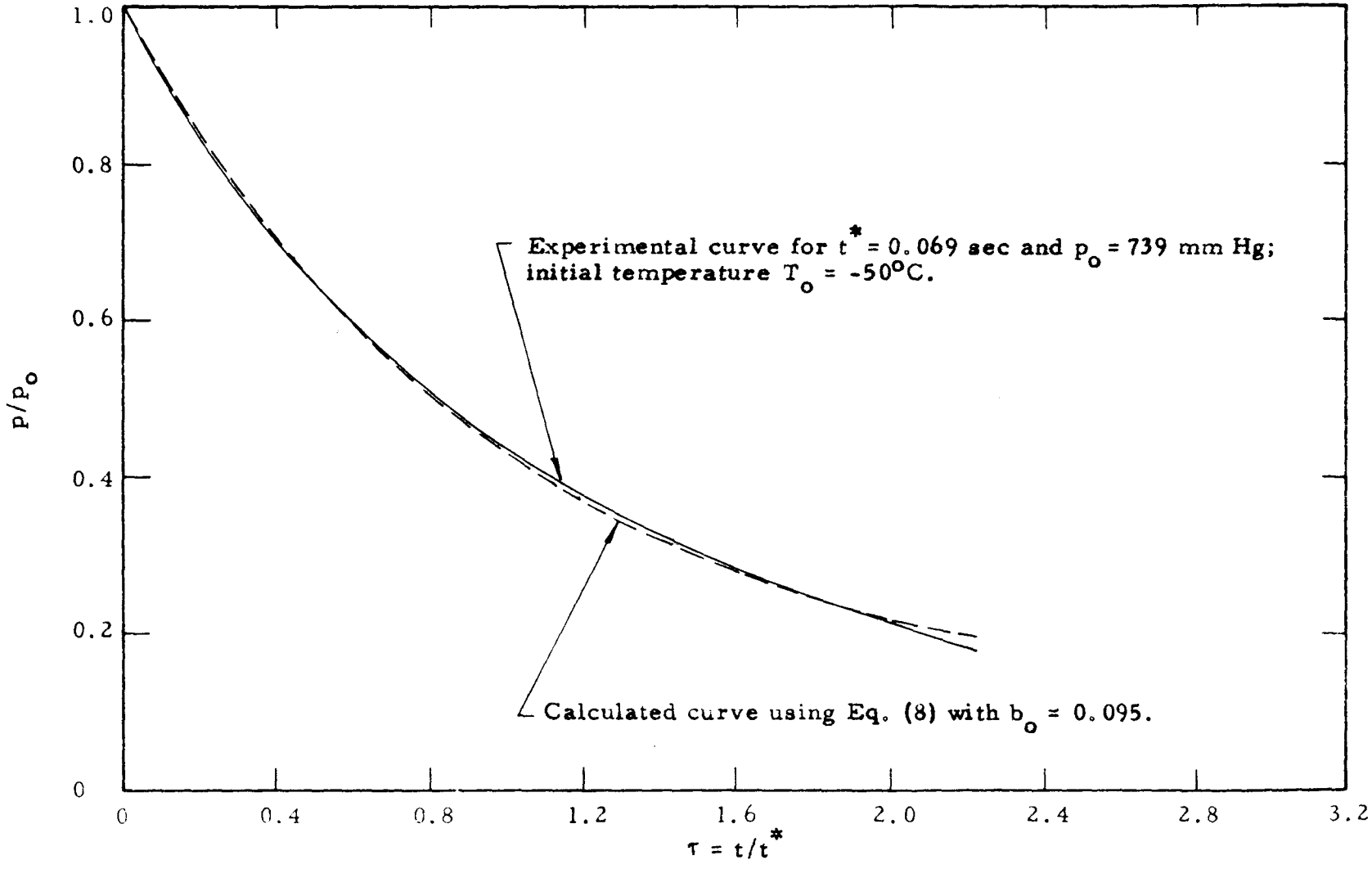

Fig. 45. The reduced pressure p/p_o as a function of the reduced time $\tau = t/t^*$ for He discharging from a vessel containing silica gel of mesh size 6-16.

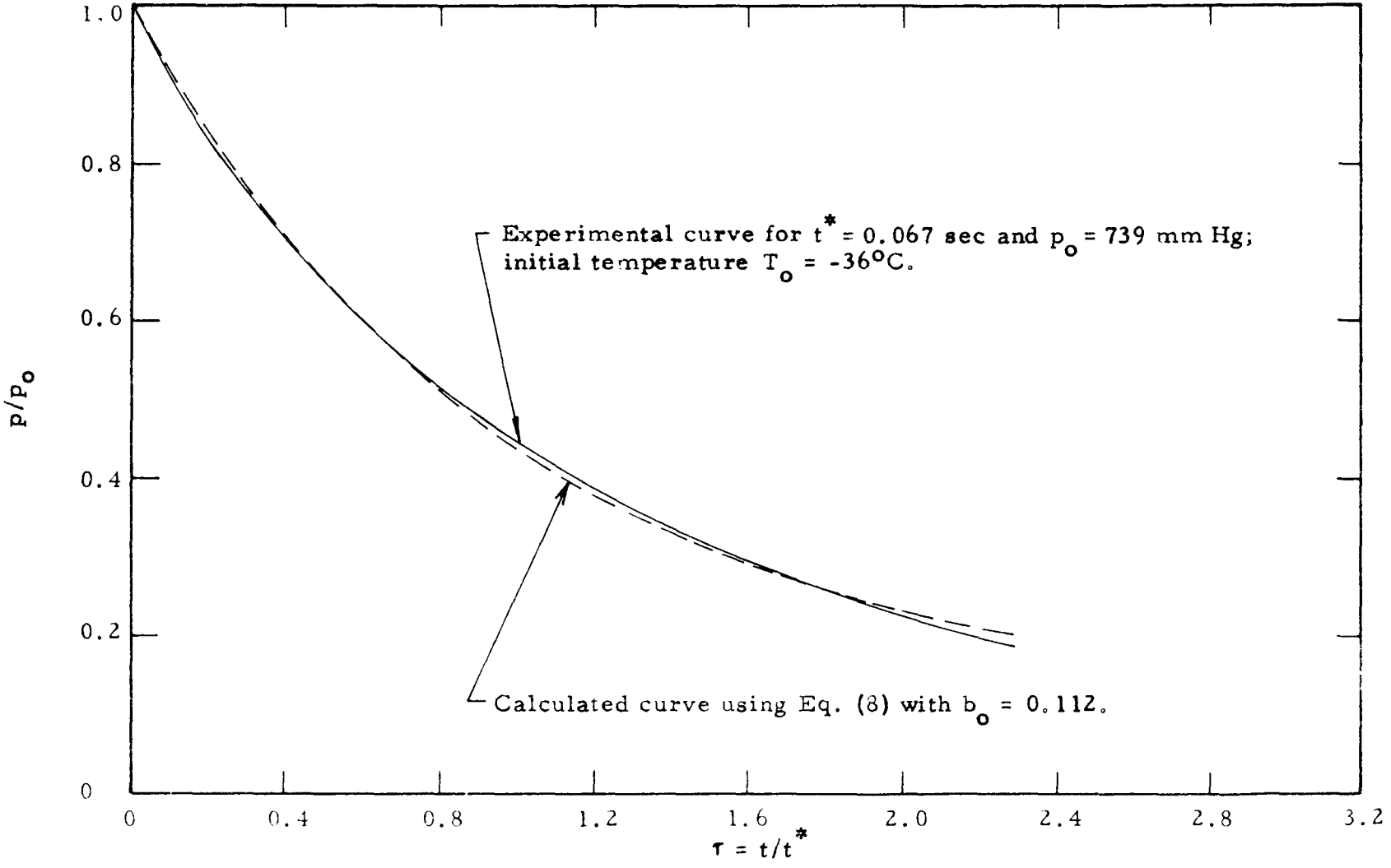

Fig. 46. The reduced pressure p/p_o as a function of the reduced time $\tau = t/t^*$ for He discharging from a vessel containing silica gel of mesh size 6-16.

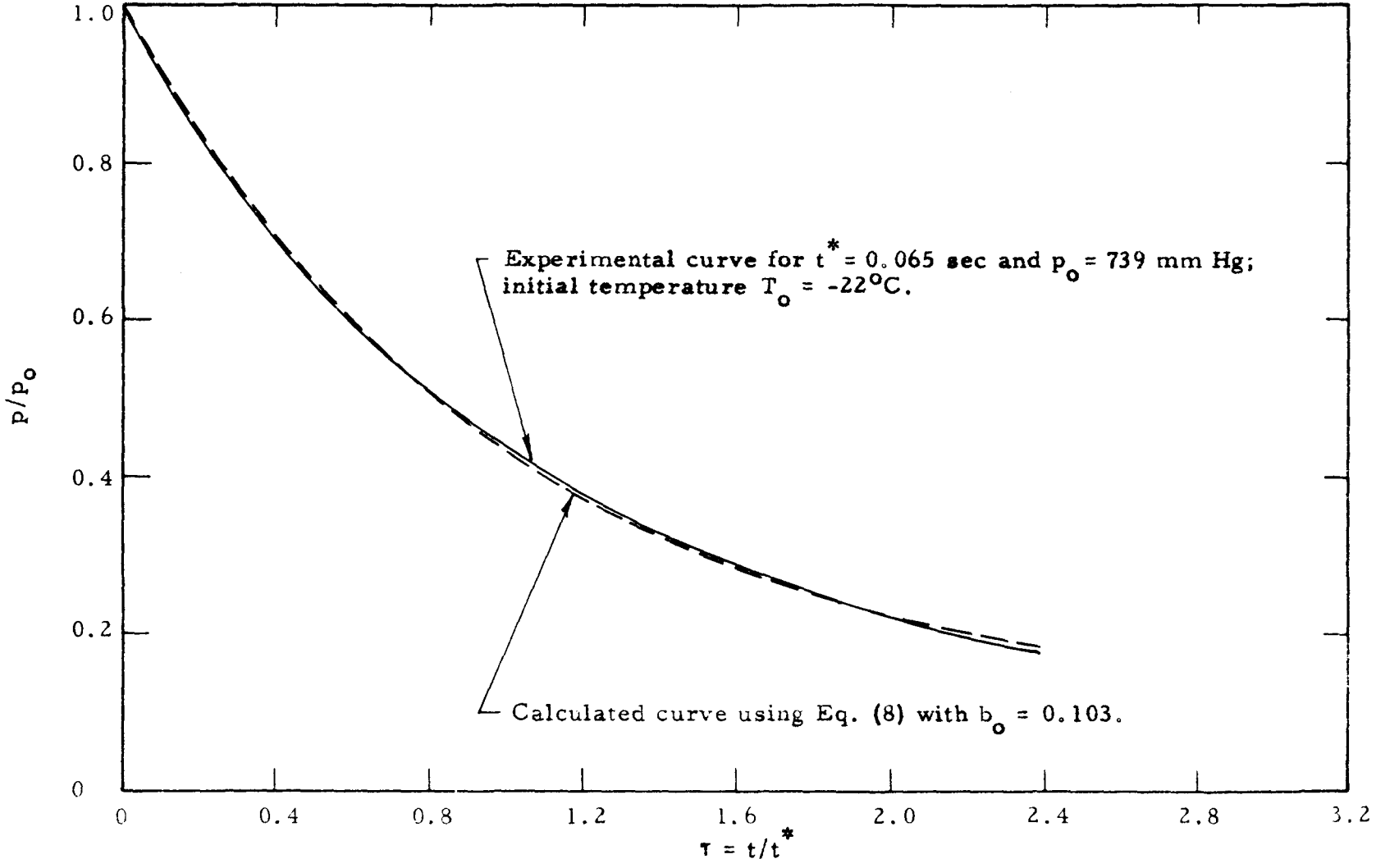

Fig. 47. The reduced pressure p/p_o as a function of the reduced time $\tau = t/t^*$ for He discharging from a vessel containing silica gel of mesh size 6-16.

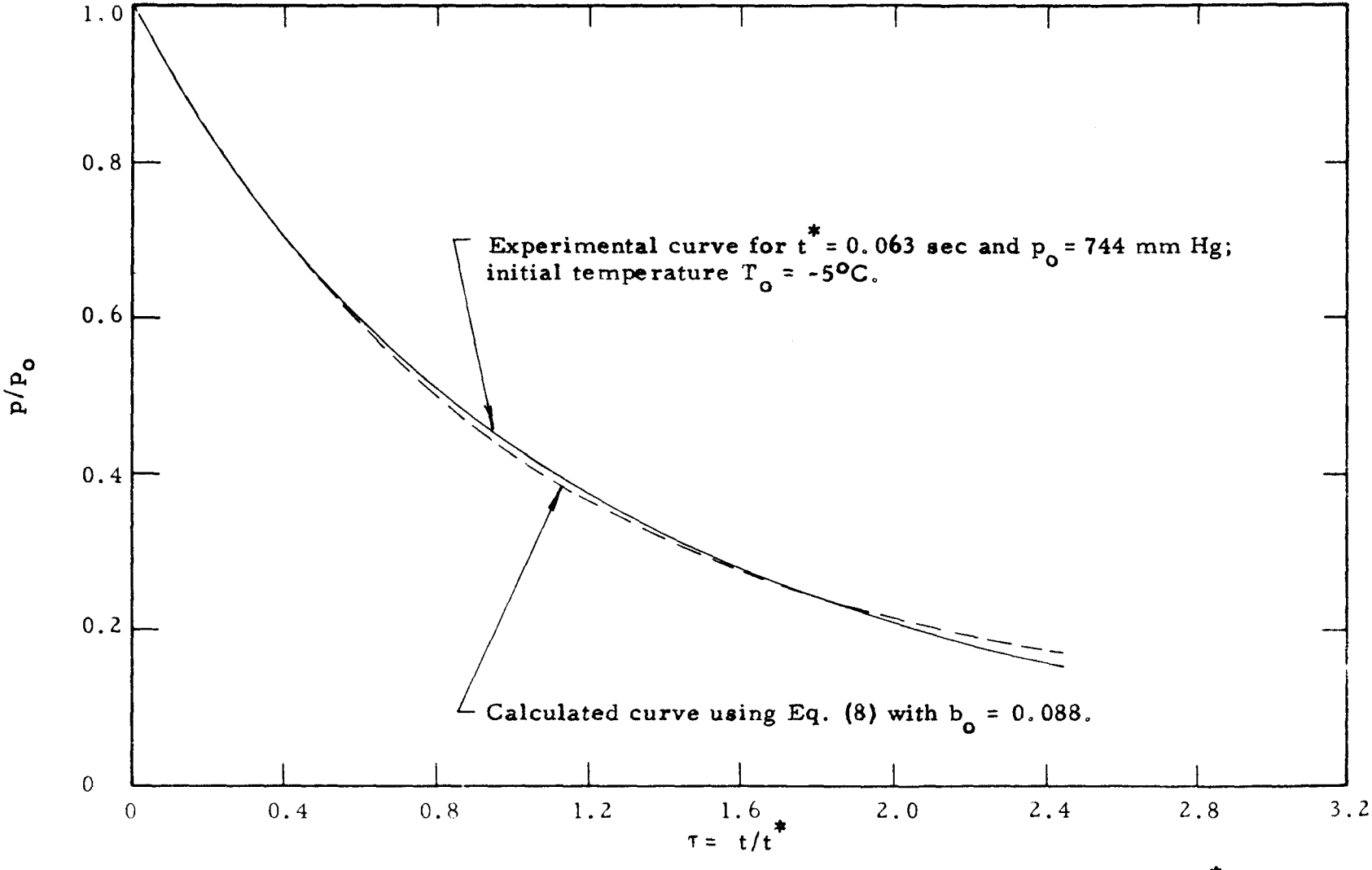

Fig. 48. The reduced pressure p/p_o as a function of the reduced time $\tau = t/t^*$ for He discharging from a vessel containing silica gel of mesh size 6-16.

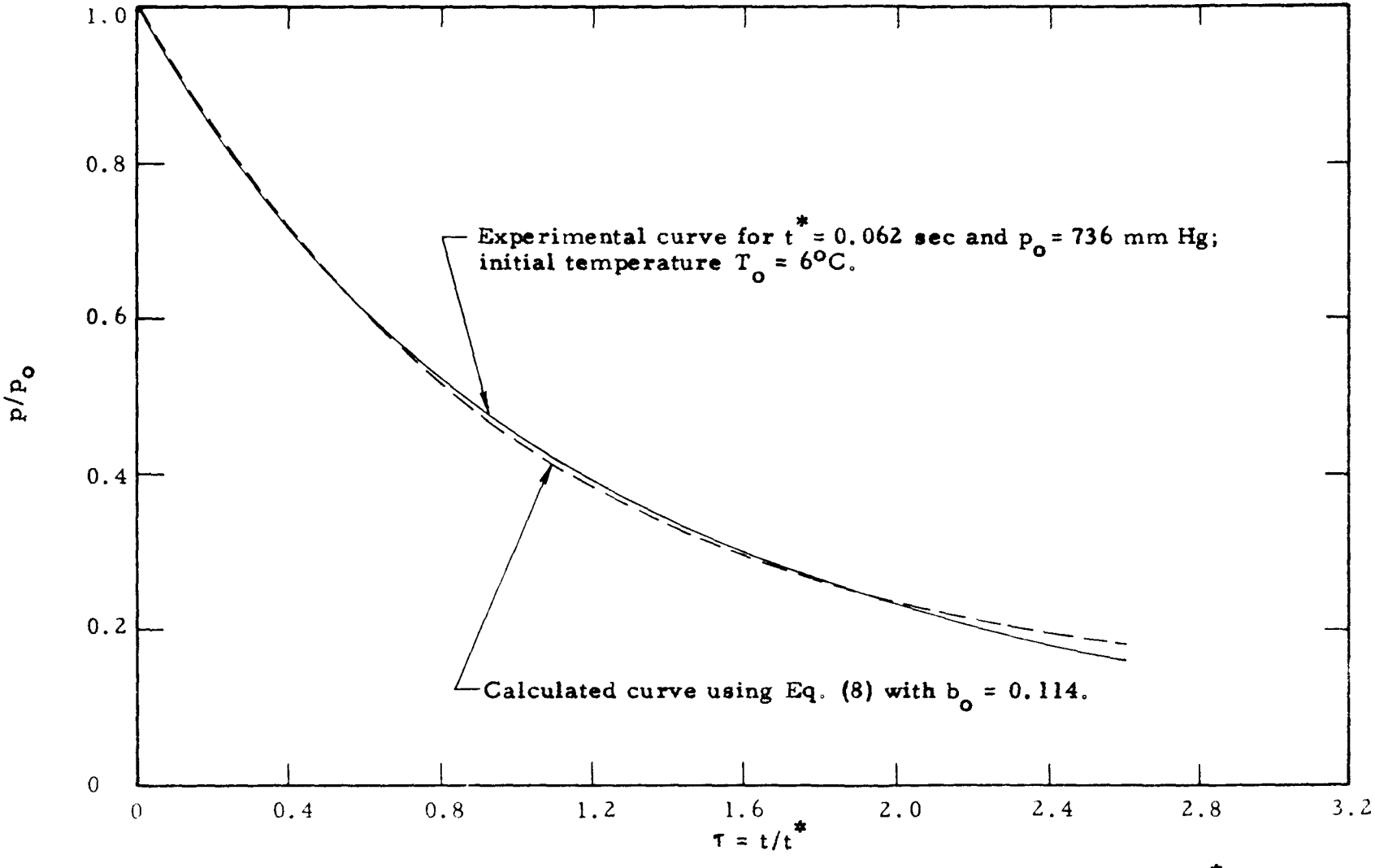

Fig. 49. The reduced pressure p/p_o as a function of the reduced time $\tau = t/t^*$ for He discharging from a vessel containing silica gel of mesh size 6-16.

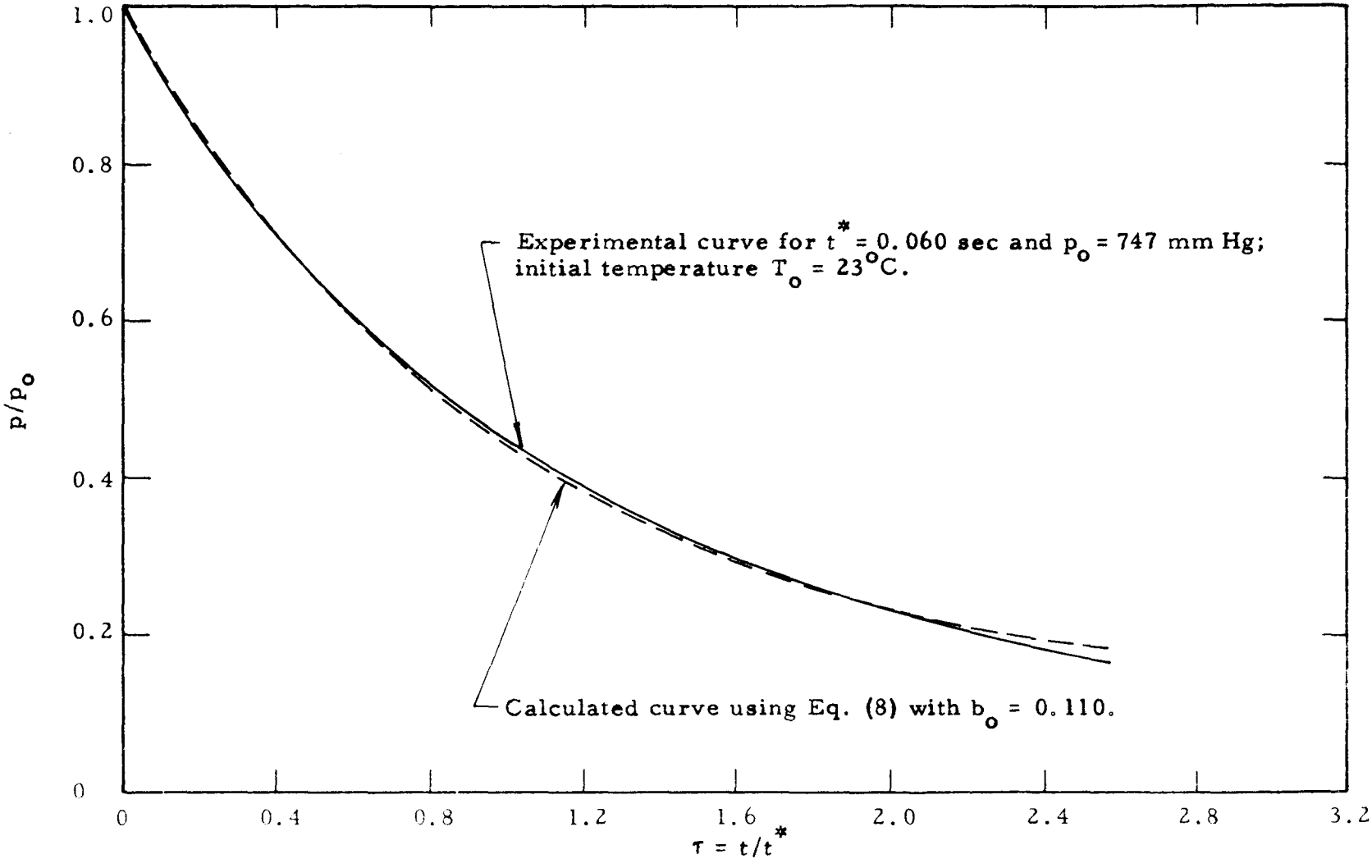

Fig. 50. The reduced pressure p/p_o as a function of the reduced time $\tau = t/t^*$ for He discharging from a vessel containing silica gel of mesh size 6-16.

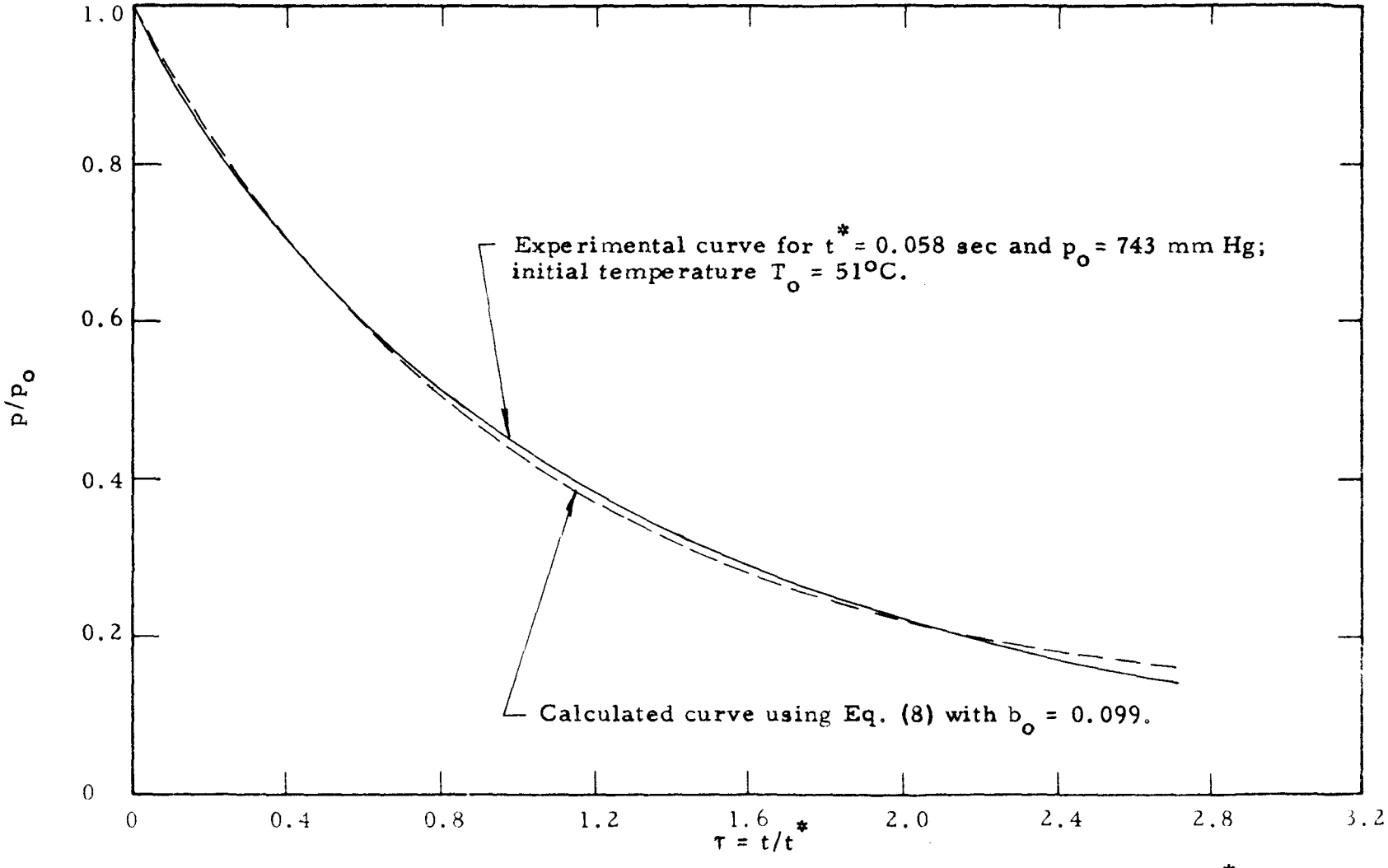

Fig. 51. The reduced pressure p/p_o as a function of the reduced time $\tau = t/t^*$ for He discharging from a vessel containing silica gel of mesh size 6-16.

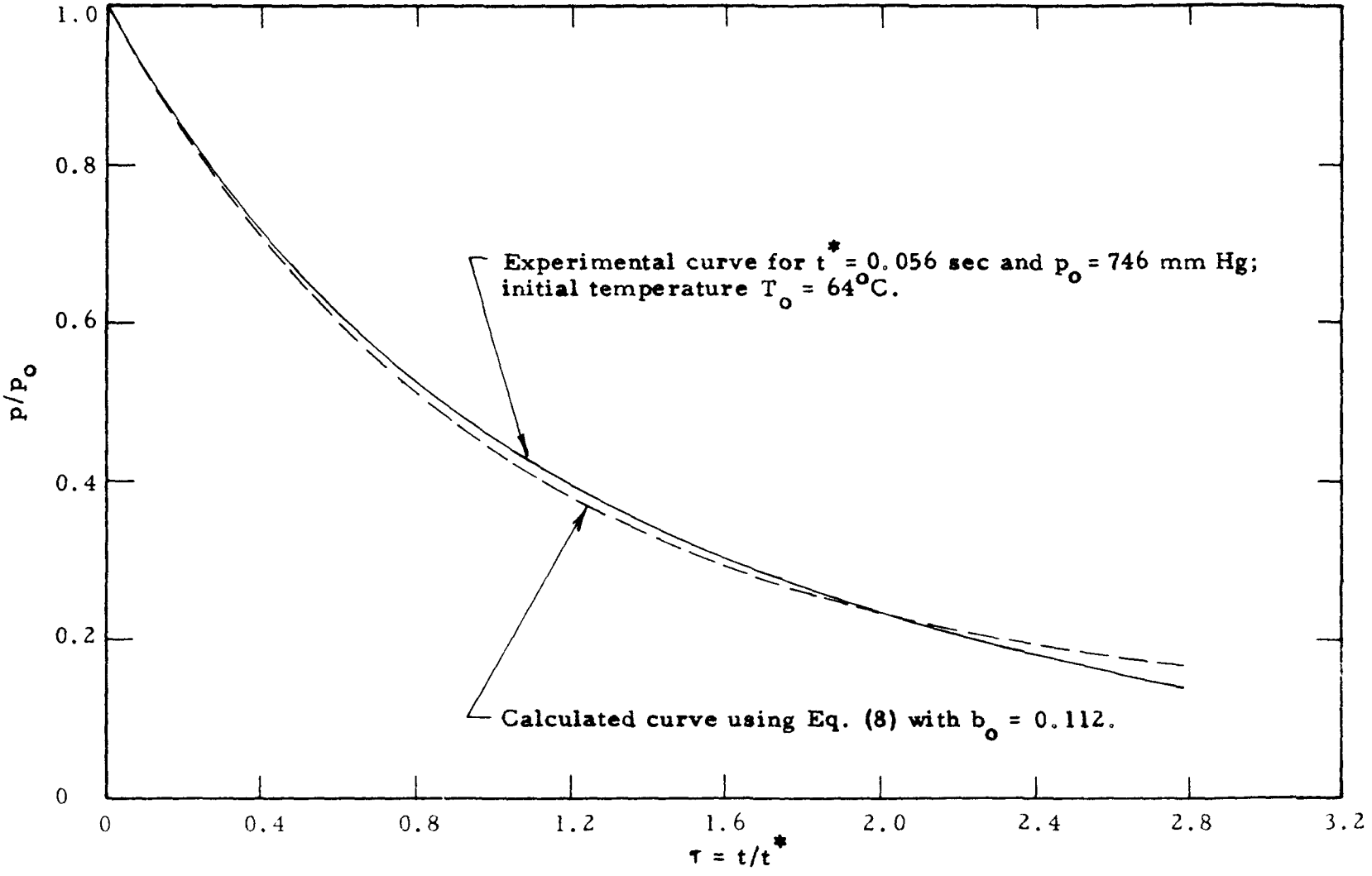

Fig. 52. The reduced pressure p/p_o as a function of the reduced time $\tau = t/t^*$ for He discharging from a vessel containing silica gel of mesh size 6-16.

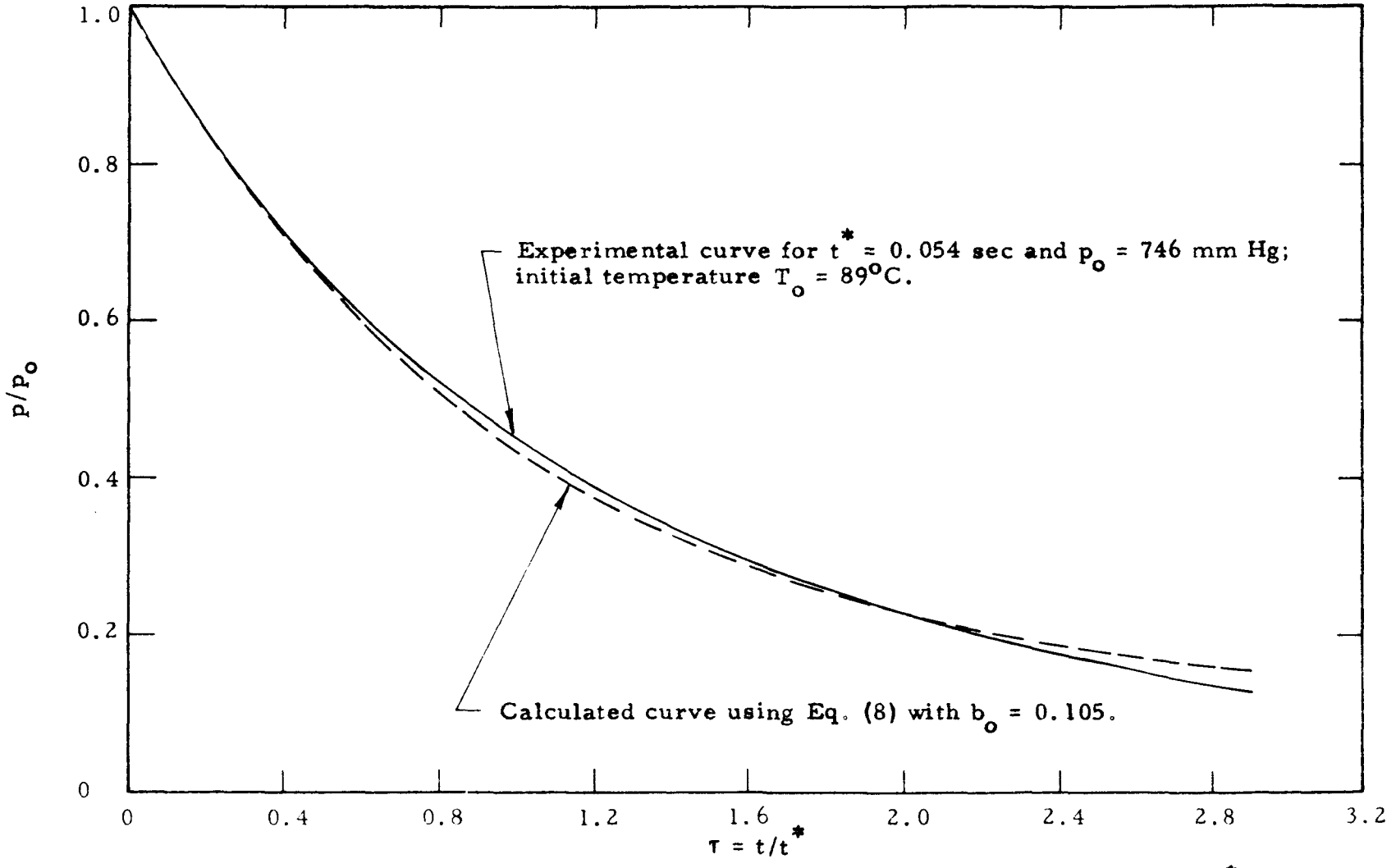

Fig. 53. The reduced pressure p/p_o as a function of the reduced time $\tau = t/t^*$ for He discharging from a vessel containing silica gel of mesh size 6-16.

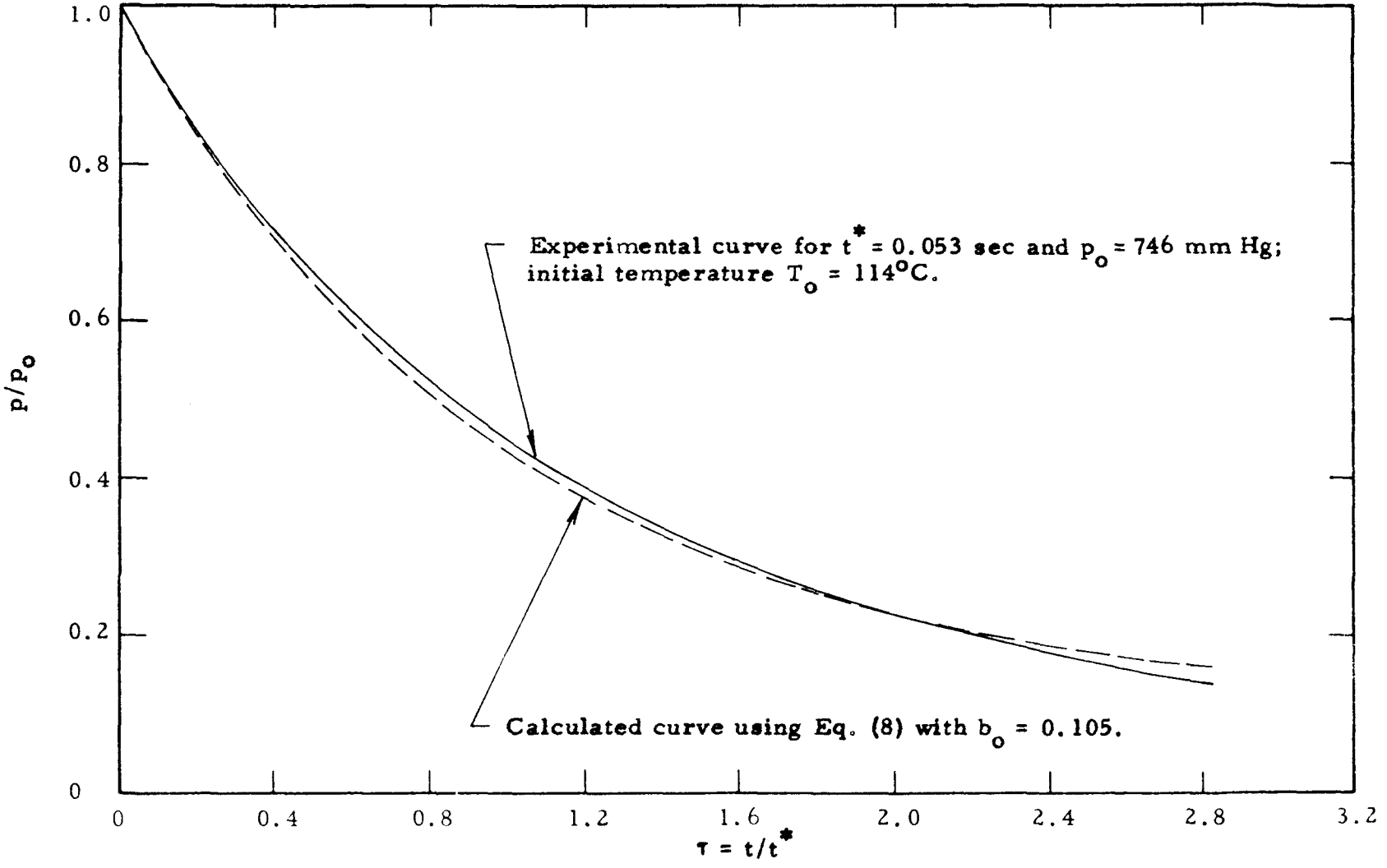

Fig. 54. The reduced pressure p/p_o as a function of the reduced time $\tau = t/t^*$ for He discharging from a vessel containing silica gel of mesh size 6-16.

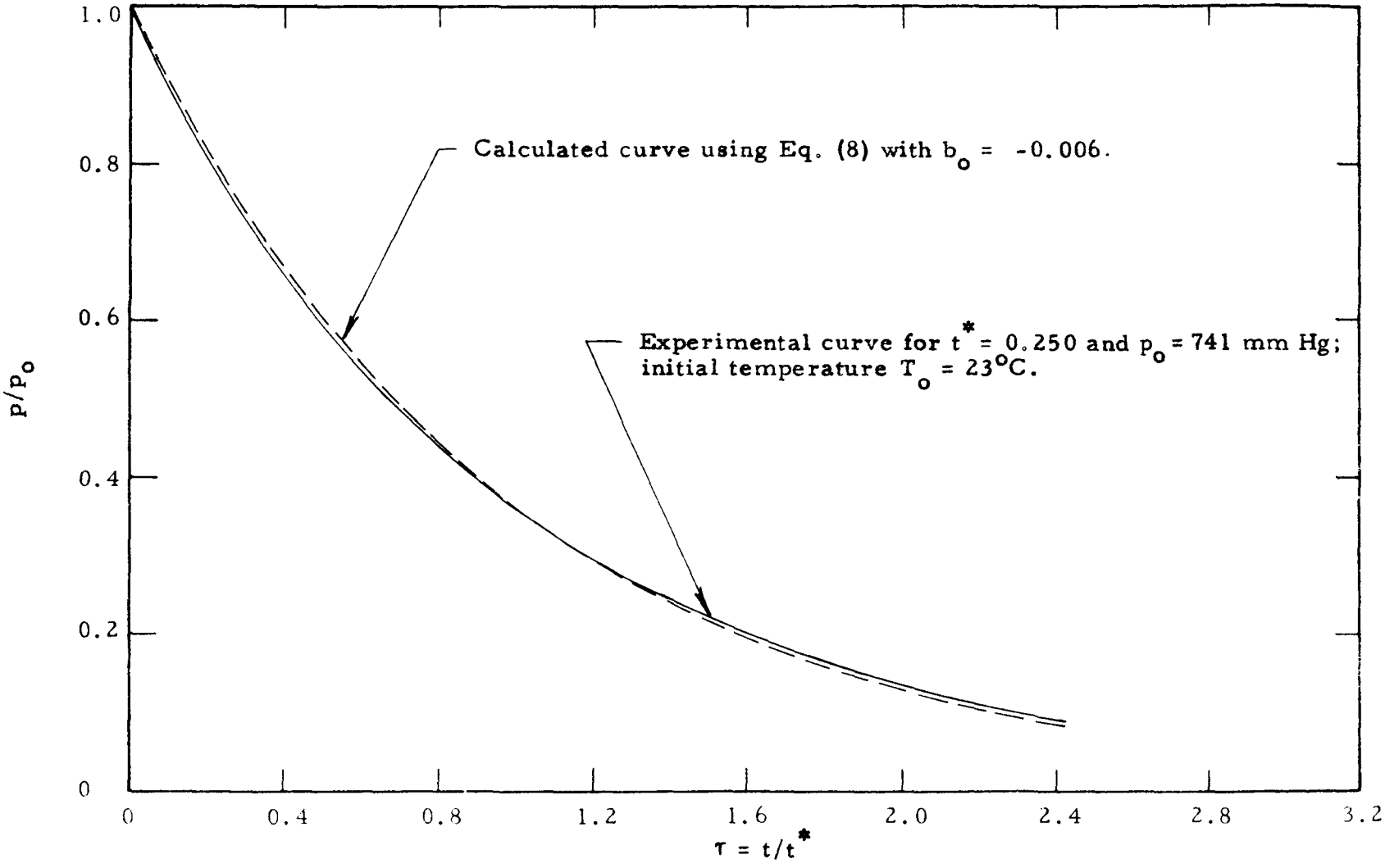

Fig. 55. The reduced pressure p/p_o as a function of the reduced time $\tau = t/t^*$ for CO_2 discharging from a vessel containing 12-mesh quartz sand.

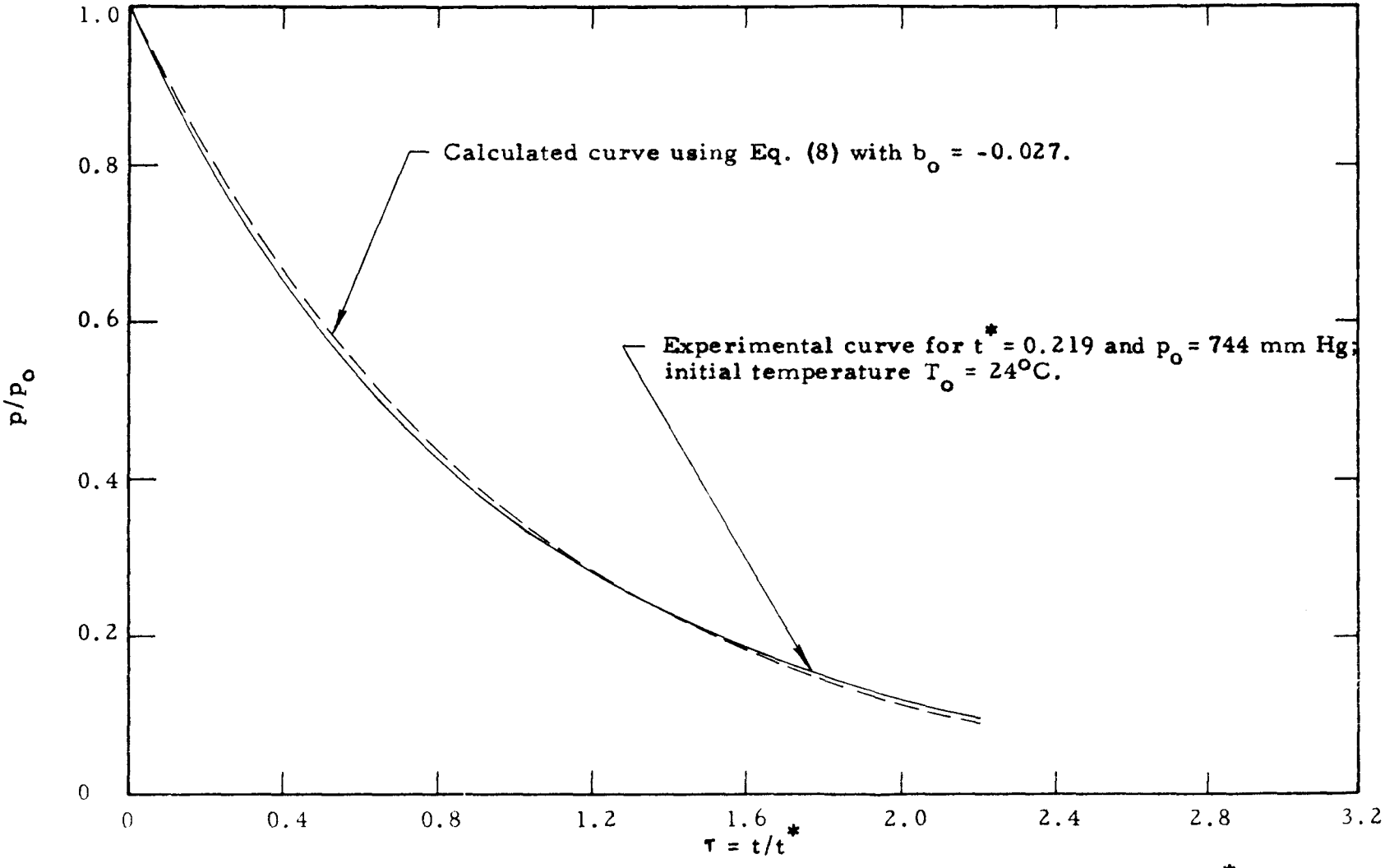

Fig. 56. The reduced pressure p/p_o as a function of the reduced time $\tau = t/t^*$ for Ar discharging from a vessel containing 12-mesh quartz sand.

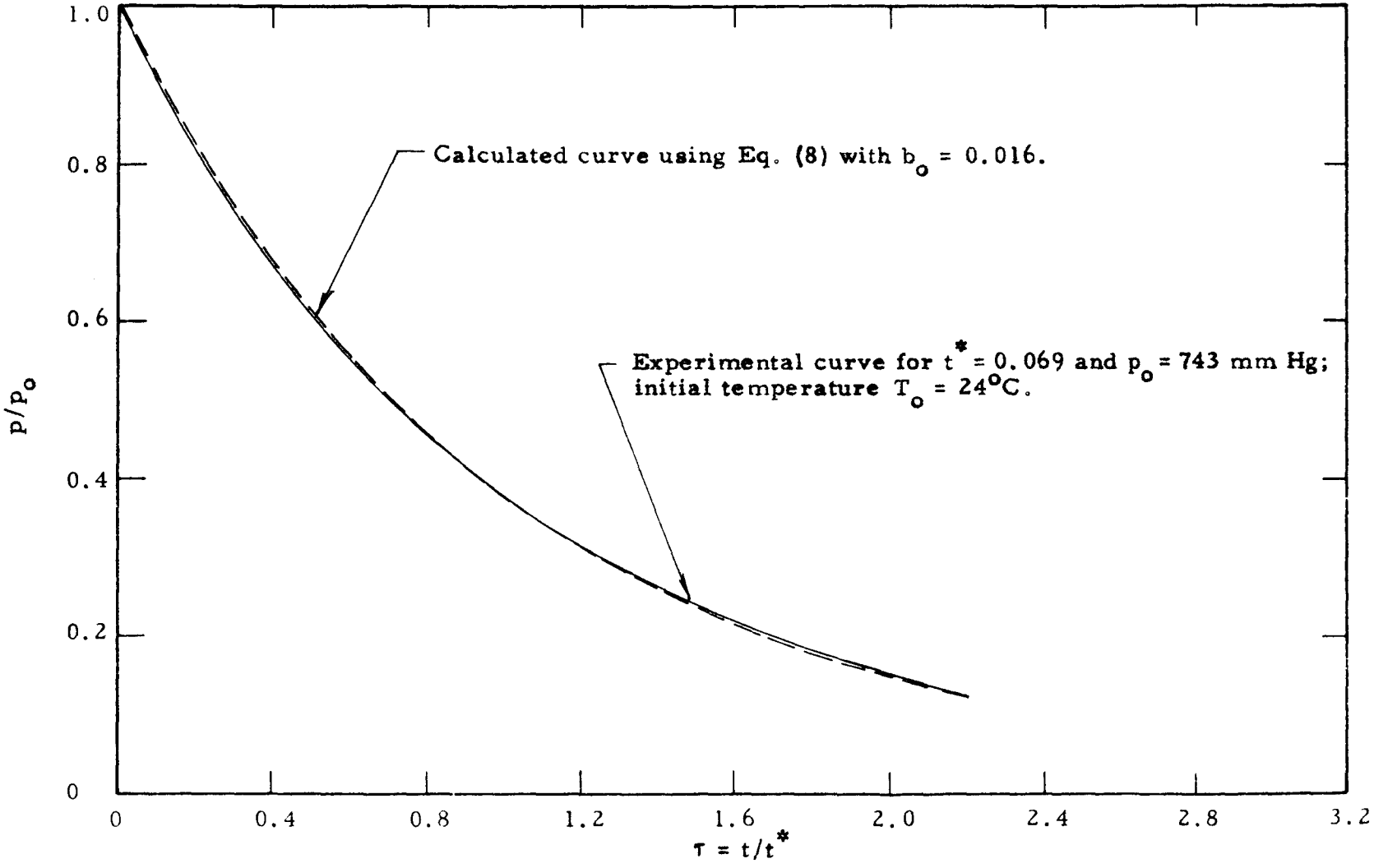

Fig. 57. The reduced pressure p/p_o as a function of the reduced time $\tau = t/t^*$ for He discharging from a vessel containing 12-mesh quartz sand.

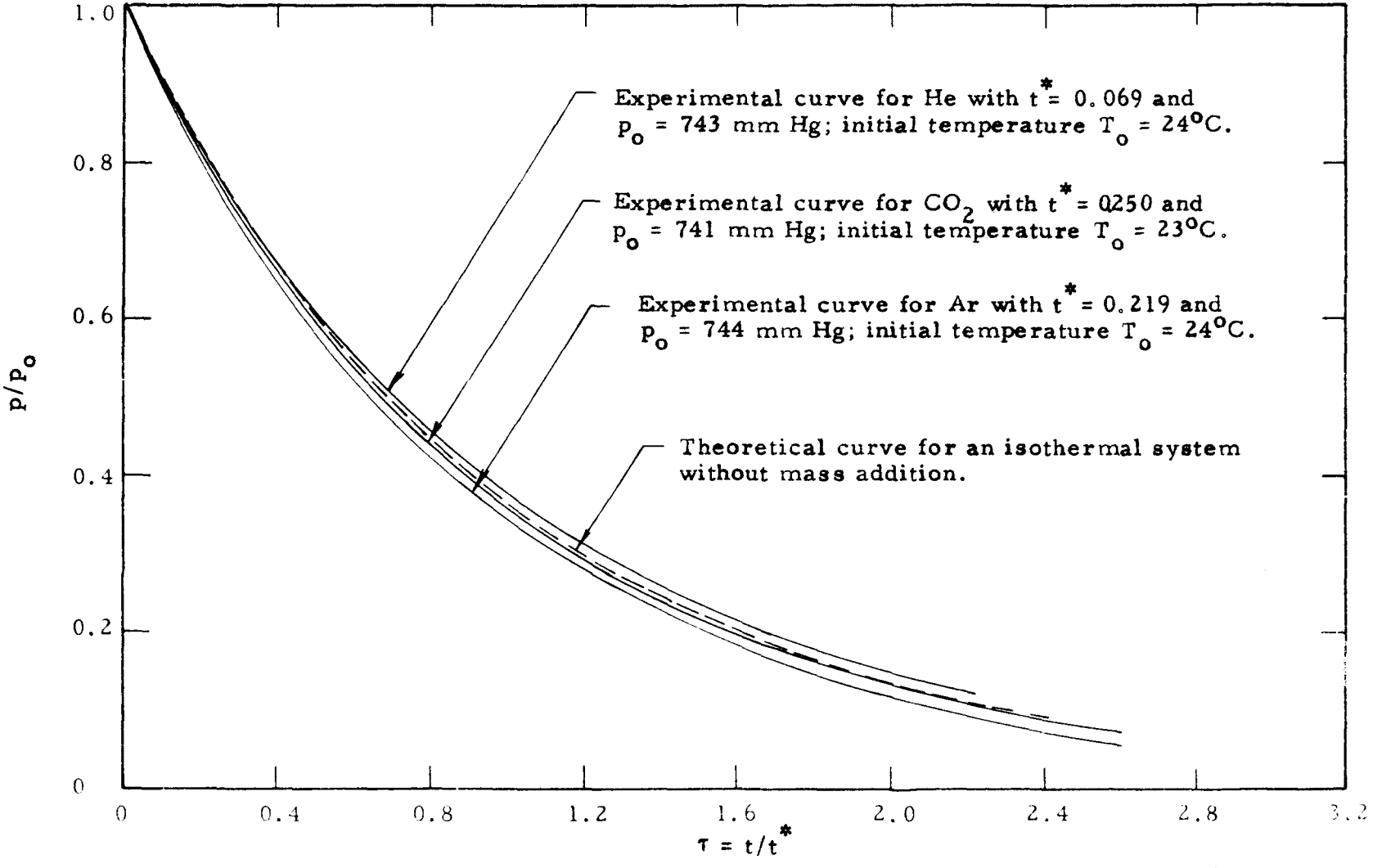

Fig. 58. The reduced pressure p/p_o as a function of the reduced time $\tau = t/t^*$ for CO_2, Ar and He discharging from a vessel containing 12-mesh quartz sand.

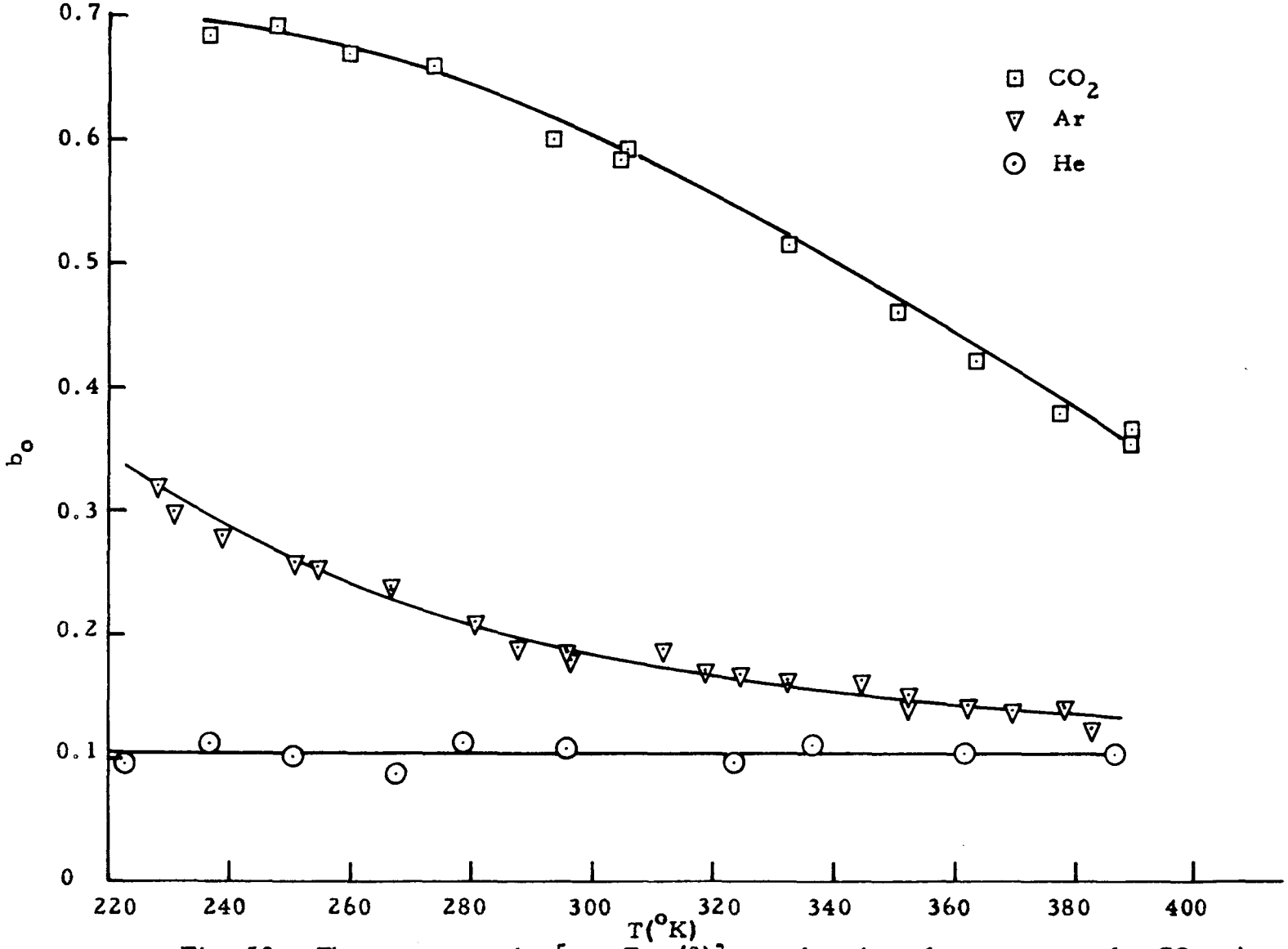

Fig. 59. The parameter b_o [see Eq. (8)] as a function of temperature for CO_2, Ar and He discharging from a vessel containing silica gel of mesh size 6-16.

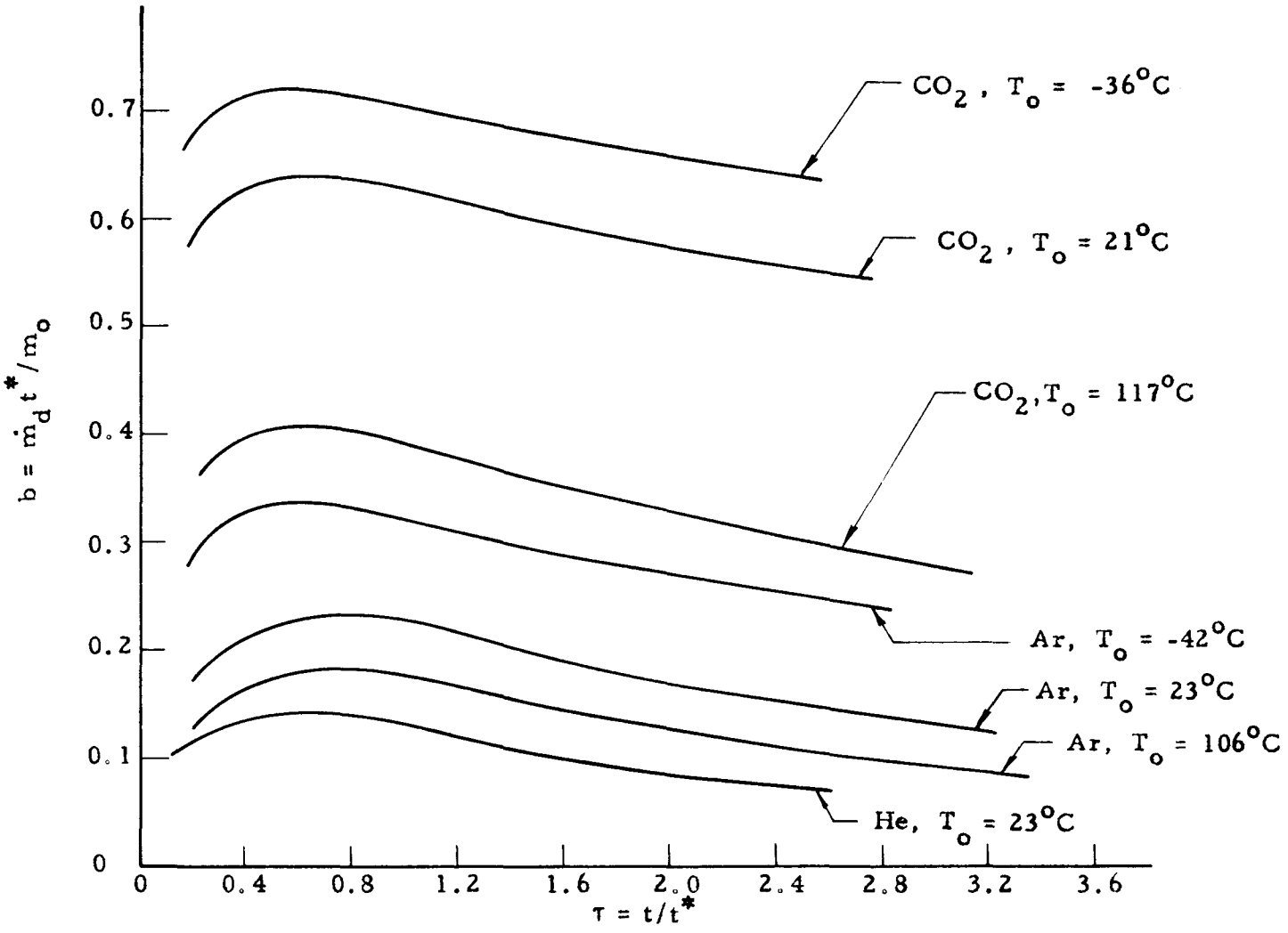

Fig. 60. Representative experimental curves showing the dimensionless desorption rate $b = \dot{m}_d t^*/m_o$ as a function of the reduced time $\tau = t/t^*$ for gases discharging from a vessel containing silica gel of mesh size 6-16.

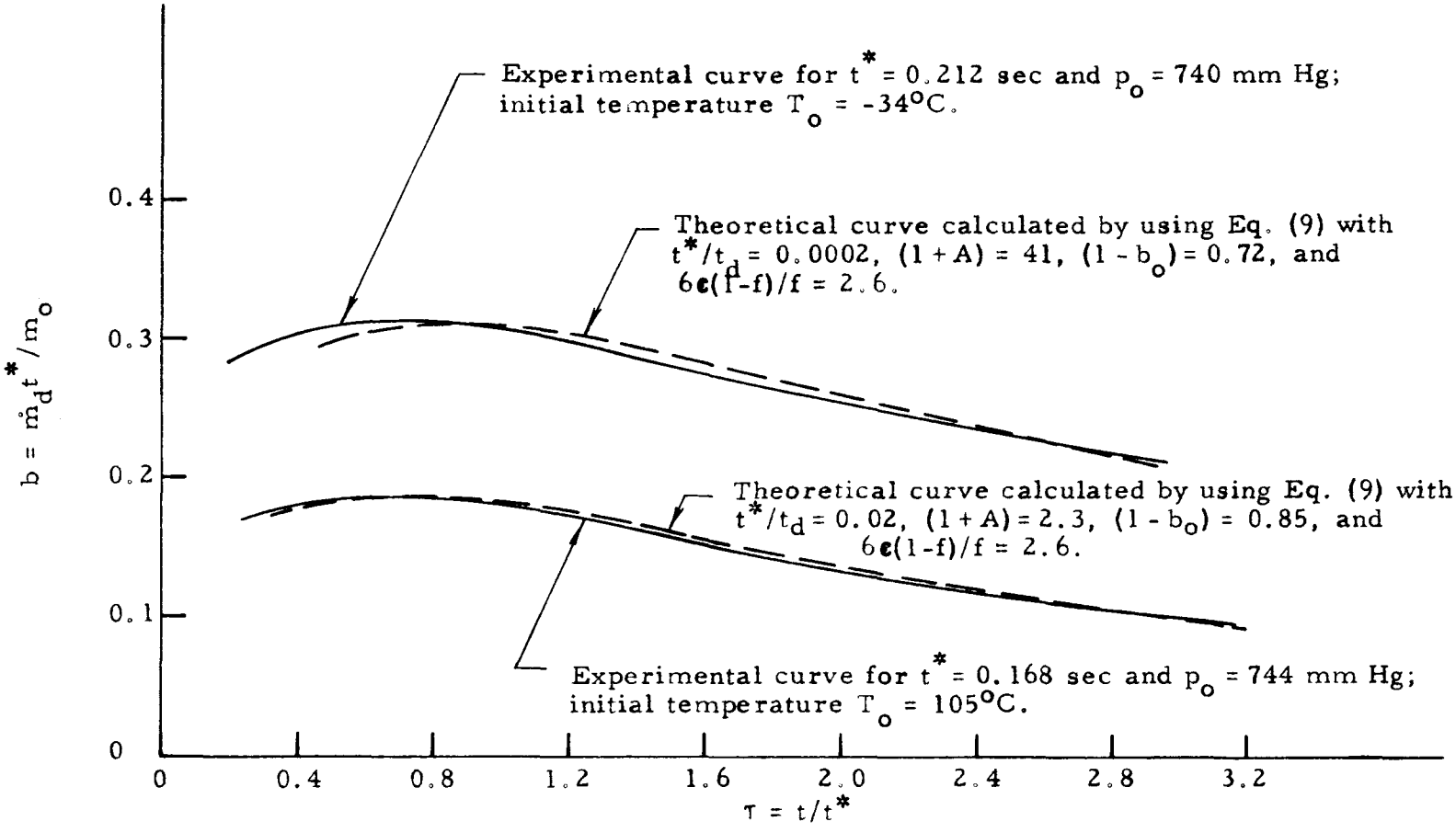

Fig. 61. The dimensionless desorption rate $b = \dot{m}_d t^*/m_o$ as a function of the reduced time $\tau = t/t^*$ for Ar discharging from a vessel containing silica gel of mesh size 6-16.

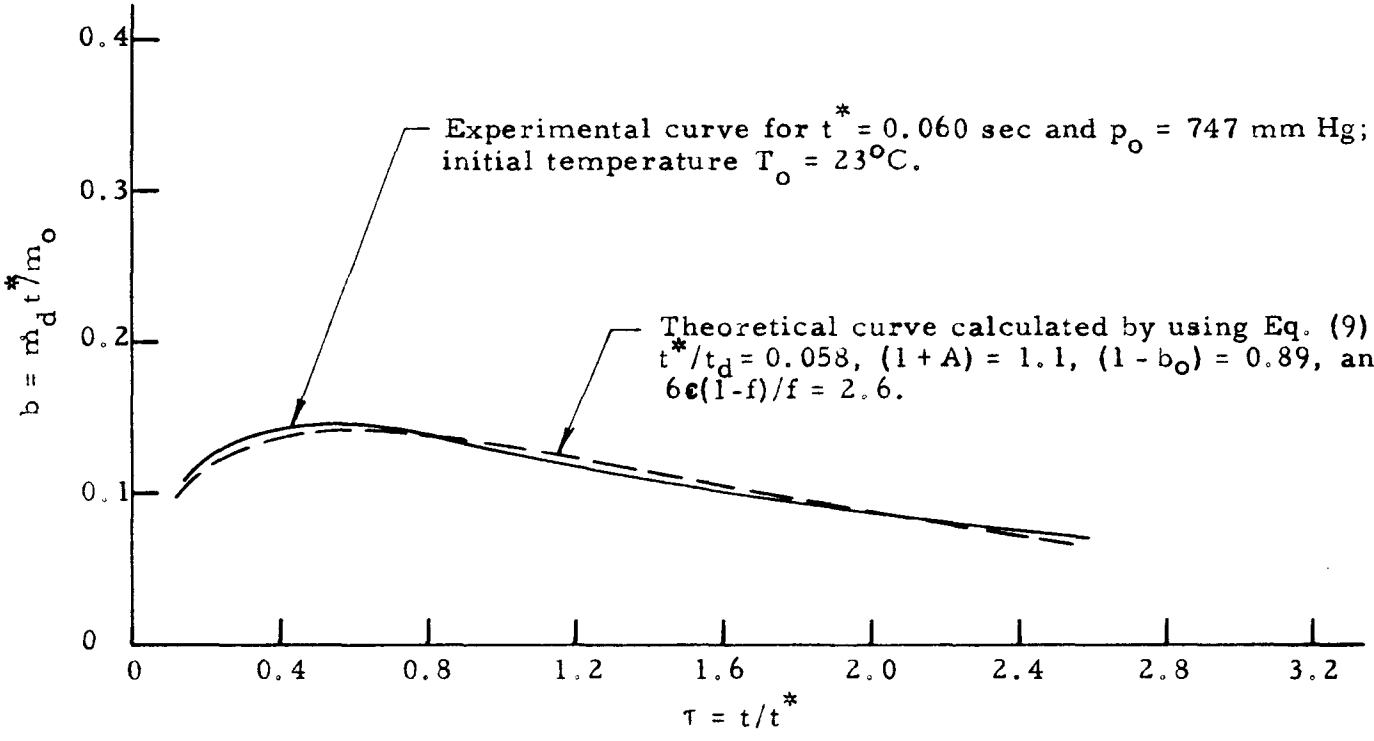

Fig. 62. The dimensionless desorption rate $b = \dot{m}_d t^*/m_o$ as a function of the reduced time $\tau = t/t^*$ for He discharging from a vessel containing silica gel of mesh size 6-16.

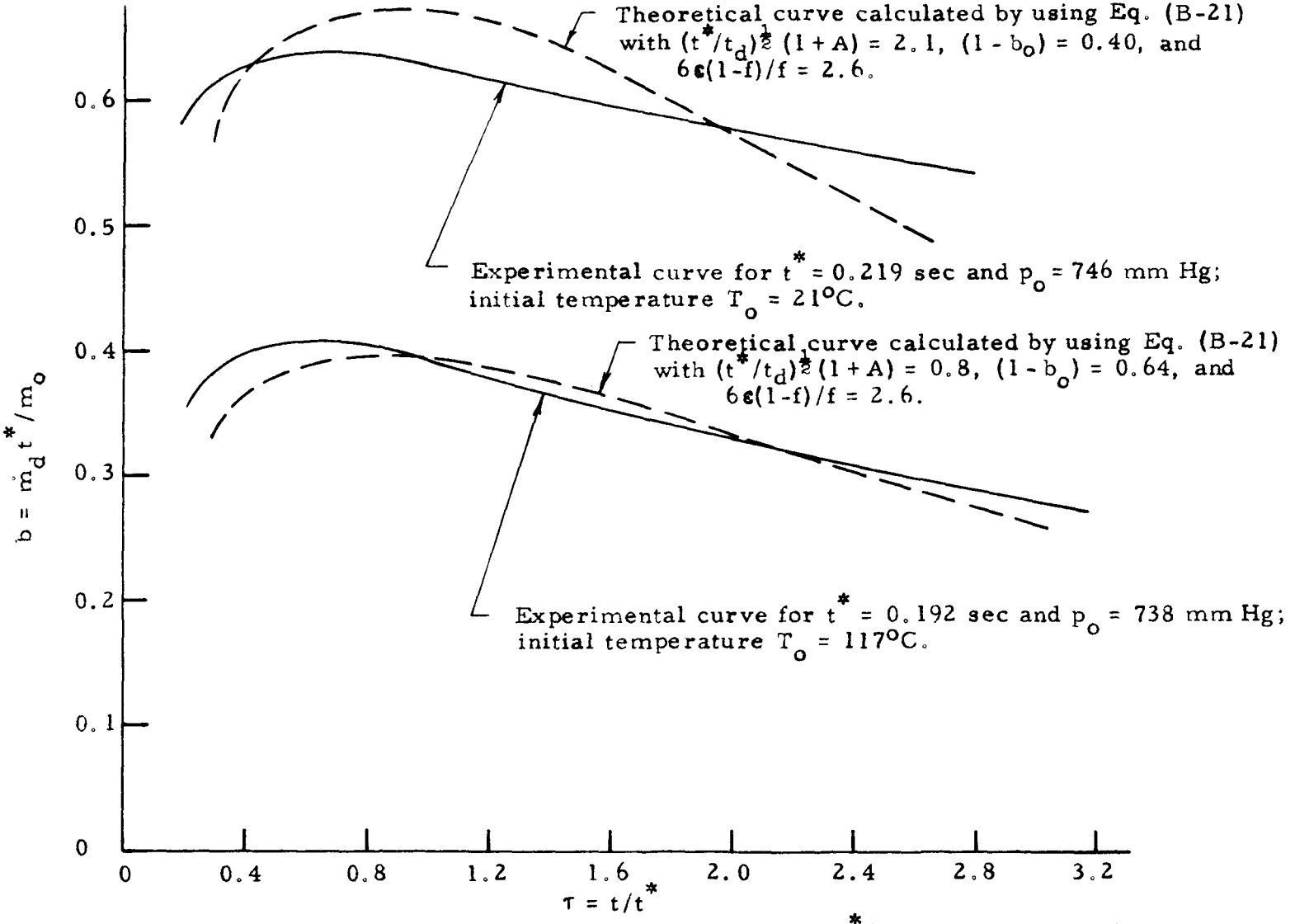

Fig. 63. The dimensionless desorption rate $b = \dot{m}_d t^*/m_o$ as a function of the reduced time $\tau = t/t^*$ for CO_2 discharging from a vessel containing silica gel of mesh size 6-16.

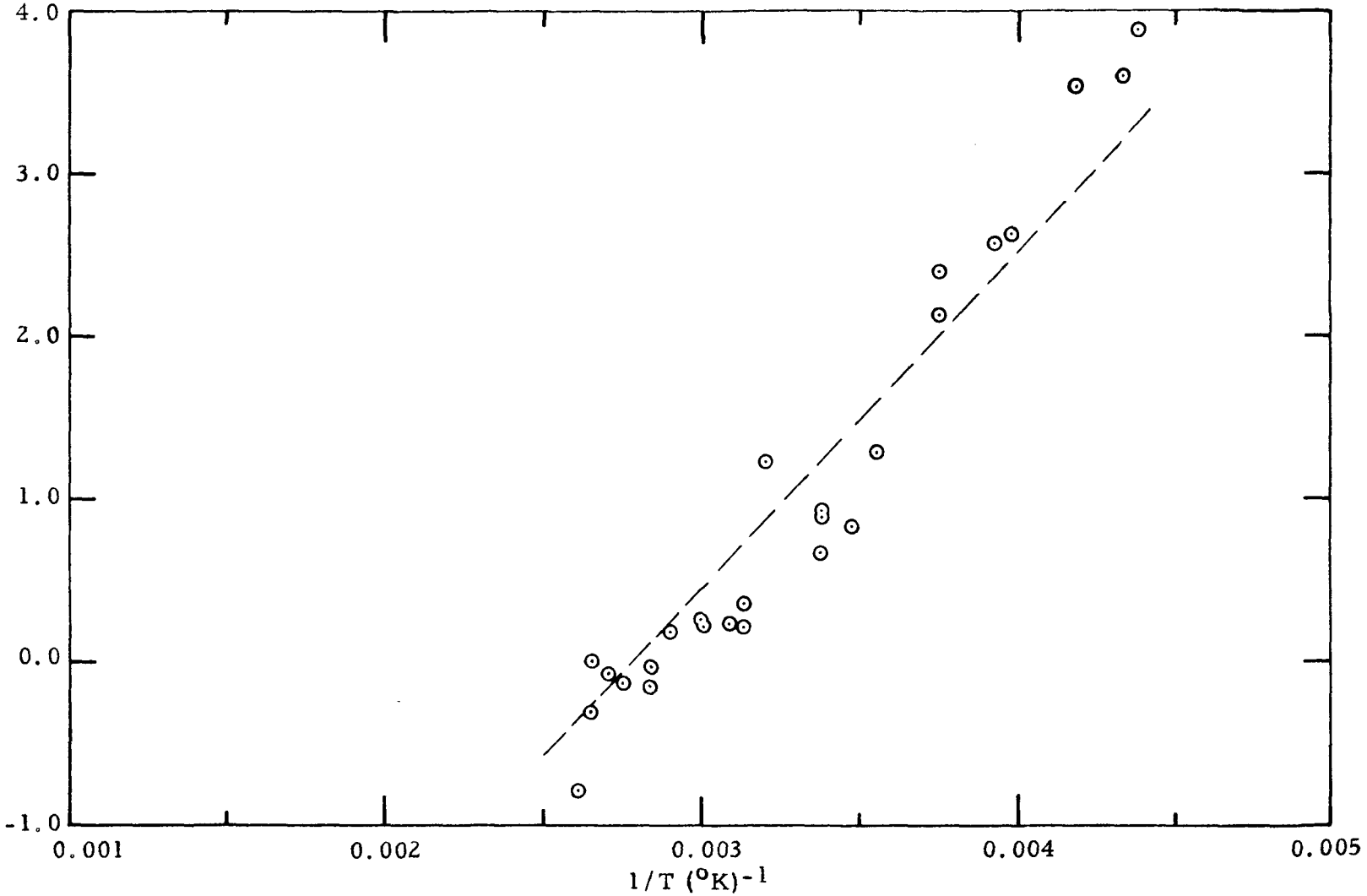

Fig. 64. The logarithm of A as a function of the reciprocal temperature 1/T for Ar.

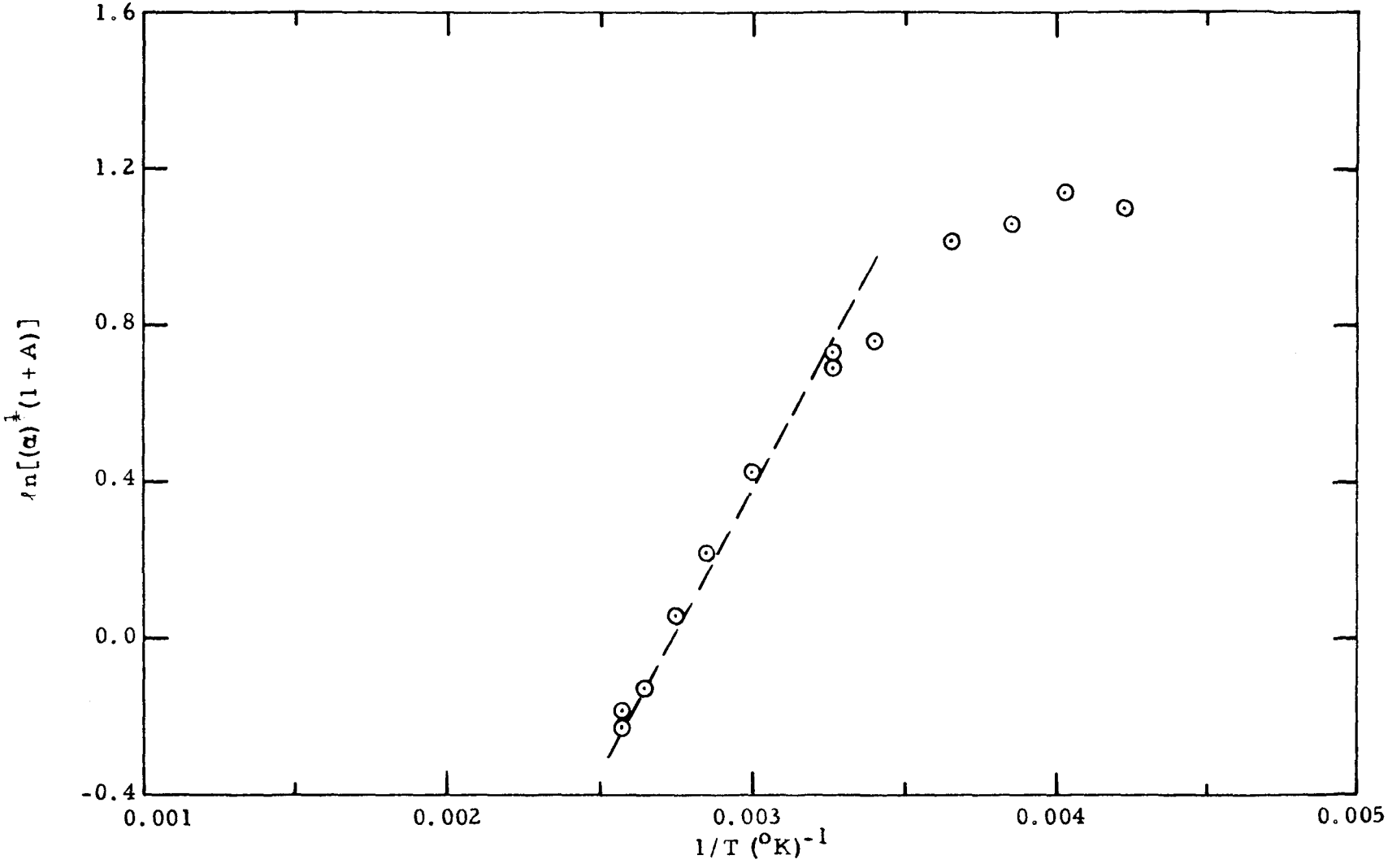

Fig. 65. The logarithm of $(\alpha)^{\frac{1}{2}}(1 + A)$ as a function of the reciprocal temperature $1/T$ for CO_2 .